ROLLING BLACKOUT IS REQUIRED FOR BOTH PHOTOTRANSDUCTION AND SYNAPTIC TRANSMISSION IN *DROSOPHILA*

By

Fu-De Huang

Dissertation to the Faculty of the

Graduate School of Vanderbilt University

In partial fulfillment of the requirements

For the degree of

DOCTOR OF PHILOSOPHY

In

Biological Sciences

May, 2006

Nashville, Tennessee

Approved:

Douglas G. McMahon

Todd R. Graham

Randy D. Blakely

H. Alex Brown

Kendal S. Broadie

To my wife Xiaodan, my kids: Connie, Jason and Richard

and my mother Shengqiu

ACKNOWLEDGEMENTS

The dissertation reflects an extensive and creative work. Without help, support and encouragement from several people, it would not be possible for me to finish. Thus, I like to acknowledge them with my most enthusiastic gratitude.

First of all, I would like to thank Kendal Broadie for advice and support, and establishing an extremely well equipped lab so that I can conveniently work on the project in a variety of ways. I will also give special thanks to Sean Speese for notice and acquirement of the temperature sensitive mutant of *rolling blackout* gene which is the base of my dissertation, for his instructions in molecular biology and molecular genetics. He also contributed significantly to this work by initiation of this project, embryo injection to obtain transgenic animal, and optic imaging. Heinrich Matthies for lipids measurement, biotin labeling and productive disicussion, Mark Smith for early participation in electroretinogram recording, and Elvin Woodruff for electron microscope imaging and related data collection. I am very grateful to Jeffery Rohrbough for assistance in electrophysiology and his invaluable comments on my manuscripts, Emma Rhuston for instructions in genetics.

At last, I would like to give my most special thank to my wife for understanding, supporting and love to me and my three kids.

The Neuroscience program in University of Utah and Biological Science department of Vanderbilt provided education and financial support.

Table of contents

LIST OF TABLES

LIST OF FIGURES

Figure page

Chapter II

Chapter III

CHAPTER I

INTRODUCTION

The synaptic vesicle cycle

Synaptic transmission is mediated by the fusion of a neurotransmitter containing synaptic vesicle (SV) with the presynaptic plasma membrane. To sustain repeat transmission, the SV is recycled from plasma membrane through endocytosis. The recycled SV is refilled with neurotransmitter, and goes through trafficking, docking and priming steps to participate in another round of transmission, therefore forming a cycle. Essential proteins in both SV exocytosis and endocytosis have been identified; central proteins in SV exocytosis are the fusogenic SNARE proteins and a critical endocytic protein is dynamin GTPase (see below). These central protein components are regulated by other proteins and also regulatory lipids, particularly PtdIns(4,5)P_2 (PIP_2) and its metabolite diacylglycerol (DAG). Our understanding of these mechanisms is incomplete, and new regulators of SV exocytosis and endocytosis are being identified.

SNARE proteins and membrane fusion

SNAREs were identified as receptors of soluble N-ethylmaleimide - sensitive fusion protein(NSF)-attachment proteins (SNAPs) (Sollner et al., 1993). SNAREs were identified from a multi-subunit complex that was isolated from bovine brain by affinity purification with NSF and α-SNAP. Three SNARE proteins were identified, including synaptic vesicle (SV)-integral synaptobrevin

(v-SNARE), plasma membrane-integral syntaxin 1A and plasma-membrane associated SNAP-25 (t-SNARE, SNARE located at target membrane). SNARE proteins were found to be homologous to yeast proteins essential for membrane traffic, suggesting that SNAREs are essential molecules for all eukaryotic intracellular membrane fusion (Bennett and Scheller, 1993; Ferro-Novick and Jahn, 1994). Sequence analysis revealed that all SNAREs contain one or two homologous domains of approximately 60 amino acids, referred to as the SNARE motif (Terrian and White, 1997; Weimbs et al., 1997; Weimbs et al., 1998). Detergent-extracted synaptic SNAREs (syntaxin 1A, synaptobrevin and SNAP-25) can assemble into a ternary complex (SNARE complex) by the association of their SNARE motifs into a twisted parallel four-helical bundle (Sutton et al., 1998). The formation of SNARE complex has been proposed to provide the driving force to initiate membrane fusion (Lin and Scheller, 1997; Sutton et al., 1998). Soon after this model was proposed, it was shown that v- and t-SNARE proteins residing on separate liposomes can indeed assemble into SNARE complex, the trans-SNARE complex, leading to spontaneous fusion of those liposomes (Weber et al., 1998). This indicates that trans-SNARE complex formation, presumably mediated by SNARE-motif interaction, is sufficient to induce membrane fusion.

Synaptic vesicle exocytosis

SV exocytosis consists of many interconnected steps, including SV transport to, and docking at, the presynaptic active zone (AZ), SV priming (the

process rendering the SV fusion-competent) and fusion. These sequential steps involve a series of protein–protein interactions, including the regulation of SNARE proteins and the formation of SNARE complex (Sutton et al., 1998; Weber et al., 1998; Weis and Scheller, 1998; Jahn and Sudhof, 1999; Lin and Scheller, 2000; Sudhof, 2000; Chen and Scheller, 2001; Richmond and Broadie, 2002; Rizo and Sudhof, 2002; Jahn et al., 2003; Rosenmund et al., 2003; Jahn, 2004; Sudhof, 2004).

Synaptic vesicle trafficking and docking

In the presynaptic terminal there are two distinct pools of SVs; the readily releasable pool (RRP) and the reserve pool (RP). SVs in RRP cluster around the AZ and are recruited to fuse during low frequency stimulation condition, SVs in the RP are located away from AZ and are recruited only under high frequency stimulation conditions (Sudhof, 2004). The molecular mechanisms for this SV trafficking to and docking at AZ are not clear. SVs in the RP were proposed to be bound to the actin cytoskeleton through synapsins which are abundant SV peripheral membrane proteins coating the vesicle surface (Greengard et al., 1994). The N-terminal domain of synapsin can be phosphorylated by PKA and calcium/calmodulin dependent kinase I, and this phosphorylation abolishes binding of synapsins to SVs, presumably freeing SVs to be transported (Greengard et al., 1994; Hosaka et al., 1999). However, deletion of synapsin 1 and 2 (most abundant synpsin proteins at synapse) causes a reduction of SV number, but no alteration of SV clustering

(Sudhof, 2004). The mobilization of SVs from the reserve pool to AZ involves high-frequency stimulation, the cAMP cascade and activation of the actin polymerization/depolymerization (Kuromi and Kidokoro, 1998; Kidokoro et al., 2004) and actin-myosin interactions (Mochida et al., 1994; Ryan, 1999; Jordan et al., 2005). SV docking may be mediated through the interaction of SV proteins with AZ proteins (Wang et al., 1997; Lin and Scheller, 2000; Voets et al., 2001; Rosenmund et al., 2003; Weimer et al., 2003). It was proposed that SV might first dock on a protein scaffold composed of large proteins including aczonin, bassoon, or piccolo, which contain multiple protein-protein interacting domains and specifically localized at AZ. Then SV is transferred to AZ plasma membrane via the interactions of SV protein Rab3a GTPase interacting its AZ effectors RIM, Rabphilin, and UNC18/nSec1. The interactions of t-SNARE SNAP-25 with vesicle-associated Ca^{2+} synaptotagmin (Rickman et al., 2005) and Rabphilin (Tsuboi and Fukuda, 2005) may also be involved in SV docking.

Synaptic vesicle priming

The priming step involves UNC13-mediated opening of syntaxin, and the assembly of the synaptobrevin/syntaxin/SNAP-25 SNARE complex, which forces the SV into close proximity to the AZ plasma membrane in preparation for Ca^{2+} influx-triggered fusion (Augustin et al., 1999; Jahn and Sudhof, 1999; Lin and Scheller, 2000; Sudhof, 2004; Aravamudan et al., 1999; Richmond et al., 1999; Varoqueaux et al., 2002). During priming, each SNARE protein and the

SNARE complex are under the rigorous control or regulation by other synaptic proteins, such as the regulation of syntaxin by UNC13, UNC18, tomosyn and amisyn, and the SNARE complex regulation by synaptotagmin, Gβγ (heterodimer of β and γ subunit of G protein), and complexin.

In solution, isolated syntaxin 1A adopts a default "closed" configuration in which the N terminus is folded to bind the SNARE motif, occluding the interaction of the SNARE motif with synaptobrevin and SNAP-25. Thus, the default state of syntaxin 1A in synapse is assumed to be closed (Dulubova et al., 1999). A primary function of UNC13/MUNC13 is proposed to open the "closed" sytaxin 1A, allowing the open syntaxin 1A to interact with SNAP-25 and synaptobrevin to form a SNARE complex (Richmond et al., 2001). UNC13/MUNC13 contains a syntaxin 1A-binding C terminus (Maruyama and Brenner, 1991; Betz et al., 1997), and a C1 domain that binds DAG (diacylglycerol) and phorbol ester (Ahmed and Maruyama, 1992; Kazanietz and Bustelo, 1994; Kazanietz, 1995a; Kazanietz et al., 1995b; Betz et al., 1998). UNC13/MUNC13 exists as both soluble and insoluble forms (Betz et al., 2001). Insoluble UNC13/MUNC13 is tightly associated with the cytoskeletal matrix of the presynaptic active zone by a proteinaceous linker. Soluble Unc13/MUNC13 can be recruited to the plasma membrane in a DAG-dependent manner (Betz et al., 1998; Ashery et al., 2000). Proteinaceously anchored UNC13/MUNC13 is proposed to establish a basal, fusion-competent SV pool that possesses high releasable probability but slow refilling rate (Rhee et al., 2002). The DAG-recruited UNC13/MUNC13 is proposed to be required for the formation of

another pool of fusion competent SVs, characterized by low release probability but fast refilling rate, which may be the major source for neurotransmitter release during stimulation by high frequency action potentials (Brose and Rosenmund, 2002; Rhee et al., 2002).

In addition to UNC13/MUNC13, other SNARE regulatory proteins (Jahn and Sudhof, 1999; Jahn et al., 2003; Jahn, 2004; Sudhof, 2004) include UNC18-1/MUNC18-1, tomosyn and amisyn (Sudhof, 2004), which physically interact with syntaxin 1A. UNC18-1/MUNC18-1 forms a complex with closed syntaxin and may inhibit SNARE complex assembly (Dulubova et al., 1999; Yang et al., 2000). However, UNC18/MUNC18 is also essential for SV fusion by an unknown mechanism (Verhage et al., 2000; Rizo and Sudhof, 2002; Sudhof, 2004). Tomosyn and amisyn are soluble and have a C-terminal synaptobrevin-like SNARE motif that can substitute for synaptobrevin in the synaptic SNARE complex. However, neither tomosyn nor amisyn can form a functional trans-SNARE complex because neither tomosyn nor amisyn contains a transmembrane domain. Therefore, tomosyn and amisyn may act as competitive inhibitors of the genuine synaptobrevin-like SNARE motifs (Jahn, 2004; Sudhof, 2004; Constable et al., 2005).

During SNARE complex formation, syntaxin 1A may initially form a binary complex with SNAP-25, then binds to synaptobrevin to form a ternary complex (Sutton et al., 1998), or bind to synaptotagmin (Rickman et al., 2005). In living cells, the assembly of syntaxin 1A and SNAP-25 has been visualized by FRET signal (An and Almers, 2004). After the SNARE complex assembly, several

synaptic proteins interact to control, regulate, or stabilize the complex. These synaptic proteins include synaptotagmins, Gβγ (heterodimer of β and γ subunit of G protein), snapin, and complexins (see below).

Synaptotagmins are SV-associated proteins that contain a short N-terminal intracellular sequence, a single transmembrane region, a short linker, and two cytoplasmic calcium-binding C2 domains (the C2A and C2B domains) (Perin et al., 1990; Geppert et al., 1991). Synaptotagmins bind to the C-terminus of SNAP-25 in the assembled SNARE complex and act as Ca^{2+} sensors in evoked SV exocytosis. However, the precise mechanism how Ca^{2+} binding to synaptotagmin leads to the SNARE complex-mediated SV fusion is not known (Jahn and Sudhof, 1999; Sudhof, 2004; Rickman et al., 2005). Gβγ also binds to the C-terminal of SNAP-25 in the SNARE complex, and competes with synaptotagmin for binding (Blackmer et al., 2005; Gerachshenko et al., 2005; Sullivan, 2005). Snapin is exclusively located on SV membrane, and associates with the SNARE complex by directly binding to SNAP-25 (Ilardi et al., 1999). Snapin protein enhances the synaptotagmin-SNARE complex physical interaction by binding to SNAP-25 in the SNARE complex (Ilardi et al., 1999; Tian et al., 2005). Snapin is a possible target of PKA, and PKA-phosphorylation of snapin enhances its binding to SNAP-25, and the interaction of both snapin and synaptotagmin with the SNARE complex (Chheda et al., 2001).

Complexins are small neuronal proteins that bind to assembled SNARE complexes (McMahon et al., 1995) possibly by inserting into a groove in the C-terminal half of the complex. Complexs may be involved in the stabilization of

assembled SNARE complexes, but are not essential for SV exocytosis (Reim et al., 2001; Tokumaru et al., 2001; Chen et al., 2002; Sudhof, 2004).

Synaptic vesicle fusion

SV fusion is a rapid (≤50 μS) Ca^{2+} influx-triggered process, which involves regulated fusion pore opening and expansion. It is widely accepted that the SNARE complex is essential for fusion. The SNARE complex is sufficient for *in vitro* liposome fusion (Weber et al., 1998), but physiological SV fusion involves other proteins/lipids acting as facilitating cofactors (Weber et al., 1998; Jahn and Sudhof, 1999; Lin and Scheller, 2000; Sudhof, 2004; Tucker et al., 2004). Now the central question regarding the function of the SNARE complex in fusion is whether the SNARE complex directly executes fusion by "zippering-up" of SNARE motifs, or whether it controls downstream fusion machinery. If downstream fusion machinery exists what proteins are involved? Accumulating evidence indicates that a separate fusion machinery complex may act downstream of SNARE complex assembly. V_0-ATPase, protein phosphatase 1, and Vtc3p, among other proteins have been shown to act subsequent to trans-SNARE pairing, and may mediate SV fusion downstream of SNAREs (Peters et al., 1999; Peters et al., 2001; Muller et al., 2002; Bayer et al., 2003; Hiesinger et al., 2005). Another critical question concerns the nature of the fusion pore. One model is that the trans-SNARE complex directly executes fusion. In this model the fusion pore is considered to be a transient lipidic intermediate resulting from the dissipation of a lipid-stalk/hemifusion intermediate (Jahn and Sudhof, 1999;

Jahn et al., 2003; Sudhof, 2004). A second model, in which a separate fusion machinery exists, the fusion pore is represented by a junction-like proteinaceous pore formed by the 5-8 syntaxin transmembrane segments (Han et al., 2004; Han and Jackson, 2005; Sorensen, 2005) or by the V_0-ATPase complex (Peters et al., 2001; Bayer et al., 2003; Hiesinger et al., 2005).

Synaptic vesicle endocytosis

After exocytosis, SVs undergo endocytosis or recycling. Three pathways, “kiss-and-stay”, “kiss-and-run” and clathrin-mediated endocytosis, have been proposed for SV recycling (Sudhof, 2004). The first two are fast (<1S) pathways involving the closure of the fusion pore, SVs either remain at the AZ and are refilled with neurotransmitter (“kiss-and-stay”), or are recycled locally independently of clathrin (“kiss-and-run”). The fast pathways are thought to preferentially recycle SVs into the readily releasable pool under low frequency stimulation. In contrast, clathrin-mediated endocytosis is relatively slow (30-40S) and is employed at higher frequency stimulation (Koenig and Ikeda, 1996; Pyle et al., 2000; Richards et al., 2000; Sudhof, 2004).

The slow endocytosis pathway is the best understood. Similar to exocytosis, clathrin-mediated endocytosis involves cascades of protein-protein and protein-lipid interactions. Clathrin-mediated endocytosis is divided into clathrin coat assembly, invagination, fission, and clathrin uncoating (Cremona and De Camilli, 1997; Slepnev and De Camilli, 2000; Cremona and De Camilli, 2001). Clathrin coat assembly is proposed to start with the binding of the

heterotetrameric clathrin adaptor complex AP-2 and the accessory clathrin adaptor AP180 to both membrane protein and lipids. Subsequently, the AP-2 recruits clathrin and promotes its assembly into a basket-like lattice that distorts the plasma membrane, driving vesicle budding inside the plasma membrane. Clathrin accessory proteins are then recruited to facilitate invagination of the coated pit by changing membrane curvature and recruiting other endocytic proteins. Amphiphysin and endophilin are two such well-characterized clathrin accessory proteins (Slepnev and De Camilli, 2000).

At vesicle fission, dynamin plays a key function as an enzyme or a scaffold protein. Dynamin is a GTPase with a pleckstrin homology domain (PH domain), GTPase-enhancing domain (GED domain), and a proline-rich domain (PRD domain) in its C-terminus. Dynamin is recruited to the stalk of a deeply invaginated coated pit to form a scaffold around the stalk by SH3-domain-containing proteins, such as endophilin, amphiphysin, Src-kinase and possible others (Slepnev and De Camilli, 2000; Cremona and De Camilli, 2001). Dynamin is proposed to constrict and sever the stalk via a GDP hydrolysis-dependent conformational change (Cremona and De Camilli, 2001). However, GTP-hydrolysis by dynamin may not be critical for endocytosis (Sever et al., 1999). It has also been suggested that dynamin links endocytosis to actin polymerization via the interactions of its PRD with SH3-containing proteins, and that actin polymerization may propel SVs into the cytosol after they are pinched off from the plasma membrane (Qualmann et al., 2000; Lee and De Camilli, 2002; Merrifield et al., 2002; Orth and McNiven, 2003). The PRD of dynamin

binds to the SH3 domain of several proteins that interact with actin or the proteins that regulate actin assembly, including profilin (Witke et al., 1998; Gareus et al., 2005), Abp1 (Kessels et al., 2001), cortactin (McNiven et al., 2000), syndapin (Qualmann and Kelly, 2000; Slepnev and De Camilli, 2000; Kessels and Qualmann, 2002), intersectin (Slepnev and De Camilli, 2000; Hussain et al., 2001), Grb2 (Miki et al., 1994), and Nck (Benesch et al., 2002).

After internalization, clathrin-coated vesicles are required to shed the clathrin coat to allow cycling of endocytic proteins. This process involves ATPase heat shock protein cognate (Hsc70) and its cofactor auxilin. Auxilin recruits Hsc70 to the clathrin coat, stimulates Hsc70's ATPase activity and works together with Hsc70 to release clathrin (Schmid, 1997; Slepnev and De Camilli, 2000; Fotin et al., 2004a; Fotin et al., 2004b). Dephosphorylation of PIP_2 by synaptojanin1 might be a switch for uncoating. Synaptojanin1 is a polyphosphoinsitide phosphatase enriched at nerve terminals, and hydrolyzes several phosphoinositide species, including PtdIns(4,5)P_2 and PtdIns(3,4,5)P_3 (McPherson et al., 1996; Cremona and De Camilli, 2001). Disruption of synaptojanin1 function by gene mutation, antibody, or peptide injection prevents SV formation and uncoating and recycling (Cremona et al., 1999; Gad et al., 2000; Harris et al., 2000; Cremona and De Camilli, 2001).

PIP_2 and metabolites regulate synaptic vesicle cycle

In addition to putative fusogenic and endocytic proteins, PIP_2 and its PLC hydrolysis product DAG, play critical roles in the SV cycle by recruiting (as an

anchor), regulating/activating (as a regulator) synaptic proteins, converting to other regulatory lipids (as a precursor), or by directly altering membrane physical properties (Goni and Alonso, 1999; Peters et al., 1999; Cremona and De Camilli, 2001; Martin, 2001; Brose and Rosenmund, 2002; Di Paolo et al., 2004; Fratti et al., 2004; Jun et al., 2004; Wenk and De Camilli, 2004; Rohrbough and Broadie, 2005).

As a lipid anchor, PIP_2 has been proposed to regulate SV targeting to the plasma membrane during exocytosis, and to recruit endocytic proteins to their functional sites during clathrin-mediated endocytosis. For example, PIP_2 recruits the AP-2/AP-180 clathrin adaptor complex and accessory proteins (amphiphysin, endophilin) to start coat assembly. PIP_2 recruits dynamin together with SH3-containing proteins, to the stalk of endocytic pits (Cremona and De Camilli, 2001; Martin, 2001), and recruits N-WASP in cooperation with Rho-type GTPase to nucleate actin polymerization (Rohatgi et al., 1999; Zigmond, 2000; Cremona and De Camilli, 2001).

As a regulator, PIP_2 has been implicated the SV cycle by binding to and stimulating both fusogenic proteins, including synaptotagmin, rabphilin, SNAP-25, MUNC18-interacting Mint1/2, and endocytic proteins, such as dynamin (Cremona and De Camilli, 1997, 2001; Martin, 2001; Rosenmund et al., 2002; Wenk and De Camilli, 2004; Rohrbough and Broadie, 2005). Dynamin binding and stimulation by PIP_2 is also critical for dynamin's function in endocytosis (Barylko et al., 1998; Lee et al., 1999; Vallis et al., 1999; Cremona and De Camilli, 2001). In addition, PIP_2 interacts with the syntaxin1A/SNAP-25 binary

complex and reduces its lateral mobility in a phosphatidylcholine lipid background, and thereby may stabilize the interaction of t-SNARE complex with SV proteins (Wagner and Tamm, 2001; Wagner and Tamm, 2001).

As a precursor, PIP_2 is hydrolyzed by phospholipase C (PLC) to produce soluble inositol triphosphate (IP_3) and membrane-anchored DAG. IP_3 is well known to induce calcium release from internal stores by binding to IP_3 receptors (Berridge, 1993; Berridge et al., 2003), and this process has been suggested to be involved in synaptic plasticity (Barbara, 2002). DAG activates MUNC13 and PKC (Brose and Rosenmund, 2002; Brose et al., 2004). MUNC13 activates syntaxin 1A and is essential for SV priming (Aravamudan et al., 1999; Richmond et al., 1999; Richmond et al., 2001; Brose and Rosenmund, 2002; Rhee et al., 2002). PKC phosphorylates many synaptic proteins, including synapsin, rabphilin (Fykse, 1998; Foletti et al., 2001), synaptotagmin (Hilfiker et al., 1999; Roggero et al., 2005), voltage-gated Ca^{2+} channel (Catterall, 2000), SNAP-25 (Shimazaki et al., 1996; Morgan et al., 2005), and MUNC18-1 (Barclay et al., 2003; Morgan et al., 2005). Particularly, the phosphorylation of SNAP-25 by PKC stimulates the localization of SNAP-25 to the plasma membrane (Iwasaki et al., 2000; Kataoka et al., 2000; Xu et al., 2004) and enhances the interactions of SNAP-25 with syntaxin and synaptotagmin (Shimazaki et al., 1996; Risinger and Bennett, 1999). PKC also potentiates the recruitment of vesicles to the plasma membrane (Nagy et al., 2002; Shoji-Kasai et al., 2002), and enhances the formation of SNARE complex (Xu et al., 2004). The phosphorylation of MUNC18-1 by PKC was suggested to disinhibit sytaxin1A and regulate the

kinetics of fusion pore opening (Fujita et al., 1996; Morgan et al., 2005). Consistent with the effects of PKC phosphorylation of SNAP-25 and MUNC18-1, specific inhibition of PKC activity causes activity-dependent depression of synaptic transmission (Rhee et al., 2002). Besides PKC and MUNC13, there are many other uncharacterized C1-domain (DAG binding domain) containing proteins (Brose et al., 2004). In general, PKC phosphorylates and regulates many fusogenic proteins functioning at multiple stages of SV exocytosis, including facilitating readily releasable pool refilling and fusion downstream of Ca^{2+} (Morgan et al., 2005).

DAG is converted to phosphatidic acid (PA) by DAG kinase, or is hydrolyzed by DAG lipase to release polyunsatuated fatty acids (PUFAs). PA together with ARF stimulates the activation of PI(4)P 5-kinase to generate PIP_2 that plays diverse roles in the SV cycle (see above) (Jenkins et al., 1994; Cremona and De Camilli, 2001). In addition, PA may directly recruit proteins required for membrane trafficking, such as NSF (N-ethylmaleimide sensitive factor)(Manifava et al., 2001). PUFAs (e.g. arachidonic and linolenic acids) directly stimulate MUNC18-regulated SNARE complex formation (Rickman and Davletov, 2005). Consistent with this finding, C.elegans of long chain PUFA deficiencies show NJM transmission defect (Lesa et al., 2003). PUFAs can also affect SV cycle via being transferred by endophilin into lysophosphatidic acid to produce phosphatidic acid (PA) to facilitate the SV endocytosis (Schmidt et al., 1999). In addition to regulating synaptic proteins, noncylindrical lipids including PIP_2, DAG, lysophosphatic acid, PA, and PUFAs, regulate SV trafficking through

changing membrane physical properties, e.g. by facilitating the formation of membrane curvature (Goni and Alonso, 1999; Huttner and Schmidt, 2002; Rohrbough and Broadie, 2005).

In general, PIP_2 and its metabolites coordinate and facilitate the SV cycle at multiple stages. Consistent with these roles, enzymes responsible for the turnover or metabolism of these lipids have also been implicated in the SV cycle (Cremona and De Camilli, 1997, 2001; Martin, 2001; Brose and Rosenmund, 2002; Wenk and De Camilli, 2004; Rohrbough and Broadie, 2005), including lipases (PLC, PLA_2, PLD), kinases (PI kinase, PIP kinase, and DAG kinase), phosphotases (PIP_2 phosphotase), and others (fatty acid desaturase, ceramidase). Furthermore, signaling pathways involving the above lipids and lipid enzymes have been implicated in regulating the SV cycle or synaptic transmission (Cremona and De Camilli, 1997, 2001; Martin, 2001; Rosenmund et al., 2002; Wenk and De Camilli, 2004). For example, mutation of genes and perturbation of pathways that positively or negatively regulate DAG level produced facilitation or inhibition of transmitter release (Lackner et al., 1999; Miller et al., 1999; Nurrish et al., 1999; Rosenmund et al., 2002).

Another neural signaling pathway that involves both protein-protein interaction and protein-lipid (particularly PIP_2 and its metabolites) interaction is the phototransduction in *Drosophlia* (see below).

Drosophila phototransduction

The *Drosophila* eye is a compound eye that consists of approximately 800 simple eyes called ommatidia. Each ommatidium contains 8 photoreceptor cells, named as R1 to R8. Each photoreceptor contains a rhabdomere, a specialized microvillar structure, where phototransduction occurs, which is the functionally equivalent to outer segments of human rods and cones (Montell, 1999). *Drosophila* phototransduction starts with the activation of rhodopsin, a G protein (Gq) coupled receptor, and is mediated by a PLC_{β}-dependent cascade resulting in the opening of TRP and TRPL cationic channels. The entire process happens within 20ms. Thus *Drosophila* phototransduction is the fastest known G protein-coupled signaling pathway (Ranganathan et al., 1991; Montell, 1999; Hardie and Raghu, 2001).

Rhodopsin consists of a chromophore and opsin, a 7-pass transmembrane protein. At rest, the chromophore is a 11-*cis*-retinal covalently attached to a lysine residue in the 7^{th} transmembrane domain (Palczewski and Saari, 1997). Light exposure causes the conversion of the 11-12 double bond in the chromophore from a *cis* to *trans* configuration, resulting in a conformational change to opsin, and conversion of rhodopsin to metarhodopsin. Metarhodopsin activate the coupled heterotrimeric G protein by promoting the exchange of a bound GDP for GTP and subsequent dissociation of the $Gq\alpha$ from $G\beta\gamma$. The inactivation of metarhodopsin involves the binding of arrestin to rhodopsin. This interaction is similar to that in vertebrates, except that in *Drosophila* the binding of arrestin to rhodopsin does not require rhodopsin to be phosphorylated (Vinos

et al., 1997). Moreover, the rhodopsin regeneration cycle in *Drosophila* is very different from that in vertebrates (Montell, 1999). In *Drosophila*, chromophore and opsin do not dissociate from each other, and the regeneration of rhodopsin from metarhodopsin requires only the absorption of a second photon. In vertebrates, opsin and chromophore dissociate and rhodopsin is regenerated through a multistep process involving association of a newly synthesized chromopore with opsin.

The G-protein downstream effector in *Drosophila* is also different from that in vertebrates. The downstream effector in *Drosophila* is PLC-β, encoded by the *norpA* gene (Pak et al., 1970; Inoue et al., 1985; Bloomquist et al., 1988). PLC-β hydrolyzes PIP_2 into IP_3 and DAG, leading to the activation of light-induced Na^+ and Ca^{2+} influx, and depolarization of photoreceptors (Montell, 1999; Hardie and Raghu, 2001). In vertebrates, the downstream effector for G protein is phosphodiesterase (PDE), which hydrolyzes cGMP into GMP, resulting in the closure of the cGMP-gated cation channels, decrease of Na^+ and Ca^{2+} influx through these channels, and the hyperpolarization of photoreceptors.

The light-induced current is mediated in *Drosophila* by the cation channels TRP and TRPL encoded by *transient receptor potential* gene (*trp*) and *trp-like* gene (*trpl*) (Cosens and Manning, 1969; Montell and Rubin, 1989; Hardie and Minke, 1992). The long-standing question is how the hydrolysis of PIP_2 by PLC leads to the activation of TRP and TRPL channels. A couple of models have been proposed (Montell, 1999; Hardie, 2001; Hardie and Raghu, 2001; Minke and Cook, 2002). The first model proposes IP_3 as the excitatory factor: IP_3

activates IP_3 receptor on the endoplasmic reticulum to release internal Ca^{2+}, which in turns activates TRP and TRPL channels. However, IP_3 knockout flies display normal phototransduction (Acharya et al., 1997), and release of caged IP_3 or caged Ca^{2+} failed to activate cationic channel in photoreceptors (Hardie, 2001). Thus, this "store-operated" model is apparently wrong. The alternative DAG branch of PLC-PIP_2 signaling then gained attention. DAG was proposed to activate TRP and TRPL directly or indirectly via its hydrolysis product PUFA, or via activation of PLC (Chyb et al., 1999; Estacion et al., 2001; Hardie, 2001; Hardie and Raghu, 2001). An unidentified DAG lipase was proposed to hydrolyze DAG to produce PUFA (Hardie, 2001; Hardie and Raghu, 2001). The most attractive model is that the activation of TRP and TRPL may result from the immediate effects of PLC activation, via removal of PIP_2 inhibition and the activation by PLC product DAG (Hardie, 2001; Hilgemann et al., 2001). The unlikely model is that the cascade PLC-PIP_2-DAG-PUFA leads to the activation of TRP and TRPL channels, because this lengthy cascade does not seem consistent within the 20 mS latency of *Drosophila* phototransduction. However, a modified form of the latter model proposes that pre-existing PUFA near TRP and TRPL channels stimulates these channels when PIP_2 inhibition is removed by PLC.

PIP_2 and its metabolites regulate ion channels or transporters

PIP_2 and its metabolites acutely regulate or modulate numerous ion channels and transporters. PIP_2 stimulates the plasmalemma Ca^{2+} pump,

Na^+/Ca^{2+} exchanger, inward rectifier K^+ channel, voltage-gated K^+ channels (Kv2.1, KCNQs), and inhibits the *Drosophila* TRP and TRPL phototransduction channels, the mammalian capsaicin-activated TRP (VR1) channel (Hilgemann et al., 2001; Suh and Hille, 2002). PIP_2 has dual, concentration-dependent effects on voltage-gated Ca^{2+} (P/Q type) channels, stimulating at low concentration, and inhibiting at high concentration *in vitro* and *in vivo* (Wu et al., 2002).

The PIP_2 hydrolysis product DAG is also believed to modulate various ion channels via both PKC-dependent and PKC-independent pathways. For example, DAG activates PKC to phosphorylate and regulate voltage-gated Ca^{2+} channels (L, N, P/Q type) (Catterall, 2000), voltage-gated Na^+ and K^+ channels (Standen and Quayle, 1998; Schreibmayer, 1999), and light-activated TRP channels in *Drosophila* (Smith et al., 1991; Hardie et al., 1993; Huber et al., 1998; Liu et al., 2000). Independently of PKC, DAG attenuates voltage-gated Na^+ and K^+ channels (Bowlby and Levitan, 1995; Renganathan et al., 1995), and activates many TRP channels including TRPL (Clapham et al., 2001; Benham et al., 2002). The DAG hydrolysis product PUFAs also regulate channel activity (Meves, 1994), including the direct activation of *Drosophila* TRP and TRPL channels (Chyb et al., 1999; Hardie, 2001).

Thus, PIP_2 signaling in the nervous system is an intricate cascade, with multiple metabolites balanced to control fundamental neuronal signaling processes. Much greater insight into the coincident control of PIP_2, IP_3, DAG,

PA, and PUFAs levels *in vivo* is required to understand the coordination of PIP_2–dependent signaling in neurons.

Drosophila temperature-sensitive paralytic mutants

Screening for *Drosophila* mutant temperature-sensitive (TS) paralysis was initially designed to isolate conditional mutations affecting nerve and/or muscle. The first isolated TS mutation is $para^{ts}$ (*paralytic-temperature-sensitive*) (Suzuki et al., 1971). Subsequently, many *Drosophila* TS paralytic mutants have been isolated, such as *shibire* ($shibire^{ts1}$, (Grigliatti et al., 1973)), *comatose* ($comt^{ts17}$, com^{ts53}, (Siddiqi and Benzer, 1976)), *maleless* (mle^{ts}, (Belote and Lucchesi, 1980)), *stambhA* ($stmA^{1}$, (Shyngle and Sharma, 1985)), *temperature-induced-paralytic* ($tipE^{unspecified}$, (Elkins and Ganetzky, 1990)), *cysteine string protein* (csp^{E1}, csp^{E2}, (Zinsmaier et al., 1994)), *syntaxin1A* (syx^{3-69}; (Littleton et al., 1998)). Identification and characterization of *Drosophila* TS paralytic mutants have revealed numerous key proteins or genes in neuronal signaling, examples include *paralytic* (encoding α subunit of Na^+ channel)(Loughney et al., 1989), *shibire* (encodes dynamin GTPase)(van der Bliek and Meyerowitz, 1991), *comatose* (encoding N-ethylmaleimide-sensitive fusion factor)(Ordway et al., 1994), and *cacophony* (the only gene encoding Ca^{2+} channels)(Kawasaki et al., 2000) among many others (Littleton et al., 1998; Kitamoto et al., 2000; Rao et al., 2001; Wang et al., 2004).

These TS mutants are of value because they provide the opportunity to study a neuronal function when function of the gene product is acutely removed,

and thus bypass its requirement for cell viability or development. The best example is the study of SV cycle with *shibire* TS mutants, which has revealed some fundamental principles in SV cycle(Koenig et al., 1983; Koenig and Ikeda, 1996; Kidokoro et al., 2004). In addition, *shibire*^{ts1} mutants have been successfully used in the studies of complicated biological questions, such as behavior, learning and memory (Dubnau et al., 2001; Waddell and Quinn, 2001).

TS paralytic mutants fall into two categories classified by Siddiqi and Benzer (Siddiqi and Benzer, 1976): the first class of mutants, such as *para*^{ts1}, *tipE*^{1} paralyze rapidly when environmental temperature is shifted to a transition temperature. The other class of mutants, such as: *shibire, comatose*, paralyze gradually. There is no sharp transition temperature for the second class of mutants, the higher the temperature, the faster paralysis occurs. The paralysis in the first class is due to action potential failure, while the latter is due to a synaptic transmission defect.

CHAPTER II

ROLLING BLACKOUT, A NEWLY IDENTIFIED PIP_2–DAG PATHWAY LIPASE REQUIRED FOR DROSOPHILA PHOTOTRANSDUCTION

Abstract

The *rolling blackout (rbo)* gene encodes a plasma membrane-bound lipase required for *Drosophila* phototransduction. RBO protein is enriched in photoreceptors and temperature-sensitive *rbo* mutants show reversible elimination of phototransduction within minutes, demonstrating an acute requirement for the protein. The block is activity–dependent, indicating that RBO acts in a use–dependent mechanism. Conditional *rbo* mutants show activity–dependent depletion of diacylglycerol (DAG) and concomitant accumulation of phosphatidylinositol phosphate (PIP) and phosphatidylinositol 4,5 bisphosphate (PIP_2) within minutes of induction, suggesting rapid down–regulation of phospholipase C (PLC) activity. The RBO requirement identifies an essential regulatory step in G protein–coupled, PLC–dependent inositol lipid signaling mediating activation of TRP and TRPL channels activation during phototransduction.

Introduction

Drosophila phototransduction is mediated by phospholipase C (PLC_β)–dependent opening of transient receptor potential (TRP) and TRP–like (TRPL) channels (Bloomquist et al., 1988). PLC_β cleaves phosphatidylinositol 4,5 bisphosphate (PIP_2) into inositol triphosphate (IP_3) and diacylglycerol (DAG), which is further cleaved by DAG lipase to produce polyunsaturated fatty acids (PUFAs). PIP_2, IP_3, DAG and PUFAs have all been implicated in the activation of TRP and TRPL channels (Montell, 1999; Estacion et al., 2001; Hardie, 2001; Minke and Cook, 2002; Hardie, 2003). PIP_2 reportedly inhibits the TRPL channel (Estacion et al., 2001), suggesting that PLC–dependent PIP_2 cleavage may alleviate inhibition. IP_3 may have a role in the activation of TRP and TRPL activation (Hardie and Minke, 1992), although recent evidence argues against this mechanism (Acharya et al., 1997; Hardie, 2003). DAG may directly or indirectly activate TRP and TRPL channels (Raghu et al., 2000; Estacion et al., 2001), and also stimulates an eye–specific PKC, which negatively regulates TRP channels (Smith et al., 1991; Huber et al., 1998; Liu et al., 2000). Finally, DAG hydrolysis generates PUFAs that may directly activate TRP and TRPL channels (Chyb et al., 1999). These putative interactive effects of the PIP_2 signaling system, including the coincident removal of PIP_2 and production of DAG and its metabolites, indicate that the activation of TRP and TRPL channels may result from the coordinated effects of lipid signaling (Hardie, 2001; Hilgemann et al., 2001).

A particularly fruitful genetic screening strategy in *Drosophila* focuses on the identification of temperature–sensitive (TS), conditional mutations blocking neuronal signaling. Such mutants have repeatedly revealed key proteins involved in the acute mediation of signal transduction (Loughney et al., 1989; van der Bliek and Meyerowitz, 1991; Ordway et al., 1994). Here, we characterize a TS mutant in the *rolling blackout* (*rbo*) gene encoding an integral plasma membrane lipase. Conditional *rbo* mutants exhibit acute, total block of phototransduction within a few minutes at restrictive temperature. The block is activity–dependent, and recovers rapidly in the absence of light. Conditional *rbo* mutants display activity–dependent depletion of DAG and concomitant accumulation of PIP and PIP_2. These results reveal a novel regulatory step in the G–protein coupled–PLC_β cascade upstream of TRP and TRPL channels.

Materials and Methods

Genetics

Drosophila stocks were cultured on standard medium on a 12:12 light:dark cycle at 25°C. The wild-type strain w^{1118} were used as control. Genomic deficiencies used include: 1) 42A region; Df(2R)nap1, Df(2R)cn88b, and Df(2R)nap9; 2) 44D region; Df(2R)H3D3, Df(2R)Np3 and Df(2R)H3C1. P–element stocks used for local hop mutagenesis were P{lacW}l(2)44Db[k08904] and P{lacW}ptc[k0507]. The TS $stmA^1$ mutant and lethal $stmA^{18.2}$ mutant were provided by S. Chandrashekaran. The *cmp44E* mutants (EMS mutant $cmp44E^1$

and intragenic deficiency (*cmp44E*^{rev499}) were provided by T. Jongens. The local P–element mutagenesis was a F3 screen based on a failure to complement existing EMS mutants. Complementation tests were done for both TS blindness and embryonic lethality. Tow P-element insertion lines that failed to complement the TS paralysis and lethality of exsiting *stmA* mutants, were isolated and named as *rbo*^{p1} and *rbo*^{p2}.

Molecular Techniques

To identify the *rbo* gene, EcoRI and BamHI (Fermentas) were used to cut genomic DNA of *rbo*^{p1} and *rbo*^{p2} P-element insertion lines. Flanking genomic DNA was isolated via inverse PCR. With BamHI template, forward primer 5'cacctctgacttgagcgtcg 3' and reverse primer 5'gacgggaccacc ttatgttatttcatcat3'. With EcoRI template, forward primer 5'cttgccgacgggaccaccttatgttatt 3' and reverse primer 5' agtgccacctgacgtctaag 3'. For sequencing EMS point mutations, both genomic *rbo* DNA and cDNA were employed. The Superscript^{TM} II reverse transcriptase kit (GIBCOBRL), and *rbo*-specific reverse primers were used in RT-PCR. The Expand Long Template PCR system (Roche) was used in all PCR experiments in this study. To generate the RBO-GFP fusion construct, EGFP coding sequence was fused to *rbo* genomic DNA (RF II in pBluescript SK(+) vector; (Faulkner et al., 1998)) just before the *rbo* stop codon by overlap extension PCR. The hybrid DNA was isolated by EcoR1/Not1 digestion and ligated into pCasper4 cut with EcoR I and Not I. The pCasper 4 plasmid containg genomic *rbo-egfp*

hybrid DNA was co-injected into w^{1118} embryos with pΔ2-3 helper plasmid to obtain transgenic lines. To express RBO in Schneider 2 cells, the cDNA of the longer RBO splice form was cloned by RT-PCR, cut with SpeI/NotI and ligated into pMT/V5-His A expression vector in frame with the C terminal V5 and poly His tag. The recombinant DNA was used in transient transfection of S2 cells. All recombinant DNAs were sequenced.

Membrane Association Analyses

rbo^2/rbo^2; *rbo–egfp/rbo–egfp* transgenic fly heads were homogenized with lysis buffer (50mM Tris–HCl, pH 7.5, 150mM KCl, 1mM EGTA, 1mM EDTA, 5mM DTT, complete protease inhibitors (Roche). The lysate was spun at 1000g for 10 min. The supernatant (total lysate) was centrifuged at 100,000g for 60 min to separate pellet from supernatant. The total lysate, pellet and supernatant were probed by Westerns with a monoclonal GFP antibody (Covance). To examine whether RBO was an integral or peripheral membrane protein, the membrane fraction was treated with PBS, 0.1M $NaCO_3$ (pH 10), 1% NP–40, or 1.0 M NaCl for 30 min, then centrifuged at 30,000g for 30 min to generate supernatant and pellet, and both were subjected to SDS-page and western blot.

To test whether RBO is an integral membrane protein, S2 cells were transfected with V5–epitope–tagged RBO, cell surface proteins biotinylated at 4^{o}C with a membrane–impermeable version of biotin (1mM) and washed with buffers (TBS and 100 mM glycine). Membranes were treated with RIPA buffer containing complete protease inhibitors and spun (100,000g for 1 hr). The

supernatant was used for immunoprecipitation with V5 antibody. The immunocomplex was washed with RIPA buffer, and probed by Western blotting with either the V5 antibody or streptavidin conjugated to alkaline phosphatase.

Imaging and Immunocytochemistry

RBO–eGFP imaging was performed on *rbo* null mutant animals (rbo^2) rescued with *rbo–egfp* hybrid DNA using a BioRad Radiance 2000 laser confocal scanning system. In the embryo, all analyses were done on living animals. The larval CNS was treated with PBS–Triton–X100 (0.3%) for 30 min at room temperature (RT), followed by 20 min with RNAse A (0.025 µg/ml). Propidium iodide (1.25 µg/ml) for nuclear staining was applied for 30 min at RT. Adult heads were fixed in 4% paraformaldahyde for 2 hours at RT.

Electroretinogram Recording

A standard ERG recording configuration was used(Broadie, 2000). Briefly: Animals were anesthetized with CO_2 and then embedded in dental wax. A reference glass microelectrode filled with standard saline was inserted into the thorax. A recording glass microelectrode filled with 3M KCl was inserted into the center of the fly's eye. Animals were dark adapted for 5 min. Light was generated with a 1460X GE lamp, and controlled with a VMM–T1 shutter (UNIBLITZ). A HCC-100A temperature controller (DAGAN) was used to control temperature. The tip of the temperature probe was embedded in the wax.

Anoxia was induced by application of N_2 through a tube of 1.0 cm diameter that was mounted 0.5 cm over the animal.

Lipid Biochemistry

Assay of PIP, PIP_2 and Phosphatidic Acid Mass

PIP, PIP_2 and PA mass was determined by high performance thin layer chromatography (HPTLC) immunohistochemistry(Fukami et al., 1988). Animals were dark adapted for 30 min, and then placed at 25°C or 37°C in the light or dark for 5 min. Animals were frozen in liquid nitrogen, sieved heads pulverized, and homogenized in lysis buffer [chloroform:methanol:1M NaCl containing 2mM EDTA and EGTA (1:2:0.8, v/v)] (10 min at RT), chloroform and 1M NaCl, 2mM EDTA and EGTA were added, and the lower phase collected(Bligh and Dyer, 1959). The interface was re–extracted with lysis buffer containing 0.2M phosphoric acid. The pooled lower phases were dried and separated on HPTLC plates (Whatman LHPKD) with a standard curve using chloroform:acetone:methanol:acetic acid:water (46:17:15:14:8). The plate was treated with PBS containing 1% polyvinylpyrrolidone and 0.5% bovine serum albumin (PBS–PV–BSA), incubated with PIP and PIP_2 antibody (1:1000, Assay Designs, Inc) followed by alkaline phosphatase conjugated secondary and developed.

Assay of DAG Mass

Frozen adult heads were isolated as above, extracted similarly as above. This mixture was incubated, chloroform and 1M NaCl containing 2mM EDTA and EGTA were added, spun, re–extracted and the lower phases collected. The dried pooled lower phases were resuspended in chloroform and DAG levels were assayed based on an E. coli DAG kinase assay(Preiss et al., 1986). The washed products and standard curve were separated by HPTLC using chloroform:methanol:acetic acid (65:15:5). [^{32}P] incorporation was assayed with a Typhoon 9400 (Amersham).

Results

Mapping and identification of the *rolling blackout* (*rbo*) gene

Twenty years ago, an EMS–induced, TS paralytic mutant named *stambhaA*^{1} (*stmA*^{1}) was mapped to cytological region 42A8-19(Shyngle and Sharma, 1985). We found that *stmA*^{1} displays acute, TS blindness (see below), and set out to clone and characterize this gene. However, three genomic deficiencies of the 42A8-19 cytological region complemented *stmA*^{1}, suggesting that the original mapping was incorrect. Therefore, deficiencies of surrounding cytological regions were employed for remapping, and the mutant was mapped to 44D2-8 with three overlapping deficiencies (**Fig. 1a**), Kumar et al.(Kumar et al., 2001) also reported a remapping of *stmA* to 44D1-2.

Figure 1. Mapping, identification and genomic rescue of rolling blackout (rbo) gene; hydrophobicity and membrane association of RBO protein

TS and null *rbo* mutant alleles were mapped to cytological region 44D2-8 on the 2nd chromosome based on complementation failure with the indicated three genomic deficiencies. A small intragenic deficiency of the *cmp44E* gene, *rev499*, fails to complement *rbo* mutants, indicating that *rbo* is allelic to *cmp44E*. (**b**) The *rbo* gene and protein structures. The top shows the *rbo* genomic organization. The insertion site of eGFP coding sequence indicated in the *rbo* genomic sequence. The positions of two P-elements (rbo^{p1} and rbo^{p2}) insertions are in the first exon of the smaller *rbo* gene transcript. The bottom shows the two predicted alternatively spliced isoforms of RBO protein. Shaded bars indicate predicted transmembrane (TM) domains. The early stop codon mutation (Q396amber) in rbo^{3} and missense mutation (G487D) in rbo^{ts1} are indicated. (**c**) Hydrophobicity diagram of RBO protein generated by TMpred software; predicted transmembrane domains (minimum 17 aa, maximum 33 aa with positive hydrophobicity value) are indicated with arrows. (**d**) Subcellular location of RBO-eGFP fusion protein in extracts from adult brain. The protein (~117Kda) is strongly associated with the membrane fraction (T: total lysate, S: supernatant, and P: membrane pellet). Right, detergent NP-40 can release RBO from the membrane, but not high pH or high [salt]. (**e**) V5-tagged RBO expressed in S2 cells was labeled by cell surface biotinylation. Left shows the RBO-V5-His probed with V5 antibody; right shows biotin-labeled RBO-V5-His with streptavidin-conjugated alkaline phosphatase.

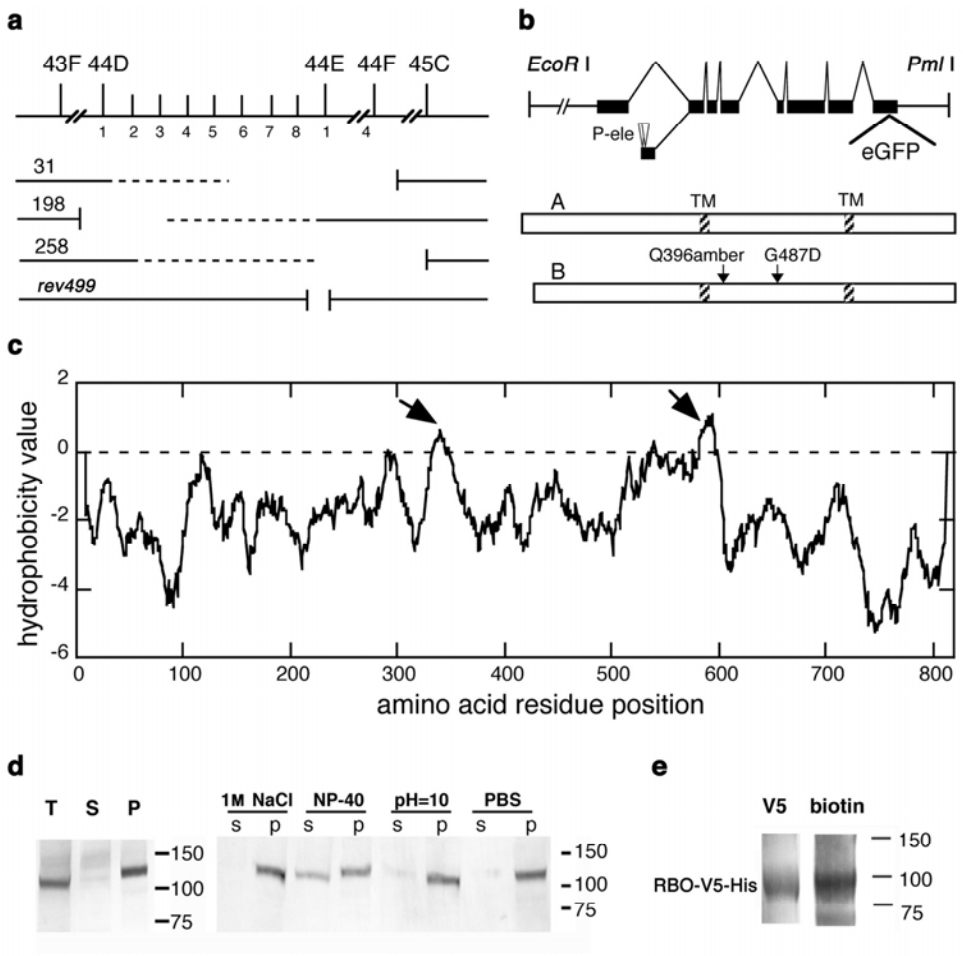

EMS–induced mutant alleles causing unconditional embryonic lethality failed to complement either the TS mutant or the deficiencies covering 44D2-8 (**table 1**). To transposon–tag the gene, two P–elements in 44D were independently mobilized (see Materials and Methods), and two new P–element insertion lines were isolated based on failure to complement both embryonic lethality and temperature–sensitivity of existing EMS mutants (**Fig. 1b**, and **table 1**). Inverse PCR cloning revealed that both P–element inserts are in the recently cloned gene *conserved membrane protein at 44E* (*cmp44E*) (**Fig. 1b**). This gene was

reported to encode a predicted transmembrane protein essential for cell viability(Faulkner et al., 1998).

Complementation tests between *stmA* and *cmp44E* mutants confirmed that both affect the same gene (**Table 1**). Subsequent sequencing of TS and EMS lethal alleles revealed a single missense (G487D), and nonsense (Q396amber) mutation, respectively (**Fig. 1b**). A single copy of wild-type genomic DNA fully rescued both TS defects and embryonic lethality of all homozygous and transheterozygous mutant alleles (**table 1**). Based on the distinctive phenotype of the conditional mutant, the single descriptive name *rolling blackout (rbo)* was adopted for this gene; rbo^{ts1} (TS allele), rbo^{P1} and rbo^{P2} (P-element insertion lines), rbo^{2} (genomic deficiency, *rev499*), rbo^{3} and rbo^{4} (EMS lethal mutations) (**table 1***)*.

Table 1. *stmA*, cmp44E and *rbo* mutants are the same gene
stmA, *cmp44E* and *rbo* mutants are allelic to each other, based on both lethality and conditional blindness complementation studies. " * " indicates phenotype was fully rescued by genomic *rbo-egfp* expression. A single naming strategy was adopted for all mutant alleles of the locus, as indicated. rbo^{ts1} = $stmA^{1}$, rbo^{2} = $cmp44E^{rev499}$, rbo^{3} = $stmA^{18.2}$, rbo^{4} = $cmp44E^{1}$.

	rbo^{ts1}	rbo^{2}	rbo^{3}	rbo^{4}	rbo^{p1}	rbo^{p2}
rbo^{ts1}	blind*	blind*	blind*	blind*	blind*	Blind*
rbo^{2}		lethal*	lethal*	Lethal	lethal*	lethal*
rbo^{3}			lethal	lethal*	lethal	lethal
rbo^{4}				Lethal	lethal	lethal
rbo^{p1}					lethal	lethal
rbo^{p1}						lethal

RBO pioneers a family of lipolytic enzymes

RBO homologs exist in species ranging from yeast to man (Faulkner et al., 1998). Sequence analysis of *Drosophila* RBO and its homologs in other species indicates conservation around three motifs characteristic of carboxyesterases/lipases (**Fig. 2**). These three motifs contain serine, aspartic acid and histidine residues, which form the enzymatic catalytic triad. Moreover, the characteristic lipase motif of the serine active site, Gly-X-Ser-X-Gly(Martinez et al., 1992), is found in RBO (**Fig. 2**). In addition, RBO displays homology to three known lipases 1) recently cloned human membrane–associated sn-1 DAG lipase (42% homology)(Bisogno et al., 2003), 2) rat triacylglycerol lipase (35%), and 3) fungal mono– and diacylglycerol lipases (25–30%). Taken together, these features suggest that RBO is a lipase.

RBO is an integral membrane protein

Hydrophobicity analysis of RBO predicts a 2– or 3–pass transmembrane protein (**Fig. 1c**)(Faulkner et al., 1998). In the 3–pass model, the N–terminus containing the histidine active site is outside the plasma membrane, while the C–terminus harboring the aspartic site is inside, rendering this model invalid. In contrast, both N– and C–termini are inside in the 2–pass model, placing the histidine and aspartic active sites on the same (internal) side of the membrane. The serine active site is located in the center of a transmembrane domain. Thus, only in the 2–pass model can the three active sites assemble to form the triad

catalytic center, indicating that RBO is likely a 2–pass transmembrane protein, but only if RBO is a lypolitic enzyme.

To test the prediction that RBO is a transmembrane protein, the subcellular location of RBO was assayed in fractionation experiments (**Fig. 1d**). The heads of animals expressing RBO–eGFP were homogenized, and soluble and membrane fractions generated. RBO–eGFP was found to be associated only with the membrane pellet fraction (**Fig. 1d,** left). The membrane fractions were next treated with agents that extract peripheral membrane proteins (high [salt] and basic pH) or integral membrane proteins (detergent NP-40). RBO protein was not appreciably disassociated from the membrane with high salt (1 M) or basic pH (pH = 10), but could be released by detergent (**Fig. 1d,** right). These results are consistent with the prediction that RBO is a transmembrane protein.

To further test whether RBO is a transmembrane protein, *Drosophila* S2 cells were transfected with a V5–epitope tagged RBO, after which all cell surface proteins were biotinylated with a cell membrane impermeable version of biotin. V5–tagged RBO expressed in S2 cells was biotinylated (**Fig. 1e**), showing that the protein must span the plasma membrane. Taken together, these results demonstrate that RBO is a transmembrane protein.

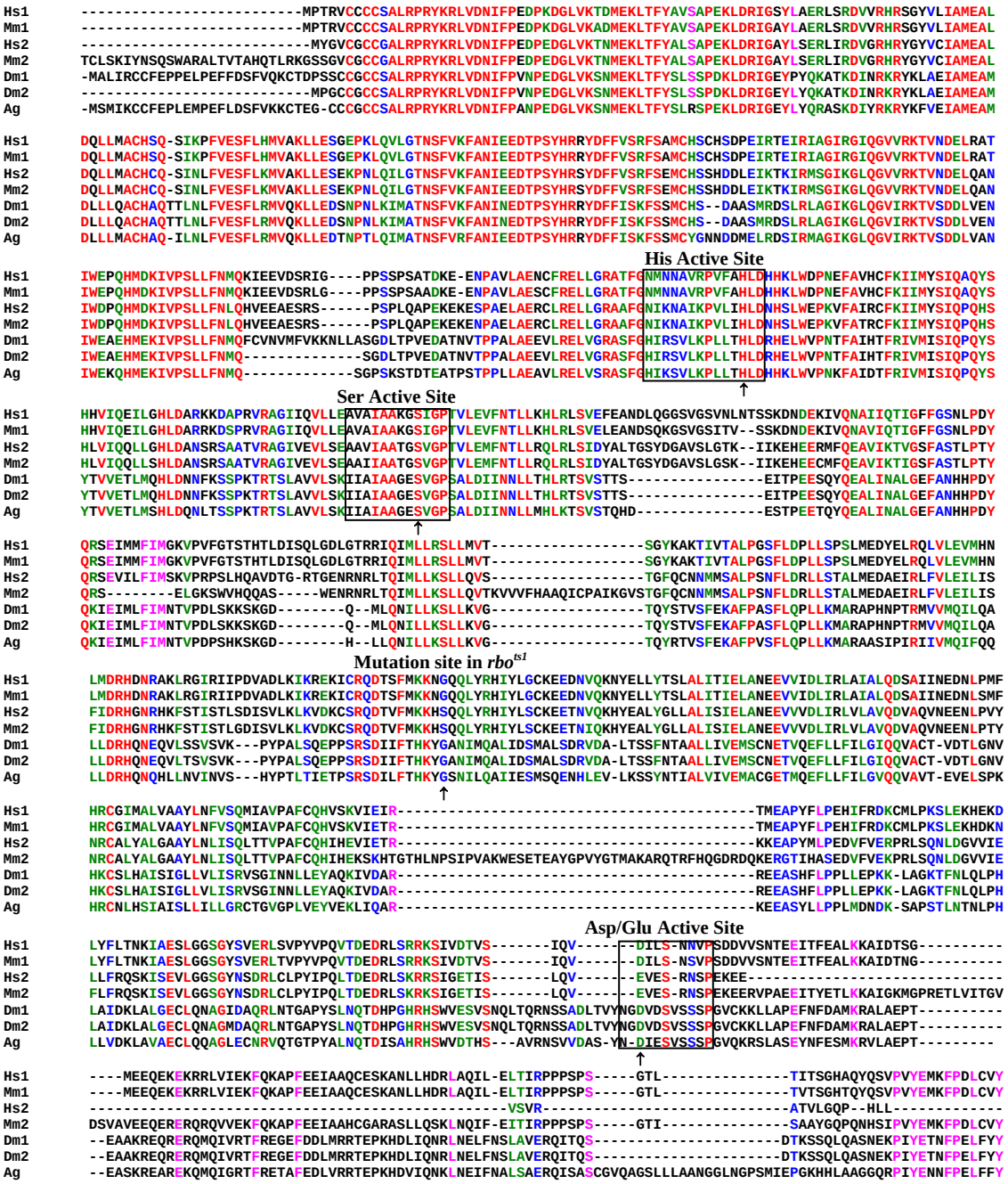

Figure 2. RBO is a predicted lipase

The RBO protein contains the domain structure of a lipolytic enzyme. Three highly-conserved lipase functional motifs (His, Ser and Asp/Glu active sites) contain the catalytic triad of His, Ser, and Asp/Glu residues, respectively. The consensus motif "GXSXG" is found in the Ser active site. The mutation site in *rbo*^{ts1} is indicated.

RBO is enriched in neuropil and photoreceptors

To study the expression of RBO, we generated transgenic lines expressing RBO–eGFP under native premotor of *rbo* regulation (**Fig. 1b**). RBO–eGFP fully rescues both TS blindness and lethality in all *rbo* mutant allelic combinations (**table 1**), demonstrating that the protein is properly expressed and functional. RBO–eGFP was expressed in the *rbo* null mutant background to assay protein expression throughout development from embryo to adult.

RBO is concentrated in the nervous system beginning during mid–embryogenesis and continuing in the mature animal (**Fig. 3**). During embryogenesis, RBO is first detected at stage 9 in the central neuropil of the developing ventral nerve cord (VNC (**Fig. 3a**). Throughout larval stages, the protein continues to remain enriched in the neuropil. In double-labeling experiments, (nuclei–red; **Fig. 3b,c**), RBO is undetectable in the cortical cell bodies, which is particularly obvious in the brain lobes (**Fig. 3c**). The RBO enrichment in neuronal processes is clearly observed in peripheral nerves penetrating the cortical somal layers to exit the VNC (**Fig. 3b,c** arrow).

In the adult, RBO remains enriched in the neuropils of thoracic ganglion and brain, but obviously absent from the cortical cell bodies (**Fig. 3d**). RBO is also enriched in the adult retina, in photoreceptor cells (**Fig. 3e**). Outside of the CNS, strong RBO expression occurs in many peripheral sensory neurons throughout development and in the adult (data not show). These observations suggest that RBO may function in multiple forms of sensory transduction, particularly phototransduction.

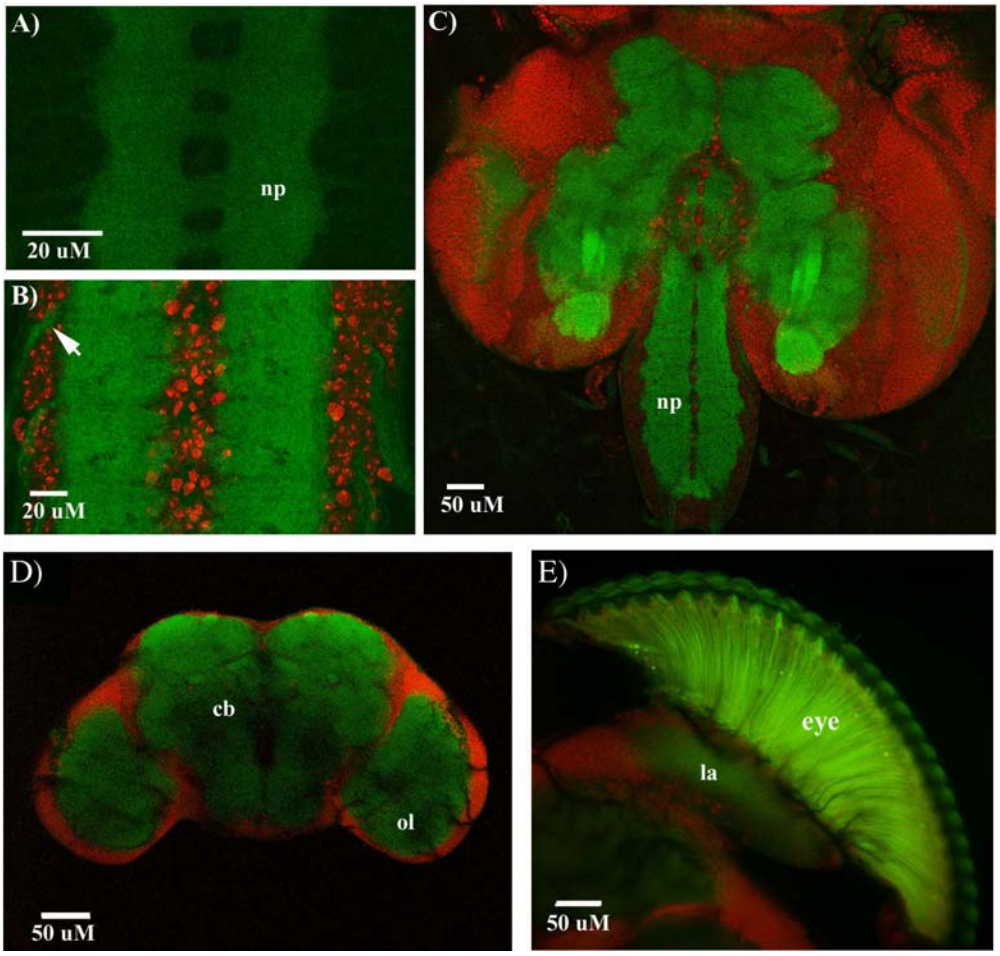

Figure 3. RBO protein is enriched in neuropil and photoreceptors
RBO-eGFP under native genomic control (green) in *rbo* null mutant (rbo^2/rbo^2). (**a**) From mid-embryogenesis, RBO is highly enriched in ventral nerve cord (VNC) neuropil (np). Two VNC segments in a stage 9 embryo are shown. (**b**) Similar VNC field from a wandering third instar larva stained with Propidium Iodide to reveal nuclei (red). RBO is abundant in the neuropil and axons exiting the VNC (arrow). (**c**) Entire larval CNS showing the two brain lobes and the VNC. RBO is abundant throughout the CNS neuropil, but excluded from the cortical neuronal cell bodies (nuclei, red). **d**. RBO expression in the adult brain. As throughout development, RBO is strikingly restricted throughout the neuropil, including the central body (cb) and optic lope (ol) neuropils, and excluded from neuronal cell bodies (nuclei, red). **e**. RBO expression in the adult visual system. Expression is seen in photoreceptors as well as in visual neuropil including the lamina (la).

RBO is required for phototransduction in an activity–dependent manner

Drosophila phototransduction was assayed by electroretinogram (ERG) recording(Hotta and Benzer, 1969; Pak et al., 1969). During a light stimulus, the ERG is composed of an initial rapid depolarization (amplitude 1, **Fig. 4a**) and a sustained depolarization (amplitude 2, **Fig. 4a**). At permissive temperature (25ºC), *rbo* TS mutants display normal light–induced ERG responses (**Fig. 4**). In contrast, at non–permissive temperature (37ºC), the ERG was completely eliminated, in either constant light (<1 minute) or during repetitive light flashes (**Fig. 4**). This complete blockade of phototransduction is due only to loss of *rbo* function, since the addition of a single copy of the wild-type genomic *rbo* gene fully restored the ERG (**Fig. 4a**). Interestingly, during the progressive loss of phototransduction, the ERG manifests a transient depolarization (**Fig. 4a**, at 2.5 minutes), similar to *transient receptor potential* (*trp*) mutants (see below). Quantification of ERG amplitudes show that *rbo* mutants display normal phototransduction at 25ºC, lack a detectable ERG at 37ºC, but that ERG amplitudes are fully restored by a single copy of wild-type *rbo* (**Fig. 4b**). These results demonstrate that RBO is acutely required for phototransduction.

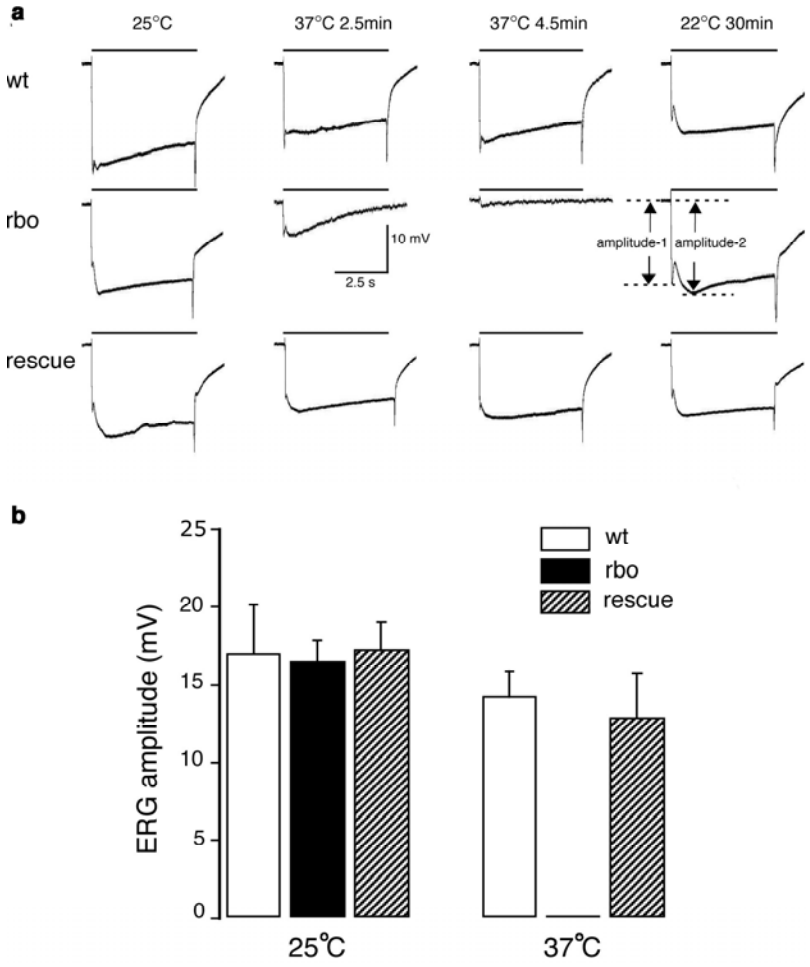

Figure 4. Block of phototransduction in *rbo* mutants
(**a**) Phototransduction is abolished at restrictive temperature (37°C) in TS *rbo* mutants. Representative electroretinogram (ERG) recordings from wild-type (*wt), rbo*^{ts1}/*rbo*^{2} mutant *(rbo)* and *rbo*^{ts1}/*rbo*^{2} mutant expressing a single copy of the *rbo-egfp* transgene (rescue) at the indicated times and temperatures. A light flash of 5 seconds (indicated by line) was given at regular interval of 25 seconds. Phototransduction in *rbo* mutants progressively decays over minutes, generating a *transient receptor potential* (*trp*) phenotype before the light-induced current is abolished (~4.5 minutes). This phototransduction block is fully reversible at permissive temperature. A single copy of *rbo-egfp* fully rescues the phototransduction block (bottom). (**b**) Quantification of ERG amplitudes in control (w^{118}), *rbo* mutant (*rbo*^{ts1}/*rbo*^{2}) and the transgenic rescue (*rbo*^{ts1}/*rbo*^{2} with a single copy of the *rbo-egfp* transgene). The ERG response was quantified by the measurement of amplitude-2 as shown in A. *n* = 5 for each. Error bars represent s.d.

By altering frequency and duration of light stimuli, the phototransduction block in *rbo* mutants was found to be activity–dependent (**Fig. 5**). At 37ºC, continuous light blocked phototransduction within 40 seconds, but repetitive one-second-light flashes at low frequency induced robust ERGs even after 30 mins at 37ºC. Repetitive one-second-light flashes separated by darkness of 20 seconds (*rbo* mutants at high frequency; *rbo–h*), caused block of phototransduction in <5 minutes (**Fig. 5a**). In contrast, repetitive one-second-light flashes separated by darkness of 3 minutes (*rbo* mutants at low frequency; *rbo–l*) allowed phototransduction to persist (**Fig. 5a**). Quantification of initial ERG depolarization (amplitude 1) showed that *rbo* mutants maintained normal amplitudes during low frequency light stimulation, indistinguishable from wild-type, whereas high frequency stimulation caused a block in <5 minutes (**Fig. 5b**, top). The sustained ERG depolarization (amplitude 2) was similarly unchanged compared to control during low frequency stimulation, whereas high frequency stimulation blocked the ERG (**Fig. 5b**, bottom). Note that longer-term stimulation at low frequency did cause a significant reduction in ERG amplitudes (~30% amplitude-1, ~70% amplitude 2; **Fig. 5b**). These results demonstrate an acute activity–dependent requirement for RBO in phototransduction.

When maintained in darkness for 3 minutes following complete suppression of phototransduction, *rbo* mutants displayed strong recovery (~80%) in ERG amplitude-1 but relatively weak recovery (~25%) in ERG amplitude-2, suggesting differential RBO–dependence of the initial and sustained phototransduction events (Fig. 5a–b, *rbo–m*). To study in detail the

Figure 5. Activity–dependent block of phototransduction in *rbo* mutants
Phototransduction block in *rbo* TS mutants is activity–dependent and recovers in the dark at restrictive temperature. (**a**) Representative traces show ERG recordings with repetitive 1-second light stimulation at 20 second intervals (high (h) frequency) in wild-type (*wt-h*) and *rbo* mutants (rbo^{ts1}/rbo^{2}*; rbo-h*), at 3 minute intervals (low (l) frequency) in mutants (*rbo-l*), and a mix of high/low frequency in the mutants (*rbo-m*). Lower traces show the simultaneously recorded temperature, in each case shifted from 25°C to 37°C as indicated. At the high frequency of light stimulation, phototransduction is abolished in *rbo* mutants within 5 minutes, whereas at the low frequency of light stimulation robust ERG responses persist. (**b**) Quantification of ERG amplitudes. The upper and lower panel shows the mean values of amplitude-1 and 2 respectively (shown in **Fig. 3a**). $n = 5$ in each case. Significance is indicated by "#" ($P < 0.05$) and "*" ($P < 0.01$). C. Recovery of ERG amplitudes following continuous light-induced total blockade. Effects of dark interval and temperature decrement on recovery of initial peak amplitude (1, left), sustained peak amplitude (2,middle) and amplitude at 10 seconds of illumination (3,right) at room temperature (RT) or 37°C, as indicated. $n = 5$ for each. Error bars represent s.d.

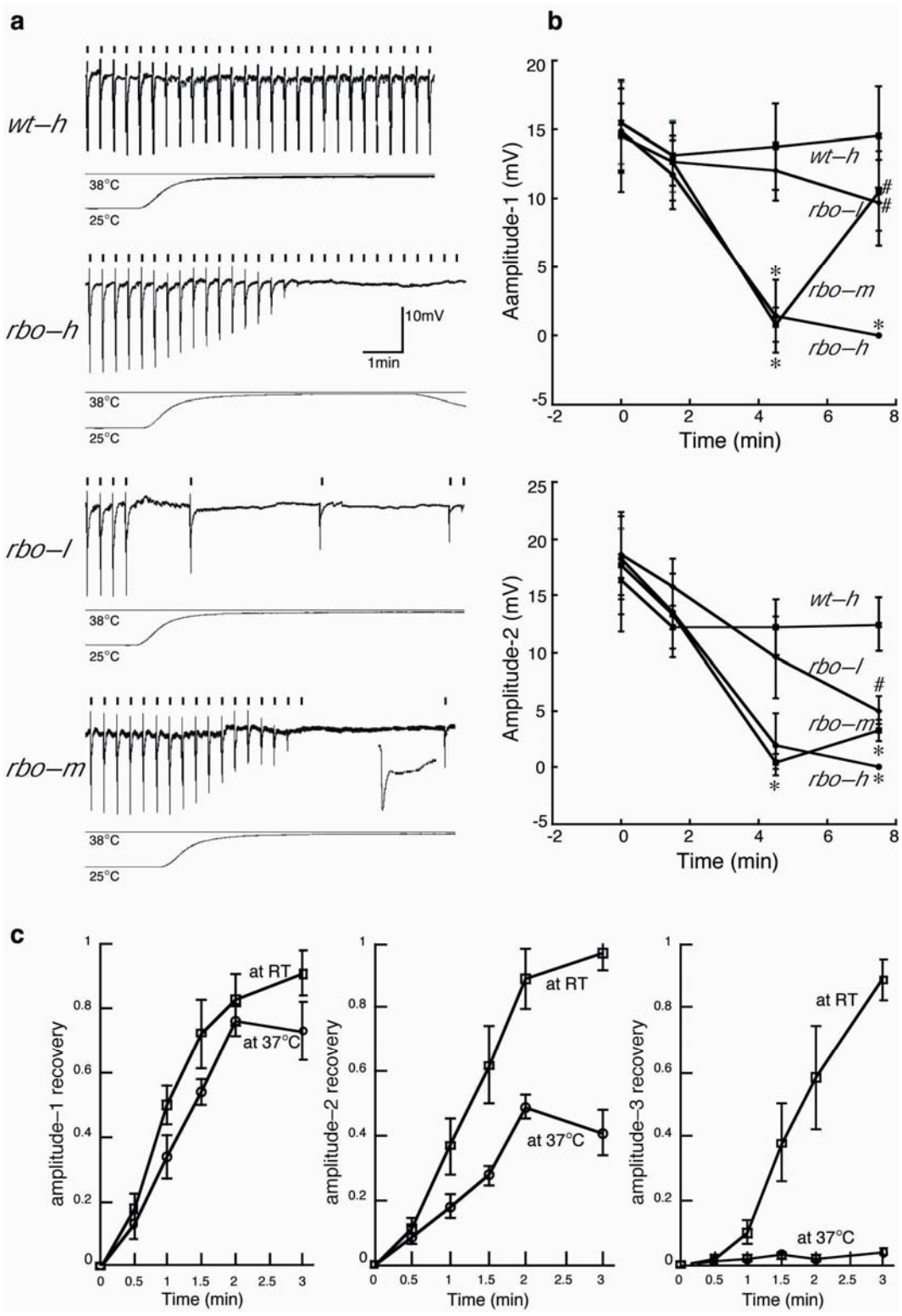
a
wt–h
38°C
25°C
rbo–h
10mV
1min
38°C
25°C
rbo–l
38°C
25°C
rbo–m
38°C
25°C
b
Aamplitude-1 (mV)
wt–h
rbo–l
rbo–m
rbo–h
Time (min)
Amplitude-2 (mV)
wt–h
rbo–l
rbo–m
rbo–h
Time (min)
c
amplitude–1 recovery
at RT
at 37°C
Time (min)
amplitude–2 recovery
at RT
at 37°C
Time (min)
amplitude–3 recovery
at RT
at 37°C
Time (min)

Figure 5

recovery of phototransduction in *rbo* mutants, continuous light at 37ºC was used to block phototransduction, then variable dark intervals were given before the next test light (**Fig. 5c**). Three ERG amplitudes were quantified: amplitude-1 (initial peak), 2 (sustained peak) and 3 (amplitude of sustained depolarization at 10 seconds). Recovery of both amplitude-1 and 2 was dark-interval-dependent, with amplitude 1 recovering faster and more completely, whereas amplitude-3 did not recover appreciable even after 3 minutes (**Fig. 5c**, right). When *rbo* mutants were returned to permissive temperature (25ºC) to restore RBO function, all 3 ERG amplitudes showed complete (>90%), dark-interval-dependent recovery within 3 minutes (data not shown). These results demonstrate that progressively sustained ERG depolarization is more dependent on RBO function.

RBO acts upstream TRP/TRPL channels

The loss of phototransduction current could be due either to a direct defect in TRP and TRPL channels, or to an upstream defect. In darkness, anoxia produces a rapid depolarization of photoreceptor cells that is largely dependent on the functional integrity of TRP and TRPL channels(Agam et al., 2000). Therefore, to test the integrity of TRP and TRPL channels, anoxia was produced in *rbo* mutants after phototransduction blockade at 37°C. Brief anoxia application produced a similar rapid depolarization in *rbo* mutants (15.9 ± 1.0 mV) and wild-type (16.8 ± 2.1 mV; **Fig. 6**). The amplitude of anoxia-induced depolarization in both *rbo* mutants and wild-type controls was twice that of

trpl^{302};*trp*^{343} double mutants (7.4 ± 1.5 mV, $P < 0.01$; **Fig. 6**). In addition to attenuated anoxia-response amplitudes, the response kinetics in *trpl;trp* mutants was much slower than in either *rbo* mutants or wild-type (**Fig. 6**)(Agam et al., 2000). These data suggest that normal TRP and TRPL channels persist in *rbo* mutants under conditions where phototransduction is abolished. Thus, the phototransduction block in *rbo* mutants maps to a defect upstream of TRP and TRPL channels.

Activation of TRP and TRPL channels is completely dependent on PLC (*norpA* gene). Reduced PLC activity is reflected by slowed ERG response kinetics, particularly the slope of the initial ERG depolarization(Pearn et al., 1996). ERG records from *rbo* mutants and controls were therefore quantified by measuring slope from lights on to 1/2 of amplitude-1 (Fig. 4a). Controls displayed a significantly ($P < 0.05$) increased slope as a function of temperature, from 1.43 ± 0.15 (25ºC) to 2.2 ± 0.18 mV/mS (37ºC) (Fig. 7), consistent with increased PLC activity at elevated temperatures(Juusola and Hardie, 2001). In contrast, the ERG slope in *rbo* mutants was significantly ($P < 0.01$) decreased during a 25ºC to 37ºC temperature shift, from 1.58 ± 0.18 to 0.45 ± 0.04 mV/mS, (Fig. 7). This observation suggests that PLC activity is inhibited by loss of RBO function.

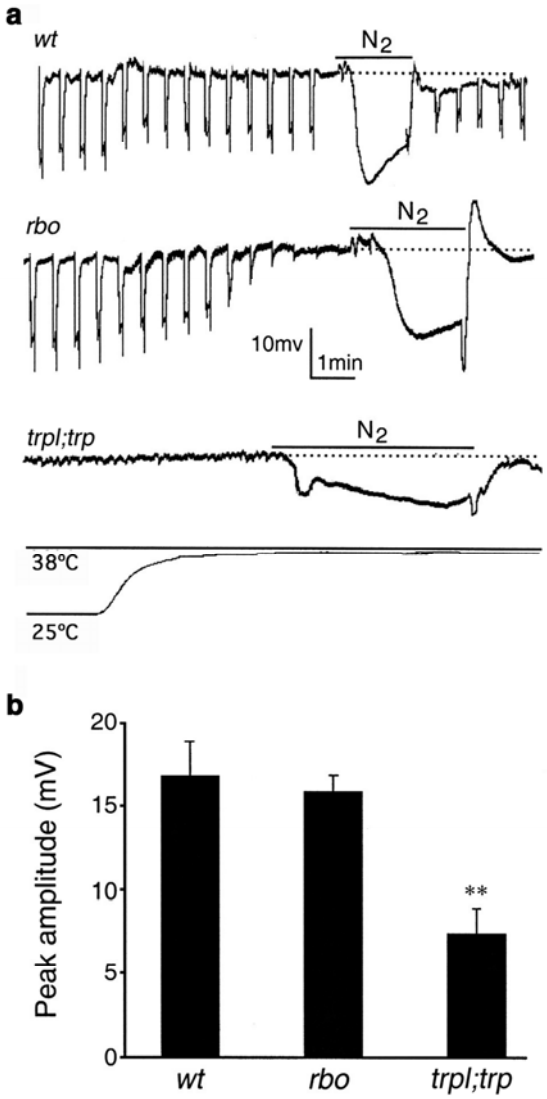

Figure 6. Sustained anoxia response in *rbo* mutants
(**a**) Representative anoxia-induced depolarization in wild-type (wt, top), rbo^{ts1}/rbo^{2} (*rbo*, middle) and *trpl;trp* double mutants (bottom) mutants. The 25-37ºC temperature shift was recorded simultaneously with repetitive 10 sec light flashes. Anoxia was induced by N_2 application as indicated. (**b**) Quantification of anoxia-induced depolarization amplitude. The peak amplitude of wt and *rbo* mutants are similar, but highly significantly ($p < 0.01$, **) greater than *trpl;trp* mutants. = 5 for each. Error bars represent s.e.m.

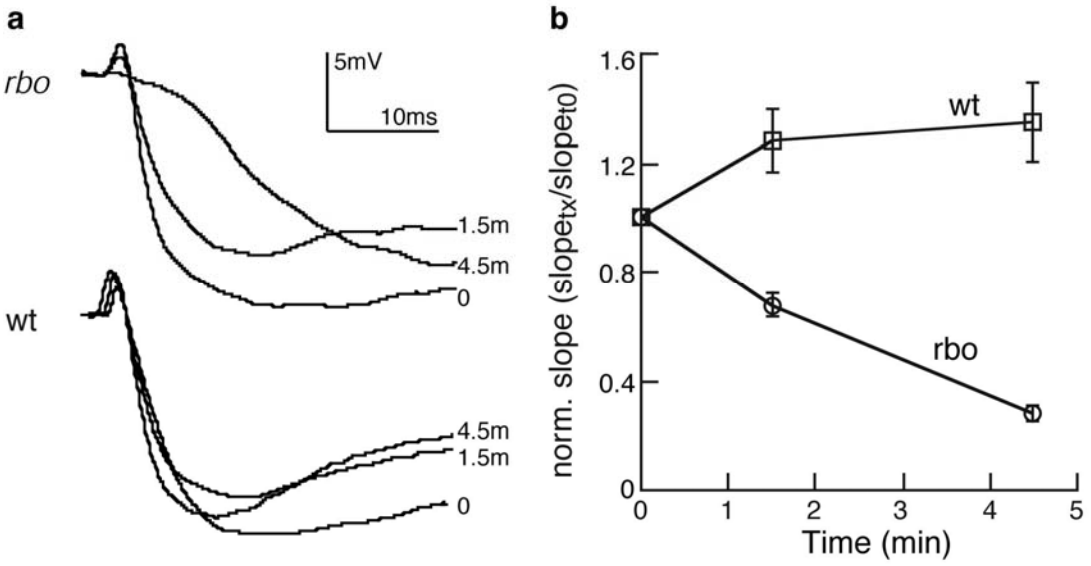

Figure 7. Reduction in the slope of initial ERG response in *rbo* mutants
(a) Representative ERG traces in *rbo*^{ts1}/*rbo*^{2} mutants (*rbo*, top) and wild-type (wt, bottom) at 0, 1.5 min and 4.5 min after a temperature shift from 25ºC to 37ºC. Note that the temperature elevation caused a slightly increased depolarization rate in wild-type, but the depolarization rate was rapidly decreased in *rbo* mutants. b. Normalization plot of the slope of initial ERG depolarization as a function of time at 37ºC. n = 5 for each. Error bars represent s.e.m.

Misregulation of PIP/PIP$_2$ and DAG levels in *rbo* mutants

The above studies show that RBO is essential in an activity-limited phototransduction mechanism, upstream of TRP and TRPL channels. The nature of the phototransduction block is most consistent with disruption of PLC activity, or in the PLC–dependent lipid signaling cascade leading to TRP and TRPL channel activation. To test this hypothesis, PIP$_2$ pathway lipids (PIP, PIP$_2$, DAG and PA) were assayed in *rbo* mutant and wild-type (WT) heads at 25ºC and 37ºC, in conditions of constant light (active state) or constant darkness (resting state).

PIP, PIP_2 and phosphatidic acid (PA) were assayed by immunostaining of high performance thin layer chromatography (HPTLC) plates (Fig. 8). At 25ºC, under either light or dark conditions, there was no detectable difference in the levels of PIP, PIP_2, or PA between *rbo* mutants and wild-type (Fig. 8). At 37ºC, both PIP and PIP_2 were elevated relative to wild-type. Analysis of PIP levels showed a highly significant elevation in *rbo* mutants in both light (1.97 $\pm$ 0.13 *rbo* vs. 0.8 $\pm$ 0.05 pmol in WT) and dark (1.6 $\pm$ 0.07 *rbo* vs. 1.0 $\pm$ 0.09 in WT; Fig. 8a). As expected by PIP_2 consumption in light, the level of PIP_2 in wild-type was strongly reduced by shifting from dark (2.34 $\pm$ 0.09) to light (1.3 $\pm$ 0.13 pmol), whereas no change at all occurred in the *rbo* mutant (1.7 $\pm$ 0.07 dark vs. 1.85 $\pm$ 0.16, light; Fig. 8b). This defect strongly suggests a block in light-activated PLC activity in *rbo* mutants. As a consequence, PIP_2 levels are significantly elevated in *rbo* mutants in the light, under conditions that block phototransduction (Fig. 8b). PA abundance appeared comparable between wild-type and *rbo* mutants under all conditions (Fig. 8c). This observation is consistent with the fact that the level of PA is independent of PLC activity(Yoshioka et al., 1985).

Figure 8.Activity–dependent elevation of PIP/PIP2 levels in *rbo* mutants
Wildtype (WT) or *rbo*^{ts1}/*rbo*^{2} mutant *(rbo)* animals were placed in either the light (open bars) or dark (black bars) at either permissive (25ºC) or restrictive (37ºC) temperatures for eight minutes, then quick frozen in liquid nitrogen and the heads analyzed for PIP (**a**), PIP_2 (**b**) or PA (**c**). Lipid mass (pmol) was determined by comparison of standard curves. Significance as indicated; $P < 0.05$ (*), $P < 0.01$ (**), $P < 0.001$ (***). Error bars represent s.e.m.

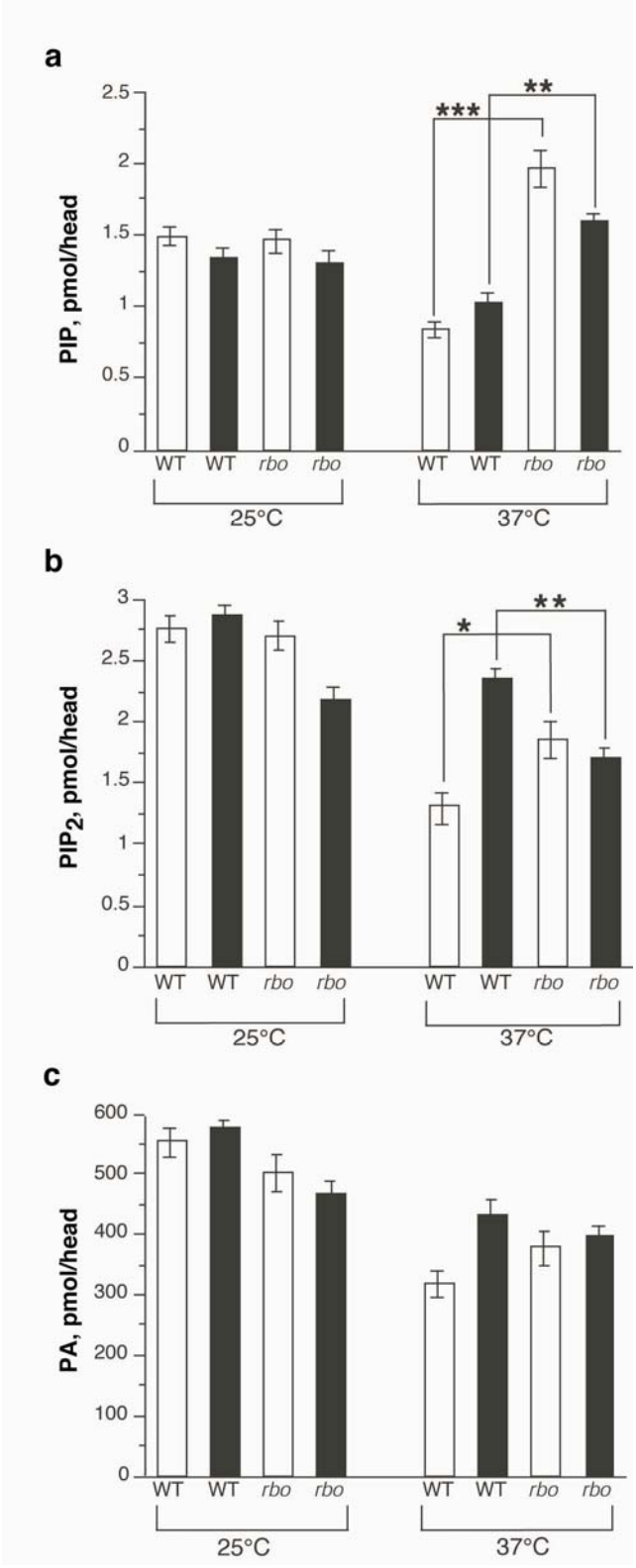
a
PIP, pmol/head
2.5
2
1.5
1
0.5
0
***
**
WT WT rbo rbo WT WT rbo rbo
25°C
37°C
b
PIP2, pmol/head
3
2.5
2
1.5
1
0.5
0
*
**
WT WT rbo rbo WT WT rbo rbo
25°C
37°C
c
PA, pmol/head
600
500
400
300
200
100
0
WT WT rbo rbo WT WT rbo rbo
25°C
37°C

The level of DAG was assayed using the DAG kinase detection method(Preiss et al., 1986) (**Fig. 9**). The most striking finding was reduction of DAG levels in the absence of RBO function and in the light (**Fig. 9**). In wild-type, DAG levels increased at 37ºC, consistent with the effect of elevated temperature to increase PLC activity(Juusola and Hardie, 2001). In contrast, in *rbo* mutants at 37ºC, the level of DAG was reduced 2 fold compared to wild-type (WT = 200 ± 10.9 pmol, *rbo* = 97 ± 4.1 pmol; **Fig. 9b**). In the dark, wild-type showed lower DAG levels. In contrast, in *rbo* mutants the level of DAG in the dark and light was the same, consistent with a failure to activate PLC in the mutants (**Fig. 9b**). Note that DAG levels in the mutant in the light are indistinguishable from wild-type in the dark, suggesting a complete failure of light-dependent PLC activity. In the dark, DAG levels were comparable in *rbo* mutants and controls (WT = 78.7 ± 3.6 pmol, *rbo* = 69.3 ± 4.0 pmol; **Fig. 9b**). There was a ~50% increase in DAG levels in the mutant compared to wild-type in both light and dark conditions at 25ºC (**Fig. 9b**). The significance of this DAG elevation under conditions in which phototransduction is not detectably altered is unclear. Taken together, these data show that the RBO–dependent mechanism modifies PIP_2–DAG signaling, consistent with disruption of PLC activity.

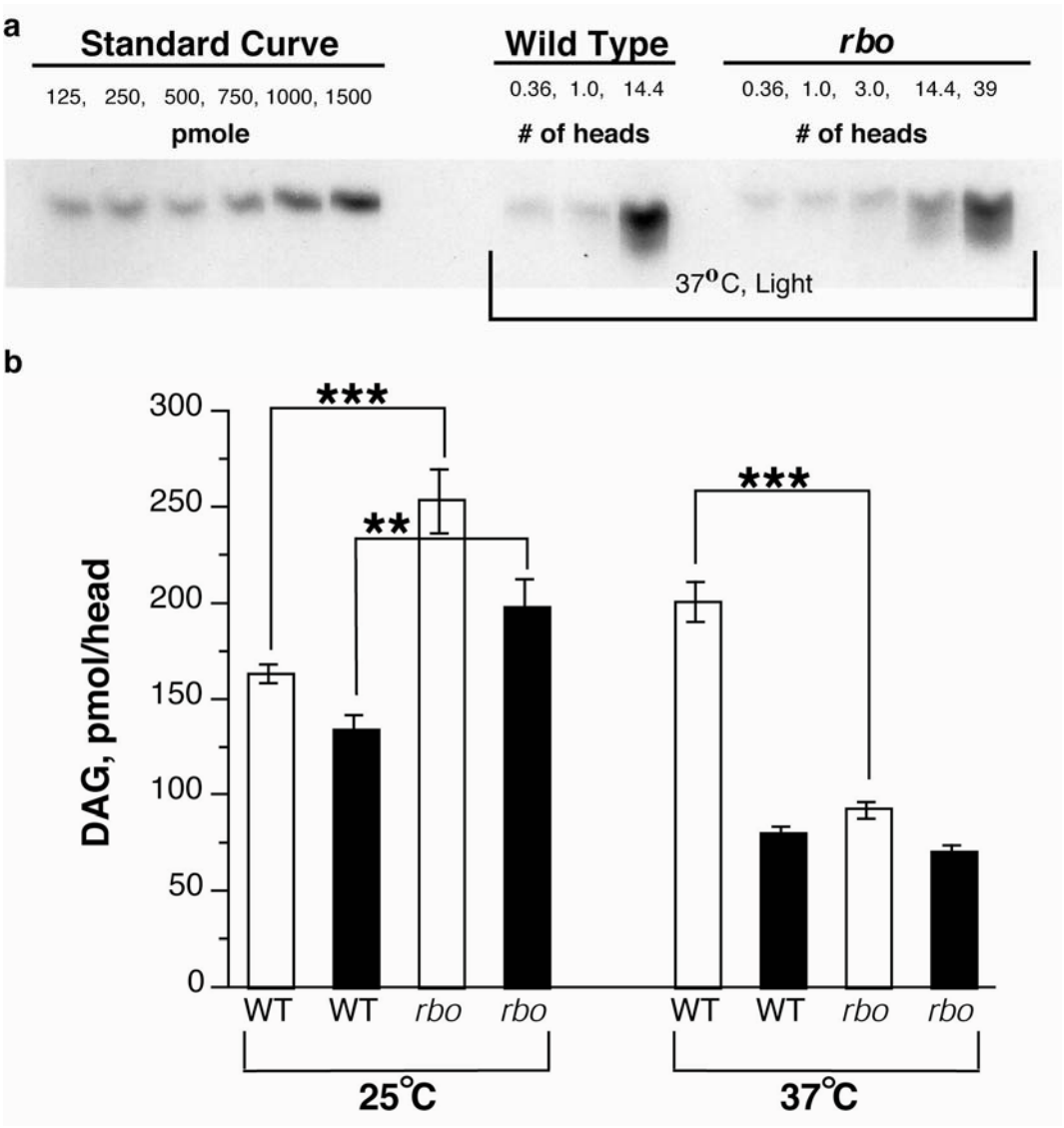

Figure 9. Activity-dependent depletion of DAG levels in *rbo* mutants
Wildtype (WT) or *rbo*^{ts1}/*rbo*^{2} mutant *(rbo)* animals were placed in either the light (open bars) or dark (black bars) at either permissive (25ºC) or restrictive (37ºC) temperatures for eight minutes, then quick frozen in liquid nitrogen and the heads analyzed for diacylglycerol (DAG) levels. (**a**) Representative example of a HPTLC showing a standard curve (left) relative to head samples from wildtype and *rbo* mutants in constant light at 37ºC. Note the loss of DAG in mutants relative to control. (**b**) Quantification of DAG levels under all conditions. Significance as indicated; $P < 0.01$ (**), $P < 0.001$ (***). Error bars represent s.e.m.

Discussion

Chromosomal deficiency mapping, transposon mutageneses and cloning, mutant genomic DNA sequencing, and genomic DNA rescue of mutant phenotypes, combine to demonstrate that the *rolling blackout* (*rbo*) gene is allelic to both *stampha A* (*stmA*)(Shyngle and Sharma, 1985; Kumar et al., 2001), and *conserved membrane protein at 44E* (*cmp44E*)(Faulkner et al., 1998). Hydrophobicity analysis, membrane fractionation and disassociation studies, and surface biotinylation assays show that RBO is an integral plasma membrane protein. RBO pioneers a new protein family with a serine/aspartate/histidine catalytic triad, and homology to known DAG lipases. RBO is enriched in the nervous system, apparently in all neurons, where it is subcellularly restricted to neuropil and in sensory neurons, including photoreceptors. Null *rbo* mutants are embryonic lethal, showing that RBO has an essential function. TS *rbo* mutants display a complete block of phototransduction, showing that RBO has a function acutely required in G–protein–coupled PLC signaling activation of TRP and TRPL channels. The accumulation of PIP/PIP_2 and depletion of DAG following conditional block of RBO function, suggest that RBO is required for PLC activity.

The activity–dependent requirement for RBO in phototransduction

Drosophila phototransduction involves PLC_{β}–dependent opening of TRP and TRPL channels(Montell, 1999; Hardie, 2001; Hardie and Raghu, 2001;

Hilgemann et al., 2001; Hardie, 2003). Conditional removal of RBO function blocks this signaling pathway completely in less than a minute under constant stimulation. The widespread expression of RBO, and its essential role in the embryo, argue that the protein is not required in a photoreceptor-specific mechanism (*e.g*. rhodopsin function). Likewise, the persistence of normal anoxia–induced depolarization under conditions where phototransduction is blocked, indicates that RBO is not required for the functional integrity of TRP and TRPL channels(Agam et al., 2000). Thus, RBO function maps between light–activated rhodopsin and the phototransduction channels; to the PLC_{β} cascade. The conditional nature of the phototransduction block, and the persistence of normal PLC activity isolated from *rbo* mutant head extracts, show that RBO is not required for PLC expression or function *per se*. Therefore, RBO appears to be required for PLC activation *in vivo*.

Two lines of evidence suggest acute block of PLC activity in *rbo* mutants. First, *rbo* mutants show rapid depletion of DAG and concomitant accumulation of PIP/PIP_2. In the absence of RBO function, the level of PIP_2 does not change with light stimulation, suggesting a complete absence of light–activated PLC cleavage of PIP_2. Likewise, the PLC product (DAG) is not elevated by light stimulation in the absence of RBO function. These results suggest that loss of RBO function may equate to loss of PLC function. A caveat of these total head lipid analyses is that *rbo* mutants block all light–activated neuronal signaling, and this could potentially cause indirect alterations in lipid metabolism. The second line of evidence is that the loss of RBO function causes a dramatic

reduction in the slope of the initial photoreceptor depolarization, which correlates with reductions in PLC activity(Pearn et al., 1996). Taken together, these results suggest that RBO may be required for regulation of PLC_{β} in photoreceptors.

RBO is required in a strictly activity–dependent manner. Only under conditions of high signaling demand (constant light, or rapid light flashes) does loss of RBO function result in complete block of phototransduction signaling. Removing the demands of light–activated signaling restores phototransduction in the absence of RBO function. Activity–dependent phototransduction block in other mutants has been linked to light–dependent exhaustion of limiting signaling factors(Minke and Selinger, 1991; Wu et al., 1995; Hardie et al., 2001). For example, mutation of CDP–diacylglycerol synthase (*cds*) causes activity–dependent phototransduction block because it is required for regeneration of PIP_2 from phosphatidic acid(Wu et al., 1995). Similarly, the activity–dependent phototransduction block in *rbo* mutants must be due to exhaustion of a critical RBO–dependent factor. The rapid decay of sustained photoreceptor depolarization in *rbo* mutants indicates that this factor is consumed during sustained light activation. The dark–interval–dependent recovery of phototransduction at restrictive temperature may indicate a secondary pathway to regenerate this factor, which is rate–limiting in the absence of RBO function due to rapid, light–activated consumption. A caveat to this conclusion is that the "secondary pathway" may simply be that TS mutant doesn't produce the complete null condition. We conclude that RBO is required to sustain

phototransduction but is not directly involved in the activation of TRP and TRPL channels.

Activation of TRP/TRPL channels and RBO function

The mechanism by which TRP and TRPL channels are activated during *Drosophila* phototransduction remains hotly debated, but there is a clear consensus that channel activation depends absolutely on PLC_{β}. Interest has focused on DAG, as a direct activator, or DAG hydrolysis products (PUFAs) as secondary activators of TRP and TRPL channels(Chyb et al., 1999; Hardie, 2001; Hardie and Raghu, 2001; Hardie, 2003). The fact that a characterized protein with over 40% similarity to RBO is a DAG lipase(Bisogno et al., 2003), immediately suggests the model that RBO–mediated hydrolysis of DAG might produce the putative PUFA trigger signal. However, the amino acid identity between RBO and sn–1 DAG lipase is low (12%), and RBO clearly belongs to a separate lipase family that does not as yet include known DAG lipases. Moreover, conditional removal of RBO results in rapid depletion of DAG, which is the opposite result to that predicted for a DAG lipase mutant. Finally, given the activity–dependent nature of the *rbo* phototransduction block, as discussed above, it does not seem probable that RBO could play any direct role in TRP and TRPL channel activation. Thus, the data do not support the hypothesis that RBO acts as a DAG lipase producing PUFAs that directly gate the phototransduction channels.

Acting as a DAG lipase, RBO might acutely regulate phototransduction via a mechanism that does not involve direct gating of the TRP and TRPL channels. Similar to *rbo* mutants, mouse DAG kinase ε mutants(Rodriguez de Turco et al., 2001) and *Drosophila rdgA* (encodes eye–specific DAG kinase) mutants(Yoshioka et al., 1984) fail to accumulate DAG, as would be predicted by the enzymatic function of their products. Indeed, the mouse mutants display DAG depletion, similar to *rbo* mutants. Moreover, PLC activity in *rdgA* mutants is reduced(Yoshioka et al., 1984; Inoue et al., 1989), and down–regulation of PLC activity was similarly suggested in the mouse mutants(Rodriguez de Turco et al., 2001). These observations suggest positive feedback loops, by which products downstream of DAG feedback to upregulate PLC activity. In the absence of this feedback, in DAG kinase mutants or, by analogy, DAG lipase mutants, PLC activity would be downregulated, resulting in accumulation of PIP_2 and loss of DAG. Moreover, disruption of such a feedback loop would be secondary to depletion of the signaling intermediates, and therefore it would take time for PLC downregulation to be manifested. All of these conclusions fit nicely with the observed phenotypes of *rbo* mutants. Thus, RBO could be a DAG lipase, as suggested by closest homology, but rather than act to produce excitatory PUFAs that directly gate TRP and TRPL channels, it may act instead as a positive regulator of PLC activity.

In summary, RBO is identified as an integral plasma membrane lipase that is essential for PLC_β–mediated phototransduction. In the absence of RBO function, the PLC–PIP_2 signaling pathway acutely arrests in an activity–

dependent manner. Multiple aspects of the *rbo* mutant phenotype are consistent with the hypothesis that RBO function is required for PLC_{β} function. We therefore propose that RBO acts as a novel positive regulator of PLC_{β} during G–protein coupled, inositol phospholipid signaling.

CHAPTER III

ROLLING BLACKOUT IS REQUIRED FOR SYNAPTIC VESICLE EXOCYTOSIS

Abstract

Rolling Blackout (RBO) is a putative transmembrane lipase required for PLC-dependent PIP_2-DAG signaling in *Drosophila* neurons. Conditional temperature-sensitive (TS) *rbo* mutants display complete, reversible paralysis within minutes, demonstrating that RBO is acutely required for movement. RBO protein is predominantly localized in presynaptic boutons at NMJ synapses, and throughout central synaptic neuropil, and *rbo* TS mutants display a complete, reversible block of both central and peripheral synaptic transmission within minutes. Electron microscopy reveals an increase in total synaptic vesicle (SV) content in *rbo* TS mutants, with a concomitant shrinkage of presynaptic bouton size, and an accumulation of docked SVs at presynaptic active zones within minutes. Genetic interaction tests reveal a synergistic interaction between *rbo* and *syntaxin1A* TS mutants, suggesting that RBO is required in the mechanism of SNARE-mediated SV exocytosis, or in a parallel pathway necessary for SV fusion. The *rbo* TS mutation does not detectably alter SNARE complex assembly, suggesting a downstream requirement in SV fusion. We conclude that RBO plays an essential role in neurotransmitter release, downstream of SV docking, likely mediating SV fusion.

Introduction

Drosophila temperature-sensitive (TS) paralytic mutants have long proven to be critical tools for the discovery and elucidation of molecular mechanisms of neurotransmission. These mutants have identified numerous classes of proteins acutely required in neuronal signaling, most prominently including ion channels (e.g. *paralytic*, Na^+ channel subunit (Loughney et al., 1989), and *cacophony*, Ca^{2+} channel subunit (Kawasaki et al., 2000)) and components of the synaptic vesicle (SV) cycle (e.g. *shibire*, a dynamin GTPase (van der Bliek and Meyerowitz, 1991), and *comatose*, N-ethylmaleimide-sensitive fusion (NSF) factor (Ordway et al., 1994)), among others (Littleton et al., 1998; Rao et al., 2001). Such conditional mutants are particularly valuable because they provide the opportunity to study neurotransmission when gene product function is acutely removed, and thus bypass any requirement in cell viability or development. Perhaps the most seminal example of this approach has been the isolation and characterization of the *shibire* TS mutant, which first revealed the essential requirement of Dynamin GTPase in SV endocytosis (Koenig et al., 1983; Koenig and Ikeda, 1996; Kidokoro et al., 2004). We report here a new TS paralytic mutant, *rolling blackout* (*rbo*), which similarly reveals a novel mechanism essential for SV exocytosis.

Dissection of the molecular mechanisms of the SV cycle particularly benefits from the study of TS mutants, which provide tools to temporally dissect the interlocked pathways of SV exocytosis and endocytosis. The exocytosis

pathway can be further subdivided into SV trafficking, tethering, docking, priming and fusion at the presynaptic active zone (AZ). During the terminal stages of SV exocytosis, the priming step involves activation of SNARE proteins via UNC-13 mediated opening of Syntaxin, and the assembly of the SNARE complex, which pulls the SV into close proximity to AZ plasma membrane to make the SV competent for Ca^{2+}-triggered fusion (Jahn and Sudhof, 1999; Lin and Scheller, 2000; Sudhof, 2004). The fusion step itself requires regulated fusion pore opening and expansion. The SNARE complex is sufficient for *in vitro* liposome fusion (Weber et al., 1998), but physiological SV fusion involves other proteins/lipids acting as facilitory cofactors (Weber et al., 1998; Jahn and Sudhof, 1999; Lin and Scheller, 2000; Sudhof, 2004; Tucker et al., 2004). Indeed, a separate fusion machinery complex may act downstream of SNARE complex assembly. The actions of V_0-ATPase, protein phosphatase 1, and Vtc3p, among others, have been mapped subsequent of trans-SNARE pairing, and may mediate SV fusion downstream of SNAREs (Peters et al., 1999; Peters et al., 2001; Muller et al., 2002; Bayer et al., 2003; Hiesinger et al., 2005). In addition to such putative fusogenic proteins, regulatory lipids such as diacylglycerol (DAG) and phosphatidylinositides (e.g. PIP_2) play critical roles in exocytosis by regulating the trafficking/activation of fusogenic proteins, and by directly altering membrane physical properties critical for SV fusion (Goni and Alonso, 1999; Peters et al., 1999; Cremona and De Camilli, 2001; Martin, 2001; Brose and Rosenmund, 2002; Di Paolo et al., 2004; Fratti et al., 2004; Jun et al., 2004; Wenk and De Camilli, 2004; Rohrbough and Broadie, 2005).

We reported previously (Huang et al., 2004) that *rbo* encodes an integral plasma membrane lipolytic enzyme that has an essential role in phospholipase C (PLC)-dependent PIP_2/DAG signaling during *Drosophila* phototransduction (Hardie, 2003; Huang et al., 2004). Here, we show that RBO protein is localized to presynaptic boutons, and that conditional *rbo* mutants are TS paralytic within minutes. At restrictive temperature, *rbo* TS mutants display a complete, reversible block of synaptic transmission, accumulate docked SVs at the presynaptic active zone, and display a strong synergistic genetic interaction with *syntaxin* mutants. These data indicate that RBO has an acute, essential role in SV exocytosis, and that RBO likely acts in the Syntaxin-dependent mechanism of SV priming/fusion, or in a parallel pathway.

Experimental Procedures

Genetics

Drosophila stocks were cultured on standard medium and entrained to a 12:12 light:dark cycle at 25°C. The wildtype (wt) strain Oregon-R (OR) and w^{1118} were used as controls. rbo^{ts1} contains a G487D missense mutation, rbo^{2} is a complete deletion null allele, rbo^{3} contains an early stop codon (Q396amber), df(2R)H3D3 is a deficiency with break points: 044D01-04;044F04-05, rbo^{2}/rbo^{2}; *rbo-egfp/rbo-egfp* is the transgenic rescue stock (Huang et al., 2004). The following TS paralytic mutant stocks were used; *cacophony* (cac^{ts2}; (Dellinger et al., 2000)), *comatose* ($comt^{ts17}$, com^{ts53}) kindly provided by Richard Ordway,

syntaxin1A (*syx*$^{3-69}$; (Littleton et al., 1998)) and *shibire* (*shibire*^{ts1}) kindly provided by Barry Ganetzky.

Behavioral Assays

For each genotype, 20 males and 20 females were tested. In each session, adult flies were transferred into a pre-warmed transparent plastic tube and placed at the indicated temperature in a hybridization oven (HO6000V, Genemate). Animals were observed continuously and the paralysis time point for each individual recorded. Paralysis was defined when an animal was inverted and immobile at the bottom of the tube, lacking any detectable leg movement. Paralyzed animals were transferred to room temperature to assay recovery time. The recovery time point was recorded when each animal achieved a standing position, and could walk when provoked. The veratridine (Sigma) resistance assay was done as described (Chandrashekaran, 1993) with slight modification: equal numbers of male and female flies were used, with assays done at 18°C, 22°C, and 28°C. Each genotype was introduced separately into vials with a 1.5 cm disc of filter paper containing 100 µg veratridine in 2% sugar. Animals were counted at 2, 4, 8, and 24 hrs.

Immunocytochemistry

RBO-eGFP imaging was performed on transgenic rescue flies (*rbo*^{2}*/rbo*^{2}*; rbo-egfp/rbo-egfp*), the expression of RBO-eGFP protein is under the control of the endogenous promoter of *rbo* gene (Huang et al., 2004). For

immunocytochemistry, dissected preparations were fixed in 4% paraformaldahyde in PBS at RT for 25 min (larvae) and 45 min (adults). Preparations were incubated in the following antibodies for 2 hrs at RT: anti-Discs Large (DLG; 1:1,000; rabbit; from Vivian Budnik), anti-Cysteine String Protein (CSP; 1:500; mouse; from Konrad Zinsmaier), anti-Synaptotagmin (1:1000; rabbit; from Hugo Bellen), and texas-red conjugated anti-HRP (1:300; goat; Jackson ImmunoResearch). Preparations were incubated for 1 hr at RT with secondary antibodies (1:1000; Molecular Probes). Images were captured on a BioRad Radiance 2000 or Zeiss LSM 510 Meta confocal system.

Electrophysiology

Excitatory junctional potential recording in Giant Fiber system

An adult fly anesthetized by CO_2 was mounted ventral side down on a glass cover slip with dental soft wax under a dissection microscope. A HCC-100A Temperature Controller (DAGAN) was used for temperature control. The tip of the temperature probe was embedded in the wax; it took ~2 min to increase temperature from 25°C to 37°C. The output from the temperature controller was transited for simultaneous recording of temperature and electrical signals. A glass reference electrode was inserted into the abdomen, and a glass stimulating electrode was inserted into each eye (Pavlidis and Tanouye, 1995). A glass recording electrode (3 MΩ) was driven through the dorsal thorax cuticle. Intracellular penetration into the muscle was monitored by a sudden potential drop of 40-60 mV. The muscle identity (DLM vs. TTM) was determined by

electrode placement and verified by recorded latency time. Signals were amplified by IX1 intracellular preamplifier (Dagan) and digitized at 100 KHz by Digidata 1200 or 1322A (Axon Instruments). Data was collected and analyzed with pCLAMP software (V8.0, Axon Instruments). All glass electrodes were filled with 3M KCl.

Excitatory junctional current recording in DLM muscle cells

An adult fly was laterally mounted over an opening of a parafilm tube and secured with soft dental wax so that air was accessible to the animal. The overlying cuticle and muscles were dissected away to expose one set of DLM cells in Ca^{2+}-free saline consisting of (in mM): 128 NaCl, 2 KCl, 4 $MgCl_2$, 5 HEPES, and 36 sucrose. The dissection saline was then replaced with 1.8 mM $CaCl_2$ recording saline, perfused at 0.3-0.4 ml/min. The posterior dorsal mesothoracic nerve carrying the DLMn axons was cut and sucked into a glass stimulation pipette (Koenig et al., 1983). Two glass microelectrodes (~10 MΩ) filled with 3 M KCl were inserted in the DLMe or d cell. The DLM resting potentials ranged from -70 to -90 mV. Two-electrode voltage clamp was performed using an Axoclamp-2B amplifier (Axon instrument), with the holding potential at –80mV(Kawasaki et al., 1998) and the voltage clamp gain over 50. The HCC-100A Temperature Controller was again used for temperature control, with coincident recording of temperature and electrical signals. Data was analyzed with pCLAMP software (V8.0, Axon Instruments).

Recording at the Larval Neuromuscular Junction (NMJ)

Standard larval NMJ recording configurations were used (Broadie, 2000). Briefly, recordings were made from muscle 6 in abdominal segments A3-4 of wandering 3rd instar larva using two-electrode voltage-clamp (–60mV) techniques (Axoclamp 2B amplifier). Intracellular recording electrodes were filled with 3M KCl and typically had a resistance of ~10MΩ. EJCs were evoked by brief stimuli (0.4-1.5ms) applied to the cut motor nerve using a suction electrode. The recording saline contained (in mM): 128 NaCl, 2KCl, 4$MgCl_2$, 5 trehalose, 70 sucrose, 5 HEPES, 1.8 $CaCl_2$, pH 7.1. A probe placed close to the preparation monitored the recording chamber temperature. Data acquisition and analysis was performed using pCLAMP software (V8.0; Axon Instruments).

Dye Imaging

FM1-43 dye imaging was done as described (Fergestad and Broadie, 2001) with slight modifications. Wandering 3rd instar larvae were dissected in Ca^{2+}-free recording with mutants and controls always prepared in the same chamber to ensure identical processing and imaging conditions (Fergestad and Broadie, 2001). The preparations were exposed to 10 µM FM1-43 (Molecular Probes) in 90 mM K^+ saline containing 1.8 mM Ca^{2+} (Fergestad and Broadie, 2001) for 3-5 min to load synaptic terminals, then washed in Ca^{2+}-free recording saline (2 mM K^+) for ~10 min, while the saline was exchanged at least 3 times. Confocal fluorescence images were acquired with a Zeiss LSM 510 confocal microscope. In each animal, 2 - 4 loaded muscle 12 and 13 NMJs were imaged

(segments A2-A4), and then samples were transferred to pre-warmed (38ºC) Ca^{2+}-free recording saline and moved to a 38ºC incubator for 15 min. Samples were then treated with pre-warmed (38ºC) high K^+ saline for 5 min to destain terminals, and confocal imaging was then repeated using identical parameters.

Electron Microscopy

Animals at room temperature (22°C) or incubated for 10 min at 37°C were fixed in 2.5% glutaraldeyde overnight. Samples were then washed in PBS for 10 min, transferred to 1% osmium tetroxide in H_2O for 1hr, rinsed with ddH_2O, and stained *en bloc* in 2% aqueous uranyl acetate for 1hr. Samples were then dehydrated through a series of graded alcohols and embedded in araldite. After placing in a vacuum oven for 30 min, animals were placed in fresh araldite and left to polymerize overnight at 60ºC. Ribbons of thin (~40-50nm) sections were obtained with a Leica Ultracut UCT 54 ultramicrotome and examined on a Phillips CM12 TEM, equipped with a 2 mega pixel CCD camera. Digital electron microscopy images were taken of synaptic boutons from the DLM NMJ. All sections for quantification contained at least one clear presynaptic T-bar, defining an AZ, identified in at least two consecutive sections. Docked vesicles were defined as those within 20 nm from the electron dense presynaptic membrane at the T-bar, as previously (Aravamudan, et al. 1999). Morphometric analysis was performed using the public domain NIH Image J software package.

SNARE Complex Assay

Animals at room temperature (22°C), or incubated for 10 min at 33°C or 37°C, were frozen in liquid nitrogen, and heads were immediately collected with a sieve. 150 mg of heads were homogenized in 3 ml ice pre-chilled hypotonic buffer (10 mM $MgCl_2$, 25 mM Tris (pH 7.4), 2.5 mM EGTA and complete mini protease inhibitor cocktail (Roche)) with a dounce homogenizer. Plasma membrane fractions were collected from the lysed cell suspension by centrifugation at 1,000***g*** (5 mins, 4°C) and subsequent centrifugation of the supernatant at 50,000***g*** (30 mins, 4°C). Protein extraction was performed by resuspending the final membrane pellet in SDS sample buffer (50 mM Tris-HCl (pH 6.8), 10% glycerol, 2% SDS, 5% 2-mercaptoethanol) for 15 min at 22°C. Total membrane protein concentration was determined by absorbance measurements at 280 nm. Bromophenol Blue was added (0.03%), and samples were subjected to SDS-PAGE and western blot with primary antibody against Syntaxin1A (8C3; Iowa Developmental Studies Hybridoma Bank), and SNAP25 (Leo Pallanck, University of Washington), and HRP-conjugated secondary antibodies (Promega). Signals were visualized by ECL and quantified by Labworks 4.5 in combination with UVP BioImaging systems.

Statistics

Statistical analyses of total SV number, bouton size and the docked SV number at active zones were done with Instat; significant differences were determined by the nonparametric Mann-Whitney test. Statistical analyses of all

other experiments were done with Microsoft Excel X software; significant changes were determined by an unpaired t test. In all cases, P values less than 0.05 were considered significant. If not specified, data is represented by mean ± S.E.M.

Results

RBO is Acutely Required for Movement

At permissive temperatures (<25°C), *rbo* TS mutant adult flies appear to act normally and cannot be distinguished from wildtype (wt) based on locomotion or gross behavior. At restrictive temperature (>37°C), all *rbo* TS mutant animals are completely paralyzed within minutes, although control animals appear unaffected. At intermediate temperatures, *rbo* TS mutants show intermediate movement impairment. At 29°C, mutants remain mobile for many hours but become progressively sluggish and die within 1 day, and at 33°C, mutants display reduced movement followed by complete paralysis in ~30 min. Thus, *rbo* TS mutants display a progressively temperature-dependent impairment in some mechanism required for movement.

The kinetics of reversible paralysis was quantified in a range of homozygous and trans-heterozygous *rbo* mutants (rbo^{ts1}/rbo^{ts1}, rbo^{ts1}/rbo^{2}, rbo^{ts1}/rbo^{3}, rbo^{ts1}/*Df(2R)H3D3*; see Methods). The time courses of paralysis and recovery are shown in Figure 1. All *rbo* mutant allelic combinations display 100% paralysis within 3-4 minutes when shifted from room temperature (22°C)

to 37°C, and recover with a similar time course after a return to room temperature (Fig. 1). Control wildtype and *rbo*/+ flies show no movement impairment under identical conditions. No difference in the kinetics of paralysis or recovery was observed between rbo^{ts1} homozygotes and rbo^{ts1}/rbo^{2}, rbo^{ts1}/rbo^{3}, rbo^{ts1}/*Df(2R)H3D3* mutants (data not shown). A single copy of a wildtype *rbo:egfp* transgene fully rescues behavioral paralysis in all of these genotypes (Fig. 1a). Therefore, the temperature-sensitive paralysis can be fully ascribed to the rbo^{ts1} mutation.

To gain insight into possible mechanisms, we compared rbo^{ts1} mutants with $paralytic^{ts1}$ (terminates action potentials; (Wu and Ganetzky, 1980)) and $shibire^{ts1}$ (blocks SV endocytosis; (Koenig et al., 1983)). The paralysis and recovery kinetics of rbo^{ts1} differs markedly from $paralytic^{ts1}$, in which paralysis/recovery are exceedingly rapid (~5 seconds; Fig. 1). This result suggests that *rbo* is unlikely to encode a protein directly mediating neuronal excitability, such as an ion channel or channel regulator. Consistent with this conclusion, rbo^{ts1} mutants do not show any visible change in death rate after exposure to veratridine for 2, 4, 8, 12 hours at 18°C, 22°C and 28°C (data not shown). Veratridine is a sodium channel-specific neurotoxin which prolongs the activation of voltage-gated Na^+ channels (Ritchie, 1979; Suzuki and Wu, 1984; Jackson et al., 1986). Na^+ channel mutants and Na^+ channel regulator mutants display increased resistance to veratridine at both permissive and restrictive temperatures, including $para^{ts}$, nap^{ts}, and *tipE* (Suzuki and Wu, 1984; Jackson et al., 1986). Further, rbo^{ts1} mutants do not show genetic interaction with $paralytic^{ts1}$, *shaker* (I_A voltage-gated K^+ channel) or *ether-*

a-gogo (a subunitcommon to different K^+ channels) mutants in terms of the kinetics of TS paralysis and recovery (data not shown).

The paralysis kinetics of *rbo*^{ts1} and *shibire*^{ts1} mutants is quite comparable; *rbo*^{ts1} mutants paralyze slightly more slowly than *shibire*^{ts1} (Fig. 1a), but recover with an indistinguishable time course (Fig. 1b). The relatively slow paralysis/recovery in *shibire*^{ts1} is caused by slow depletion/regeneration of the synaptic vesicle pool (Koenig et al., 1983). Similarly, there is an activity-dependent requirement for RBO in phototransduction (Huang et al., 2004), and loss of RBO function likely results in the loss of some resource limiting neurotransmission. Given that RBO is an integral plasma membrane lipase (Huang et al., 2004), one likely possibility is that RBO produces a limiting lipid required for neurotransmission or, alternatively, eliminates a lipid that negatively regulates neurotransmission.

RBO is Subcellularly Restricted to Neuronal Synapses

A *rbo-egfp* fusion transgene was made from genomic DNA including 3.5 kb upstream and 1.5 kb downstream of the *rbo* coding region. A single copy of this *rbo-egfp* transgene rescues all *rbo* mutant phenotypes (Huang et al., 2004). We therefore examined *rbo-egfp* expression in the *rbo* null mutant background. Previously, we showed RBO-eGFP protein to be highly enriched in the central synaptic neuropil of embryos, larvae, and adults, in the brain and the thoracic and abdominal ganglia (Huang et al., 2004). To examine RBO expression within

individual, identified neurons, we assayed motor neurons and NMJ synapses in both larvae and adults (Fig. 2).

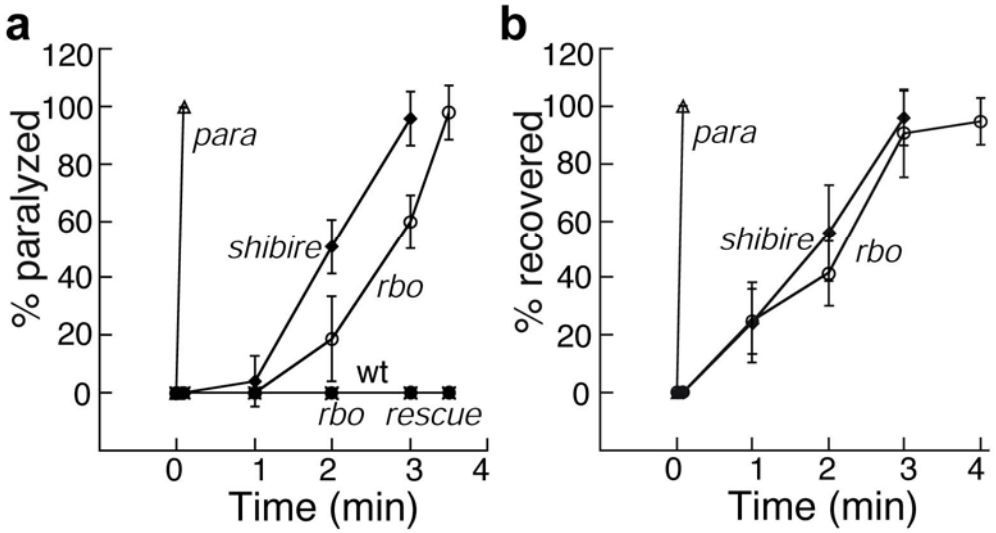

Figure 1. Temperature-sensitive (TS) paralysis and recovery of *rbo* mutants
The kinetics of TS paralysis at 37°C (a) and recovery from paralysis at room temperature (22°C) (b). The genotypes are Oregon-R wildtype (wt), rbo^{ts1}/rbo^{2} (*rbo*), rbo^{ts1}/rbo^{2}; *rbo-egfp*/+ (*rbo* rescue), $paralytic^{ts1}$ (*para*) and $shibire^{2ts1}$ (*shibire*) homozygous mutants.

RBO protein is undetectable in neuronal soma, present at low levels in axons and highly enriched specifically within synaptic boutons (Fig. 2). RBO protein is expressed at all examined NMJ synapses innervating the body musculature in both larva (Fig. 2a) and adult stages (Fig. 2b). Double-labeling experiments with either presynaptic (Synaptotagmin (Syt), Cysteine String Protein (CSP), horse radish peroxidase (HRP)) or postsynaptic (Discs Large, DLG) markers confirms that RBO is specifically subcellularly enriched within

synaptic boutons (Fig. 2). The expression pattern is consistent with a predominantly presynaptic localization for RBO, although a low level of muscle postsynaptic localization may also occur. RBO is associated with the plasma membrane throughout the synaptic bouton, without any detectable restriction in smaller membrane domains (Fig. 2a; insets). This expression pattern together with TS paralytic phenotype suggests that RBO functions in synaptic transmission to mediate coordinated movement.

Figure 2. RBO protein is subcellularly restricted to synapses
Confocal imaging of RBO-eGFP in *rbo* transgenic rescue background (*rbo*^{2}/*rbo*^{2}; *rbo-egfp*/*rbo-egfp*). (a) RBO at wandering 3rd instar larva NMJ synapses. Co-localization of RBO with synaptic markers; Discs Large (DLG), predominantly postsynaptic, and Cysteine String Protein (CSP), a presynaptic vesicle-associated protein. (b) RBO in adult abdominal NMJs. Anti-HRP recognizes the neuronal membrane. (c) Innervation pattern of DLM NMJs stained with anti-Synaptotagmin. NMJs are deeply embedded and evenly distributed in DLM muscle cells. The bottom is the projection of a single DLM muscle cell. (d) lower amplification and (e) higher amplification, showing that RBO co-localizes with HRP in DLM NMJs.

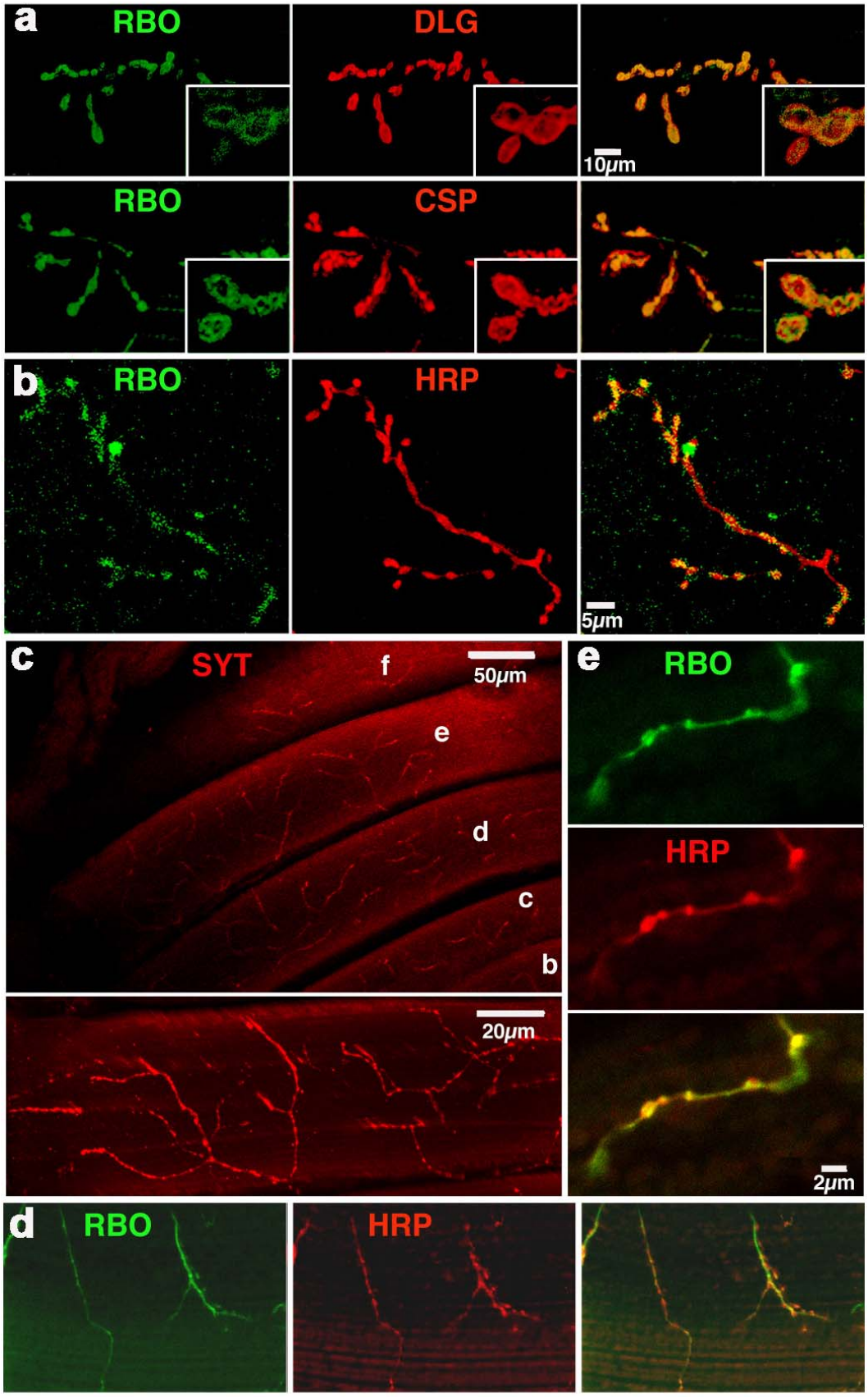
a
RBO
DLG
10μm
RBO
CSP
b
RBO
HRP
5μm
c
SYT
f
50μm
e
d
c
b
20μm
e
RBO
HRP
2μm
d
RBO
HRP

RBO is Required for Synaptic Transmission

To investigate whether the adult conditional *rbo* paralysis is associated with a failure in synaptic transmission, excitatory junction potential (EJP) recordings were made in the adult Giant Fiber (GF) escape circuit (Fig. 3), well characterized in terms of both anatomy and physiology (King and Wyman, 1980; Tanouye and Wyman, 1980; Ikeda and Koenig, 1988; Trimarchi and Murphey, 1997). GF circuit activation involves stimulation of the Giant Neuron in the brain, action potential (AP) propagation through the GF into the thoracic ganglion, electrical synaptic activation of the PSI interneuron, cholinergic synaptic activation of the dorsal longitudinal muscle (DLM) motor neuron (DLMn), AP propagation along DLMn axon in the peripheral nerve, and finally NMJ glutamatergic transmission at the muscle (Fig. 2c). Records were made by electrically stimulating the paired Giant Neurons in the brain with extracellular glass electrodes while intracellularly recording output in thoracic DLM muscles (Fig. 3a).

At permissive temperature (25°C), evoked EJP amplitudes in rbo^{ts1} mutants are indistinguishable from wildtype (rbo^{ts1}/rbo^{2}, 43 ± 6.6 mV; wt, 48 ± 4.6 mV; Fig. 3b,c). In contrast, following a shift to 37°C, evoked EJPs in rbo^{ts1} mutants are undetectable, and remain completely suppressed at 37°C, but then recover following return to 25°C (Fig. 3b-d). In wildtype, EJP amplitudes are reduced by ~25% at 37°C (36 ± 1.8 mV), but persist throughout the entire time course of the temperature shift recording (Fig. 3b-d). These results show that adult conditional paralysis in rbo^{ts1} mutants temporally correlates with neural

transmission blockade in the adult GF circuit. Interestingly, there is not an acute requirement for RBO at the larval NMJ. Excitatory junctional current (EJC) amplitudes at room temperature (20-22°C) were indistinguishable between *rbo*^{ts1} and control animals (*rbo*^{ts1}/*rbo*^{2}: 185±19 nA, n=5; wildtype: 190±10 nA, n=5). Incubation of *rbo*^{ts1} wandering 3rd instars at 37°C did not cause significant change in EJC amplitudes. At a stimulation frequency of 0.5 Hz, mean EJC amplitude was 243±18 nA for *rbo*^{ts1}/*rbo*^{2} (n=6) and 224±24 nA (n=6) for control animals, respectively. In all recordings, EJCs could be evoked as long as a stable recording configuration was maintained (>15 min at 37°C), largely excluding the possibility of a delayed onset of transmission impairment. Similarly, assays of SV cycling with FM1-43 dye loading/unloading at the larval NMJ failed to reveal deficits in *rbo*^{ts1}/*rbo*^{2} mutants (data not shown). Therefore, the acute requirement for RBO in maintaining neural transmission appears restricted to the adult.

The EJP loss in adult *rbo*^{ts1} mutants could be caused by a defect at any level of GF circuit function, including failure of AP initiation/propagation, or a blockade of synaptic transmission at either central or peripheral synapses. To distinguish between these possibilities, we took advantage of the dual DLM and tergotrochanteral muscle (TTM) outputs of the GF circuit (Fig. 3a). The DLM circuit contains a single, essential cholinergic chemical synapse between PSI and DLMn, upstream of the glutamatergic DLM NMJ, and thus behaves like a bi-synaptic pathway. In contrast, the TTM glutamatergic NMJ is the sole required

Figure 3. Conditional block of neurotransmission in the Giant Fiber circuit (a) Schematic diagram of the Giant Fiber (GF) circuit. Note in particular that output onto the TTM requires only electrical synapses prior to the glutamatergic NMJ, whereas output onto the DLM has a single prerequisite central chemical (cholinergic) synapse between the PSI interneuron and the motor neuron (DLMn). Stimulation (S) was applied to the brain to activate the GF, and in turn activate the motor neurons. (b) Representative traces of the temperature-dependent, reversible loss of DLM excitatory junctional potential (EJP) responses in wildtype (wt) and *rbo (rbo^{ts1}/rbo^{2})* mutants (arrow indicates shock artifact; removed for clarity). Bottom trace shows the concurrently recorded temperature shift (25°C to 37°C). (c) Quantification of EJP amplitude at 25°C and after 5 mins at 37°C. Bars show the mean±SEM. (d) Time-course of EJP amplitude changes. The recording temperature (right axis) was recorded simultaneously.

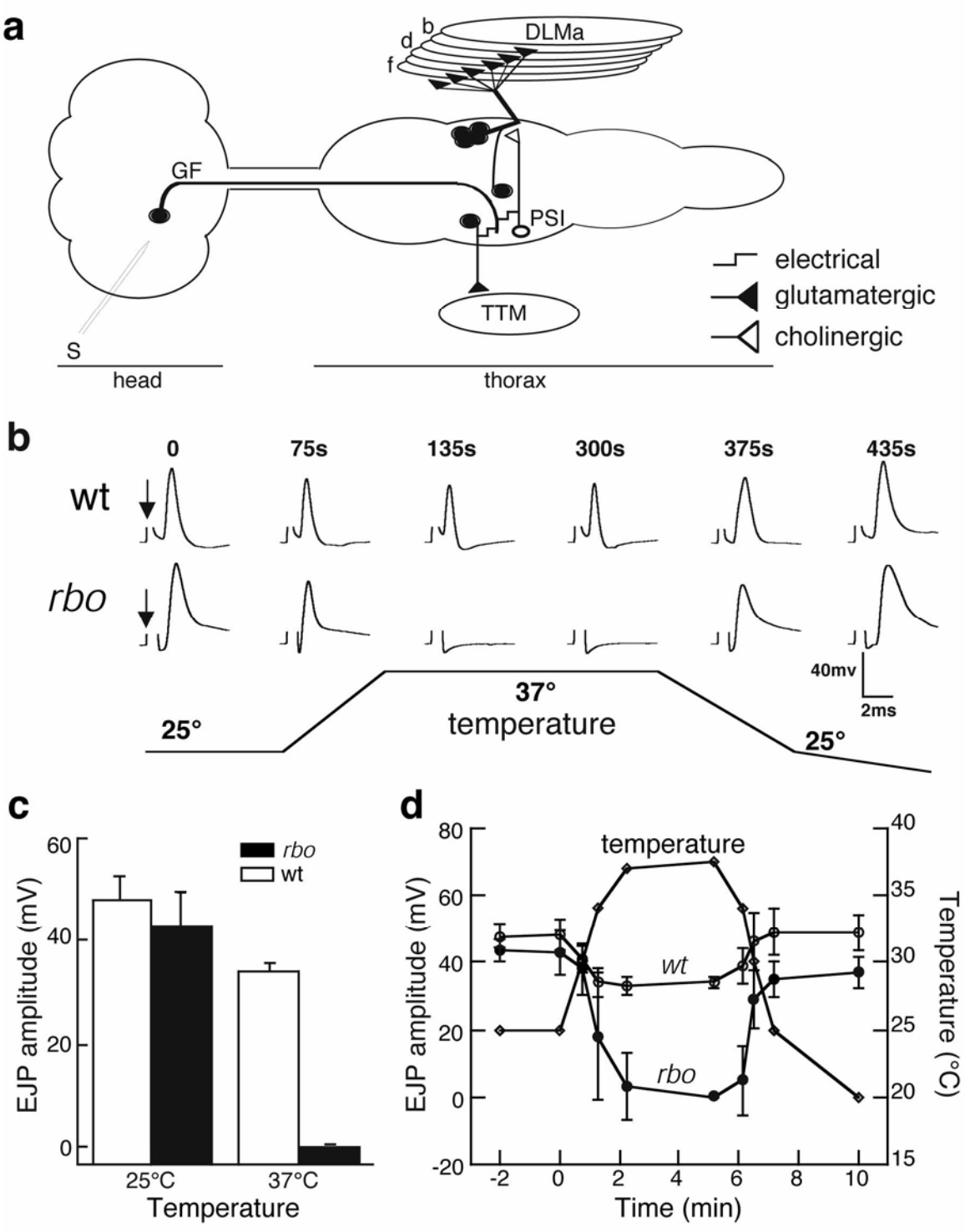
a
DLMa
b
d
f
GF
PSI
TTM
S
head
thorax
electrical
glutamatergic
cholinergic
b
0
75s
135s
300s
375s
435s
wt
rbo
40mv
2ms
37°
temperature
25°
25°
c
rbo
wt
EJP amplitude (mV)
60
40
20
0
25°C
37°C
Temperature
d
temperature
wt
rbo
EJP amplitude (mV)
80
60
40
20
0
-20
-2
0
2
4
6
8
10
Time (min)
40
35
30
25
20
15
Temperature (°C)

chemical synapse in the TTM circuit (King and Wyman, 1980): electrical synapses alone are sufficient for transmission to the TTM NMJ, which therefore behaves like a monosynaptic pathway. Any block of AP function would result in an abrupt failure of neural transmission in both outputs of the GF circuit. In contrast, any direct loss of synaptic function would be predicted to differentially block function in the two outputs. If RBO is required only at glutamatergic NMJs, we would expect both DLM and TTM EJPs to be lost in a graded, incremental fashion over several minutes, as NMJ synaptic transmission is progressively degraded. If RBO is also required for central transmission, we would predict that a blockade of the weaker cholinergic PSI synapse will lead to a failure of AP initiation in the DLMn, causing a sudden, complete loss of NMJ transmission. Similarly, if a central transmission block occurs, we would predict an abrupt recovery of the DLM EJP once the central transmission recovers versus an incremental improvement of the TTM EJP.

The results of the DLM/TTM comparison strongly indicate that *rbo* mutants are specifically defective in synaptic transmission in both central and peripheral synapses (Fig. 4). In DLM recordings in rbo^{ts1} mutants following shift to restrictive temperature (25°C to 37°C), the EJP initially declines, consistent with a progressive weakening of NMJ transmission, but then displays a sudden complete loss (Fig. 4a, middle panel). In contrast, TTM recording of rbo^{ts1} mutants always show a gradual loss of EJP amplitude over several minutes following shift to the restrictive temperature (Fig. 4b, middle), and a similar gradual recovery following return to permissive temperature (Fig. 4b, right). The

time to complete EJP loss at restrictive temperature was 4.3 ± 0.5 min (mean ± S.D., n=6), which agrees well with the time to complete TS paralysis (4.5 min). DLM and TTM EJPs in wildtype and transgenic rescue flies (*rbo*^{ts1}/*rbo*^{2}; *rbo-egfp*/+) persist through the entire recording course (Fig 4a,b, left panels).

These results predict that the DLM should show graded block/recovery if the presumed upstream block in the cholinergic PSI synapse could be by passed. To test this prediction, we used an extracellular electrode placed in the thoracic ganglion to directly excite the DLM motor neuron axon. As predicted, under this stimulation paradigm the DLM in *rbo*^{ts1}/*rbo*^{2} shows graded loss/recovery of EJP amplitude with a time course comparable to the TTM (figure 4a, right panel; n=5). Thus, the abrupt loss/recovery of the EJP in the DLM is due to a central (PSI-DLMn) synaptic defect, superimposed on a simultaneous NMJ transmission blockade. DLM EJPs evoked by brain stimulation require one or more central chemical synaptic relays (Tanouye and Wyman, 1980; Trimarchi and Murphey, 1997; Kawasaki and Ordway, 1999). Impairment of central synaptic transmission results in longer latencies of DLM EJPs (Kawasaki and Ordway, 1999). The presumed block of PSI-DLMn transmission in *rbo*^{ts1} predicts a slowing of AP generation in DLMn, therefore a longer latency of DLM EJP. To test this, we quantified the latencies of DLM EJP in wildtype and in *rbo*^{ts1}/*rbo*^{2}. During temperature elevation, both wildtype and mutant DLM EJP latencies first transiently shorten, but then begin to increase at around 33°C. Above 33-35°C, *rbo*^{ts1}/*rbo*^{2} latencies are significantly prolonged

Figure 4. The *rbo* TS mutation specifically blocks synaptic transmission
(a) Representative series of EJP traces from the DLM evoked by 0.1Hz brain or thoracic stimulation (arrow) during temperature shift from 25°C to 37°C. Numbers indicate order of the evoked response. Response amplitudes are reduced slightly in both genotypes during the temperature shift, but persist in wt (left panel) and fail in an abrupt fashion in *rbo* *(*rbo^{ts1}/rbo^{2}*)* mutants when evoked by brain stimulation (middle panel). However, *rbo* DLM EJP shows gradual loss when induced by direct simulating DLM motor neuron (right panel). (b) Representative series of TTM EJP traces from wt and *rbo* transgenic rescue ((*rbo*^{ts1}/*rbo*^{2}; *rbo-egfp*/+) (left), and *rbo* (middle and right). The left and middle panels show EJP responses during temperature shift from 25°C to 37°C, while the right shows the EJP recovery when temperature is returned to 25°C. Note the graded loss of EJP amplitude following shift to restrictive temperature (middle), and the graded recovery of EJP amplitude following shift back to permissive temperature (right). (c) Reversible block of excitatory junction current (EJC) in DLM NMJs in *rbo* mutants. Representative traces at 25°C (1), 36°C (2) and following return to 25°C (3) in both wt (left) and *rbo* (middle) mutants. (d) Quantification of EJC amplitudes; n=5 for each genotype. (e) Quantification of latency of DLM EJPs evoked by brain stimulation in wt and *rbo* mutants during temperature shift from 25°C to 37°C. " * "and " ** " indicate significant ($P<0.05$) and highly significant change ($P<0.01$) respectively, n=5 for each genotype. Bars show the mean$\pm$S.E.M.

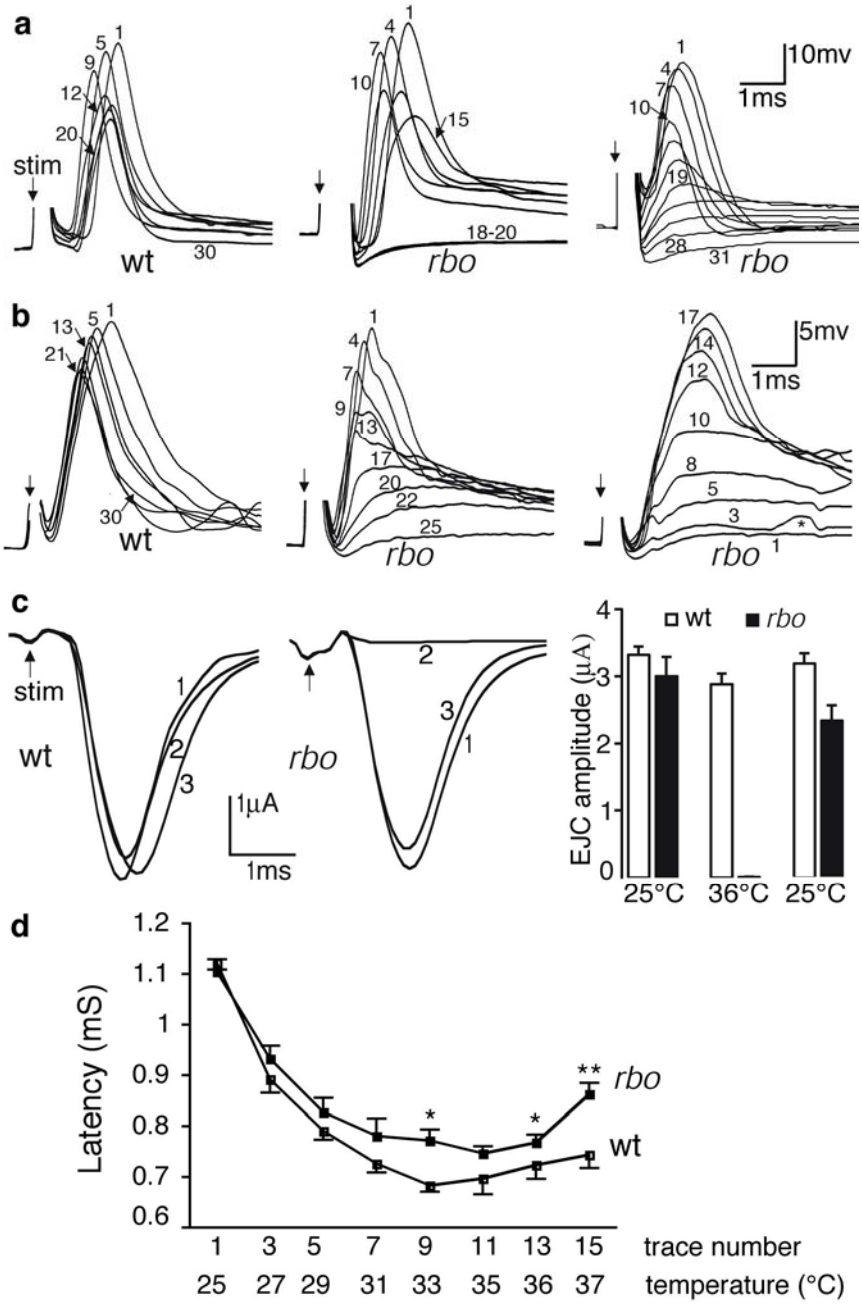
a
stim
wt
rbo
rbo
10mv
1ms
b
wt
rbo
rbo
5mv
1ms
c
stim
wt
rbo
1µA
1ms
wt
rbo
EJC amplitude (µA)
25°C
36°C
25°C
d
Latency (mS)
rbo
wt
trace number
temperature (°C)

compared to control (Fig. 4a left and middle, Fig. 4d).

The EJPs recorded in DLM/TTM are composed of both a synaptically-generated postsynaptic potential and a voltage-dependent electrogenic potential(Koenig et al., 1983; Kawasaki and Ordway, 1999). To directly examine synaptic conductance in *rbo*^{ts1} mutants, we performed two-electrode voltage-clamp EJC recordings from DLMe/d cells (Fig. 4d). The cut motor nerve was stimulated via a suction pipette, and muscle cells were clamped at –80mV. TTX was added to the perfusion solution (0.25μM) to block action potentials in nerve, allowing direct, passive depolarization of the NMJ terminal. EJCs were evoked by constant 0.1 Hz stimulation, and traces were captured at 3 time points: the initial responses at 25°C (1), after 3 mins at 36°C (2), and following return to 25°C (3) (Fig. 4c). At 25°C, EJC amplitude in wildtype and *rbo*^{ts1} mutants were indistinguishable (wt, 3.32 $\pm$ 0.12 μA, *rbo*^{ts1}/*rbo*^{2}, 3.0 $\pm$ 0.29 μA; Fig. 4c). At 36°C, *rbo*^{ts1}/*rbo*^{2} EJCs are completely abolished, but wildtype EJCs remain robust (2.88 $\pm$ 0.16 μA) throughout the entire course of the recording. After a return to 25°C, mutant transmission recovers to 87% of the initial amplitude (2.34 $\pm$ 0.23 μA; Fig. 4c). Taken together, these results demonstrate that RBO is required in a time course of minutes for both peripheral glutamatergic NMJ and central cholinergic PSI-DLMn synaptic transmission.

RBO is Required for Synaptic Vesicle Exocytosis

Our next objective was to determine the mechanistic requirement for RBO in synaptic transmission. We first attempted to carry out FM1-43 loading and

unloading to assay synaptic vesicle (SV) endocytosis and exocytosis, respectively. Unfortunately, we were unsuccessful in stimulating significant dye uptake at the adult DLM/TTM NMJs, presumably because these NMJs are embedded deeply within the muscle fibers (Fig. 2c) and poorly accessible to the applied dye. We therefore directly turned to electron microscopy (EM) to perform ultrastructural studies of DLM NMJs of both wildtype and *rbo*^{ts1} mutants. EM studies were performed both at permissive room temperature (22°C), in which mutants show no functional defects (Figs. 3,4), and 10 minutes following a shift to restrictive temperature (37°C), in which *rbo*^{ts1} mutants lack any detectable neurotransmission (Figs. 3,4).

At permissive temperature (22°C), the ultrastructure of NMJ terminals in *rbo*^{ts1} mutants and wildtype controls appears largely indistinguishable (Fig. 5). Both genotypes contain anatomically normal synaptic bouton profiles, active zones and synaptic vesicles. The synaptic bouton area and the total number of SVs per bouton section are not significantly different ($P > 0.05$) in the two genotypes (Fig. 5). Following a 10 min shift to 37°C, the picture is very different. SV number in *rbo*^{ts1}/*rbo*^{2} mutants is almost tripled within 10 minutes (mean SV number/section: 82±16, n=22 at 22°C vs. 241±29, n=51 at 37°C, p=0.001; Fig. 5c,d). At 37°C, SV number in wildtype is not changed significantly (Fig. 5d). The conditional increase in SV number is consistent with a block of exocytosis in *rbo*^{ts1} mutants. A similar increase in SV number has been reported in photoreceptor presynaptic terminals in *comotase* and *syntaxin1A* TS mutants with a SV exocytosis deficit (Kawasaki et al., 1998; Littleton et al., 1998), and

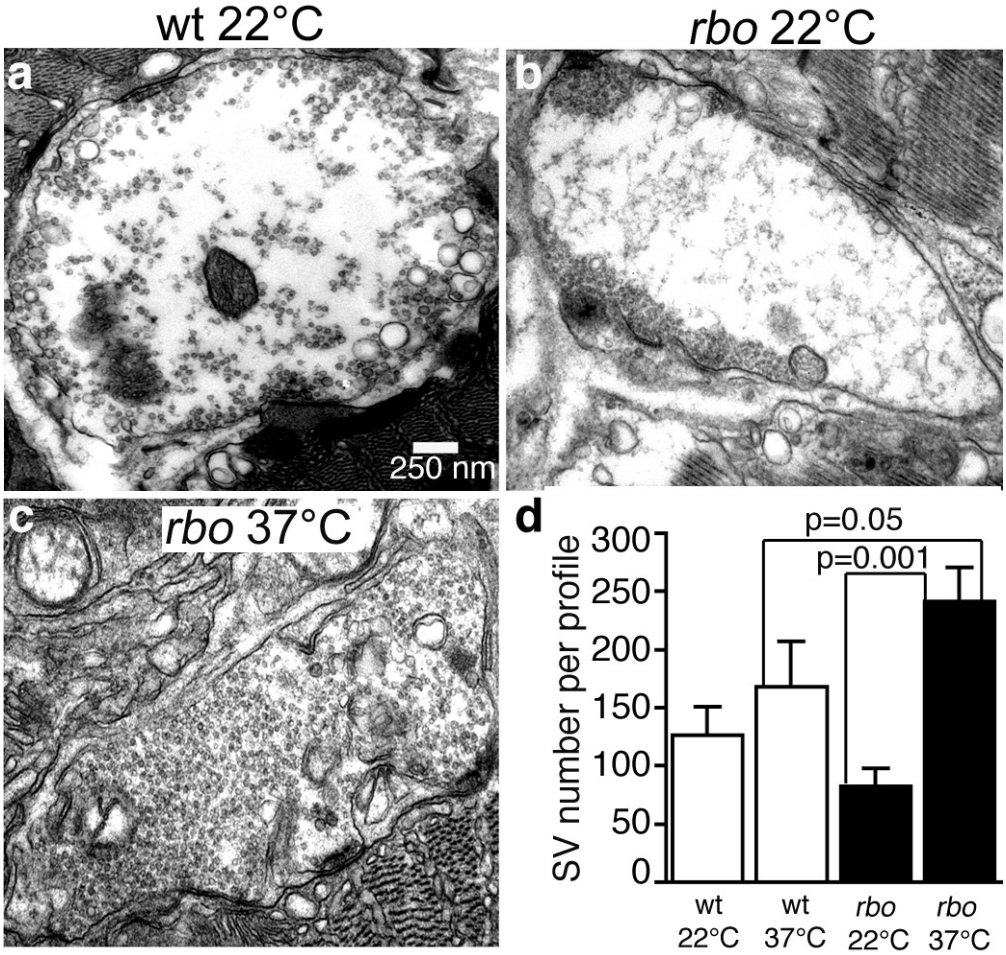

Figure 5. Conditional block of synaptic vesicle exocytosis in *rbo* mutants
(a) Representative electron micrograph of a DLM NMJ synaptic bouton from wildtype (wt) at room temperature (22°C). (b) Representative bouton of *rbo* mutant (rbo^{ts1}/rbo^{2}) at 22°C. Note that synaptic vesicles (SV) tend to be distributed toward active zones. (c) Representative bouton of *rbo* mutant after a 10 min shift to 37°C. Note dramatic increase in SV density. (d) Quantification of SV number per bouton profile. Bars show the mean±S.E.M.

presynaptic terminals of the squid giant synapse with presynaptic synaptobrevin was cleaved by terminal-injected tetanus (Hunt et al., 1994), and the opposite defect of SV depletion in *shibire* TS mutant DLM NMJs with a block of SV endocytosis (Koenig et al., 1983). The SV accumulation in rbo^{ts1} mutants

suggests disruption in the balance between SV fusion and recycling from the plasma membrane, predicting a reduction in the presynaptic terminal membrane area. To test this prediction, NMJ boutons were visualized with anti-Synaptotagmin (Fig. 2c) and bouton area quantified with confocal imaging. The temperature shift from 22°C to 37°C resulted in a slight reduction of bouton area in *rbo* mutants (from 0.99±0.02 μm^2, n=224 to 0.92±0.2 μm^2, n=180), but this change was not statistically significant. In EM studies, the largest sections from bouton serial sections containing at least one clearly define synaptic active zone were selected to quantify cross-sectional area. Following a 10 min shift to 37°C, the cross-sectional bouton area in *rbo* mutants was reduced ~38% (rbo^{ts1}/rbo^{2}; 4.84 ± 1.37 μm^2, n=22 at 22°C vs. 2.98 ± 0.5 μm^2, $p<0.05$, n=51). The bouton area of wildtype controls shows no significant change during the same temperature shift. Taken together, these data support an acute and specific block in SV exocytosis in the absence of RBO function.

To determine the stage of the putative RBO-dependent SV exocytosis block, we next quantified SV density relative to the presynaptic active zone (AZ) (Fig. 6). AZs in wildtype animals contain 1-2 SVs in contact ("docked") with the electron-dense AZ membrane (arrowhead, Fig. 6a). The rbo^{ts1} mutants at

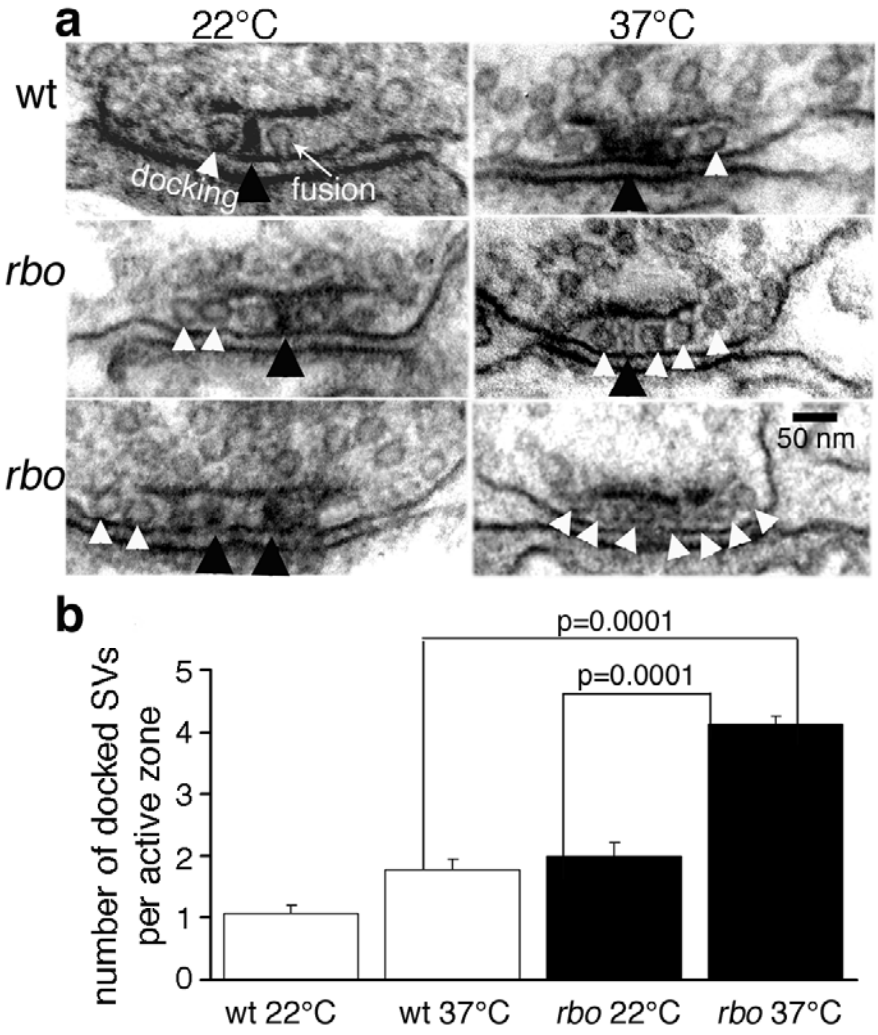

Figure 6. Docked synaptic vesicles arrest at the active zone in *rbo* mutants (a) Representative electron micrographs of presynaptic active zone (AZ) in wildtype (top) and *rbo* (rbo^{ts1}/rbo^{2}) mutants (middle and bottom) at 22°C (left column) and after a 10 min shift to 37°C (right column). The electron-dense AZ T-bar (black arrow heads) and morphologically docked SVs (white arrow heads) are indicated. (b) Quantification of the number of docked SVs per AZ. Bars show the mean±S.E.M.

permissive temperature (22°C) show a similar profile. In contrast, following 10 min shift to 37°C, there is a significant accumulation of docked SVs in rbo^{ts1}/rbo^{2} mutants (SVs/AZ: 4.1±0.1) when compared to both wildtype at 37°C (1.8±0.14, p=0.0001), and to rbo^{ts1}/rbo^{2} mutants at 22°C (2.0±0.2 p=0.0001) (Fig. 6).

Typically, all available electron-dense AZ membrane in the mutant appears occupied with docked SVs (Fig. 6a), suggesting that SV docking sites may be nearly or completely saturated. The accumulation of docked SVs is similar to that reported for *comatose* (DLM NMJs and photoreceptor synapses) and *syntaxin* (photoreceptor synapses) TS mutants with SV priming or fusion defects (Kawasaki et al., 1998; Littleton et al., 1998). This result further supports the existence of an exocytosis defect in rbo^{ts1} mutants and suggests that RBO is required at a post-docking stage of SV exocytosis, during vesicle priming or fusion stages.

SV priming is dependent on UNC-13, which can be recruited to plasma membrane by binding DAG (Brose and Rosenmund, 2002). We previously reported an acute, activity-dependent depletion of DAG in the brains of rbo^{ts1} mutants (Huang et al., 2004), and previously reported a *dunc-13* docked SV accumulation phenotype very similar to the rbo^{ts1} phenotype reported here (Aravamudan et al., 1999). To test whether the block of SV exocytosis in rbo^{ts1} may correlate with mislocalization of dUNC-13, DLM synaptic boutons were stained with a dUNC-13 antibody and confocal imaging used to assay dUNC-13 expression (Fig. 7). The rbo^{ts1} mutants at permissive temperature (22°C) showed dUNC-13 expression indistinguishable from wildtype controls. Following 10 min shift to 37°C, there was no detectable change is either the expression intensity or the bouton distribution of dUNC-13 (Fig. 7). This negative result might be due to the limited resolution of confocal imaging.

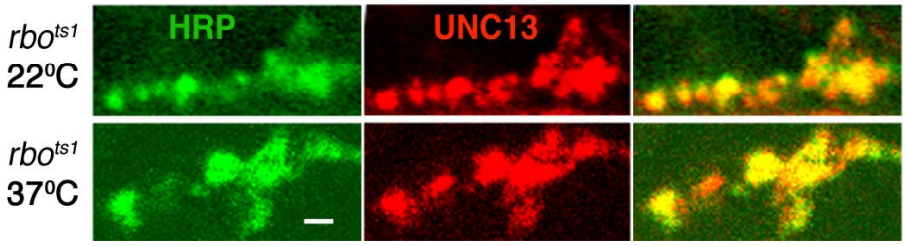

Figure 7. No detectable alteration of dUNC-13 distribution in *rbo* mutants
Adult DLM NMJ synaptic boutons double-labeled with anti-HRP (neuronal membrane; green) and an antibody to dUNC-13 (red). Representative images from *rbo* (*rbo*^{ts1}/*rbo*^{2}) mutants at permissive temperature (22°C, top) and following a 10 min shift to 37°C (bottom). Scale bar, 1.0μm.

RBO Interacts with the Syntaxin T-SNARE

To investigate the molecular mechanism underlying the RBO requirement in synaptic transmission, we next generated double mutants of *rbo*^{ts1} and other *Drosophila* TS synaptic mutants. TS mutants tested in combination with *rbo* included the *cacophony* presynaptic Ca^{2+} channel (*cac*^{ts2}; (Dellinger et al., 2000)), the *syntaxin1A* T-SNARE (*syx*$^{3-69}$; (Littleton et al., 1998)), the *comatose* NSF ATPase (*comt*^{ts17}, *comt*^{ts53}; (Siddiqi and Benzer, 1976)) and the *shibire* Dynamin GTPase (*shibire*^{ts1}; (Grigliatti et al., 1973)). To test for genetic interactions, behavioral paralysis was assayed at an intermediate temperature of 33°C, at which *rbo* single mutants (e.g. *rbo*^{ts1}/*rbo*^{ts1}, *rbo*^{ts1}/*rbo*^{2}) are only slowly paralyzed over a time course of ~30 minutes. For the first 10 minutes at 33°C, *rbo* homozygous mutants remain fully upright and mobile (Fig. 8a), thereby providing a sensitized condition in which to assay double homozygotes for accelerated paralysis. Under these conditions, *rbo* displays no obvious synergistic interaction with *cacophony, comatose* or *shibire* mutants (data not shown). In contrast, there is a strong synergistic interaction between *rbo*^{ts1} and

the *syx*$^{3-69}$ mutation. To control for genetic background contributions, both *rbo*^{ts1}/*rbo*^{ts1}; *syx*$^{3-69}$/*syx*$^{3-69}$, and *rbo*^{ts1}/*rbo*^{2}; *syx*$^{3-69}$/*syx*$^{3-69}$ mutants were examined. Both types of double mutants showed an indistinguishable synergistic genetic interaction and are pooled together in Figure 8a.

After 10 min at 33°C, *syx*$^{3-69}$ homozygotes display only ~10% paralysis. Paralyzed *syx*$^{3-69}$ flies completely recover to an upright position within 1-2 mins following return to room temperature. In contrast, *rbo*^{ts1}; *syx*$^{3-69}$ double mutants rapidly paralyze at 33°C, with ~90% of mutants completely paralyzed within 10 mins (Fig. 7a), and ~5 min are required for all paralyzed *rbo*^{ts1}; *syx*$^{3-69}$ double mutants to regain an upright position following return to room temperature (Fig. 8b). These observations suggest that RBO and Syntaxin may act in the same pathway, or parallel pathways, required for neurotransmission.

RBO May Act Downstream of SNARE Complex Assembly

The *syx*$^{3-69}$ allele is a missense mutation that causes temperature-dependent disruption of Syntaxin1A binding to SNAP25 and Synaptobrevin, and hence a defect in the formation of SNARE complex (Littleton et al., 1998).

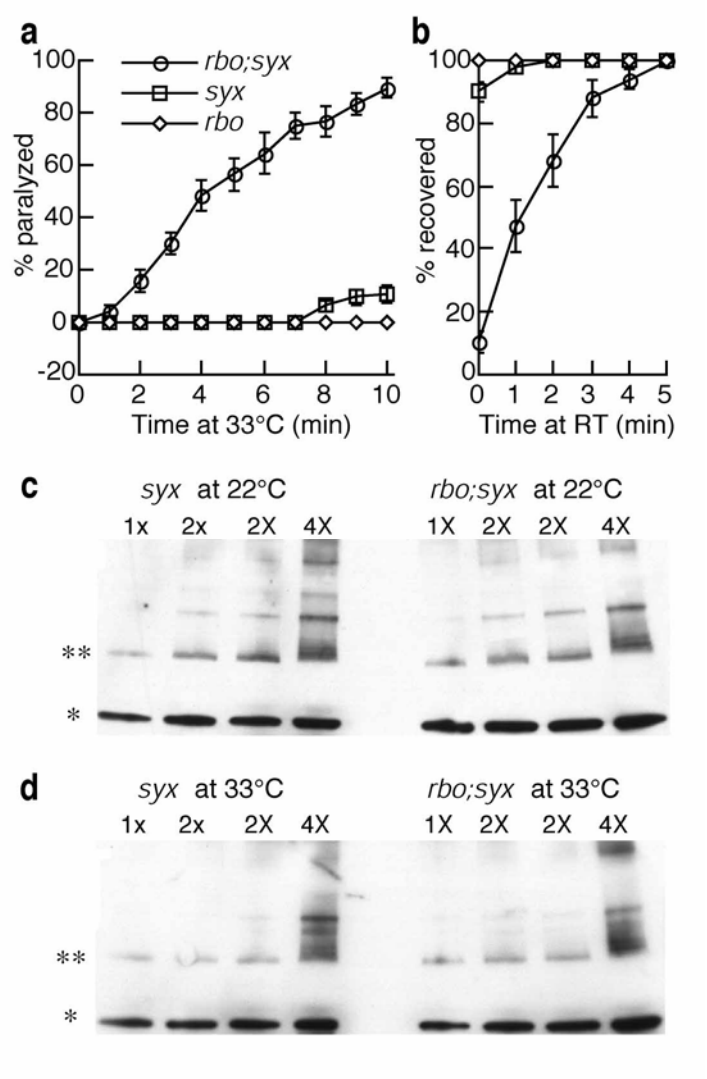

Figure 8. RBO genetically interacts with Syntaxin

The kinetics of TS paralysis at 33°C (a) and recovery from paralysis at room temperature (22°C) (b) in *rbo* (rbo^{ts1}/rbo^{2} and rbo^{ts1}/rbo^{ts1}), *syx* ($syx^{3\text{-}69}$/ $syx^{3\text{-}69}$) single mutants and *rbo; syx* (rbo^{ts1}/rbo^{2}; $syx^{3\text{-}69}/syx^{3\text{-}69}$) double mutants. The *rbo* and *syx* mutants display a strong synergistic interaction. Representative anti-Syntaxin1A Western blots of SNARE complex abundance in *syx* single mutants and *rbo; syx* double mutants. Analyses at room temperature (22°C) (c) and following a 10 min shift to 33°C (d). "1x, 2x, and 4x" indicate the loading amount of total plasma membrane protein determined by absorbance measurements at 280 nm. Equal amount of total membrane protein from *syx* single mutants and *rbo; syx* double mutants were loaded. The bands indicated by '*" and '**' represent syntaxin monomer and 7S SNARE complex, respectively.

Homozygous *syx*$^{3\text{-}69}$ mutants display reduced SNARE complex formation at room temperature, and no detectable SNARE complex formation after 20 minutes at 38°C (Littleton et al., 1998). Therefore, the synergistic genetic interaction between *rbo*^{ts1} and *syx*$^{3\text{-}69}$ mutations in behavioral paralysis could be due to an additive negative effect on SNARE complex assembly, or to a downstream Syntaxin-dependent mechanism of SV fusion. To test these possibilities, we assayed the abundance of SNARE complex in *syx*$^{3\text{-}69}$ mutants and *rbo*^{ts1}/*rbo*^{2}; *syx*$^{3\text{-}69}$/*syx*$^{3\text{-}69}$ double mutants at both room temperature and 33°C.

The ternary (7S) SNARE complex, composed of one molecule each of Syntaxin, SNAP25 and Synaptobrevin, is SDS resistant and migrates at ~73kDa in SDS-PAGE (Littleton et al., 1998; Tolar and Pallanck, 1998). Equal amounts of total membrane proteins from brain extracts of both groups of mutants were subjected to SDS-PAGE and western blot analyses with an antibody against Syntaxin1A (8C3) (Fig. 7c,d). The 7S SNARE complex and Syntaxin monomer abundance in *rbo*^{ts1}/*rbo*^{2};*syx*$^{3\text{-}69}$/*syx*$^{3\text{-}69}$ were normalized to *syx*$^{3\text{-}69}$/*syx*$^{3\text{-}69}$ of the same blot. At room temperature, double mutants contain 1.28±0.15 (n=10) and 1.16±0.06 (n=8) of 7S SNARE and Syntaxin1A monomers, respectively. After 10 minutes at 33°C, normalized quantification shows that the double mutants still contain similar relative levels of 7S SNARE complex (1.13 ± 0.10; n=20) and Syntaxin1A monomers (1.23 ± 0.07; n=19). Thus, no additive negative effect on SNARE complex assembly was detected in double mutants. We also compared SNARE complex abundance in *rbo*^{ts1}/*rbo*^{2} and wildtype (at 22°C and 37°C), and

did not observe any significant difference between mutants and controls (data not shown). Taken together, these results suggest that the *rbo* defect in SV exocytosis likely occurs downstream of SNARE complex assembly.

Discussion

RBO Functions at a Post-docking Step in SV Exocytosis

RBO is a predicted integral plasma membrane lipase (Huang et al., 2004). The protein is highly enriched within the nervous system, and is subcellularly restricted within central neurons largely to synaptic domains. At neuromuscular synapses, RBO is predominantly localized to the plasma membrane within presynaptic boutons. The protein may also be present in the postsynaptic compartment, but we are currently unable to resolve RBO-GFP localization more distinctly at a confocal level. Conditional *rbo* mutants paralyze within minutes and display a complete block of synaptic transmission within minutes. This functional block correlates with a sharp increase in SV number within presynaptic boutons and a concomitant shrinkage of presynaptic plasma membrane area. These acute changes appear to arise from the disruption of the balance between SV consumption (exocytosis) and recycling by SV formation (endocytosis). Similar SV accumulation has been reported only in mutants with defective SV fusion, including *comatose* and *syntaxin* TS mutants (Kawasaki et al., 1998; Littleton et al., 1998). In *rbo* TS mutants, docked vesicles accumulate at presynaptic active zones within minutes. This defect is most consistent with a

post-docking block of SV priming/fusion. However, since docking may be proportional to overall SV pool size (Weimer et al., 2003), the elevation in SV number might also contribute to the increased number of docked SVs.

Conditional TS paralytic mutations of *rbo* and *syntaxin1A* (syx^{3-69}) produce a strong synergistic genetic interaction. Among the pool of TS mutants tested, this interaction appears quite specific to Syntaxin. Interactions were not observed between *rbo* and TS mutant affecting presynaptic Ca^{2+} influx, SNARE complex disassembly or SV recycling. The *rbo-syx* interaction agrees well with the EM characterization indicating a requirement for RBO in post-docking SV exocytosis. The syx^{3-69} mutants display a temperature-dependent loss of SNARE complexes (Littleton et al., 1998). In rbo^{ts1}; syx^{3-69} double mutants, we found no further reduction of SNARE complex assembly. The assay included both trans- and cis-SNARE complexes, making it hard to correlate SNARE complex abundance with functional defects. Nevertheless, the absence of a discernable change in SNARE complex abundance in *rbo* mutants suggests that RBO is unlikely to function directly in SNARE assembly/disassembly. Taken together, these data therefore suggest that RBO likely acts either downstream of SNARE complex assembly, or in an unknown parallel pathway leading to SV fusion.

The acute requirement for RBO protein appears to be limited to a subset of synapses; larval NMJ synapses do not show the same requirement. One possible explanation may be functional redundancy or differences in synaptic thermal regulation between larval and adult synapses. For unknown reasons,

larva NMJ neurotransmission has proven consistently more resistant to disruption by D*rosophila* TS mutants than the adult (Suzuki et al., 1971; Siddiqi and Benzer, 1976). A second possibility is that RBO may be acutely required at synapses designed to function reliably under conditions of high demand. The central cholinergic and NMJ synapses in the adult *Drosophila* GF circuit can support 100 Hz synaptic transmission (Tanouye and Wyman, 1980; Engel and Wu, 1992; Allen et al., 2000), far beyond the usage or sustainable range of the larval NMJ.

A Role of RBO in SNARE-Dependent Synaptic Vesicle Fusion?

It has been well demonstrated that SNARE complex assembly is essential for vesicle priming, and can directly mediate membrane fusion (Weber et al., 1998; Jahn and Sudhof, 1999; Lin and Scheller, 2000; Sudhof, 2004). In addition, however, studies of yeast vacuolar homotypic fusion (Peters et al., 1999; Peters et al., 2001; Muller et al., 2002; Bayer et al., 2003), and direct studies of exocytosis of neurotransmitter vesicles including SVs (Ciufo et al., 2005; Hiesinger et al., 2005), suggest that an additional machinery may act downstream of the SNARE complex to mediate fusion. Our data suggest that RBO may similarly act downstream of SNARE complex assembly. We propose that RBO may regulate the function of the SV fusion machinery, or may be a novel component of this fusion machinery.

RBO's closest characterized homolog (42% conserved) is an integral plasma membrane sn-1 diacylglycerol (DAG) lipase (Bisogno et al., 2003;

Huang et al., 2004). We recently reported that RBO is essential for PLC-dependent neuronal signaling (Huang et al., 2004). Consistently, following a 10 min shift to 37°C, *rbo* TS mutants display an accumulation of phosphatidylinositol 4,5-bisphosphate (PIP_2) and concomitant reduction of DAG in the brain (Huang et al., 2004). Synaptically localized RBO therefore may regulate the levels of fusogenic lipids (DAG, phosphatidylinositides, polyunsaturated fatty acids) at, or near, AZ fusion sites. These critical lipids may contribute directly to the generation of membrane properties required for SV fusion. Alternatively, these lipids might regulate the activity of lipid-binding fusogenic proteins.

Both lipid partitioning and protein interactions regulate membrane changes to enable fusion. Lipids with compact head groups and space-filling tails, such as PIP_2 and DAG, favor the negative membrane curvature required for vesicle fusion, and both PIP_2 and DAG directly promote Ca^{2+}-dependent exocytosis (Hay et al., 1995; Mayer et al., 2000; Di Paolo et al., 2004). Lipases including PLC, PLD and PLA2 are known to promote secretion through the fusogenic effects of their lipid products (Cohen and Brown, 2001; Vitale et al., 2001; Brown et al., 2003; Wei et al., 2003; Staneva et al., 2004). These lipases have been proposed to increase presynaptic release site availability and/or vesicle fusion efficacy. These activities also coordinate the spatial-temporal regulation of numerous synaptic proteins (Wenk and De Camilli, 2004). SV priming is dependent on UNC-13, which binds DAG (Aravamudan et al., 1999). PIP_2 and DAG are required for the localized enrichment of SNARES and Rab GTPases at

fusion sites (Jun et al., 2004). Other known targets of PIP_2 and DAG include Synaptotagmin 1, and MUNC18-interacting MINT1,2 (Cremona and De Camilli, 2001; Wenk and De Camilli, 2004). Thus, phosphoinositides may play multiple roles in the formation of the SV fusion domain; directly determining membrane properties, serving as a precursor for other fusogenic lipids (DAG) and serving as anchors/regulators for fusogenic proteins.

Conditional removal of RBO activity in TS mutants causes acute DAG depletion and PIP_2 accumulation in the brain (Huang et al., 2004). These changes correlate temporally with the loss of neurotransmission and the arrest of docked SVs at presynaptic AZs. We have yet to develop the technology to determine whether these lipid changes occur locally at the AZ, but the synaptic localization of RBO and the acute requirement of RBO in post-docking SV exocytosis supports this conclusion.

CHAPTER IV

DISCUSSION AND FUTURE DIRECTIONS

An EMS-induced temperature-sensitive paralytic mutant gene, *rolling blackout* (*rbo*), has been conclusively identified with genomic deficiency mapping, transposon-tagging, DNA sequencing and transgenic rescue (Huang et al., 2004). The *rbo* gene expresses at least two transcripts, of 2.9kb and 3.4kb, with an identical 3' region (flybase). The smaller isoform is reported to be ubiquitously expressed throughout development and in adults, but the bigger transcript is much less abundant and is reportedly undetected until the late embryonic stage (Faulkner et al., 1998). Whole-mount *in situ* hybridization analysis in the embryo reveals that *rbo* expression is widespread, with CNS expression higher than in other tissue during the later half embryogenesis, but it is unknown which transcript is enriched in CNS (Faulkner et al., 1998).

Consistent with the high expression of *rbo* mRNA in the CNS, we found that RBO protein is specifically enriched in all CNS synaptic neuropil regions in the embryo and throughout later stages. In the peripheral nervous system, RBO protein is enriched in the cell body of sensory neurons. The subcellular distribution of RBO protein indicates that RBO is enriched in the processes of CNS neurons and the soma of sensory neurons where extensive signal transduction and membrane dynamics occur. The ubiquitous expression of *rbo* smaller transcript throughout development and its reported requirement for cell viability indicate that RBO protein should be present in all cells. However, RBO

is undetectable in the soma of central neurons, and nearly or totally undetectable in non-neuronal cells based on the examination of RBO-eGFP fusion protein in the *rbo* null background. This may be explained by two possibilities. The first is that a ubiquitous RBO isoform does exist, but its C-terminus is not tagged by eGFP. This is extremely unlikely because all identified ESTs (expressed sequence tag, total 61) cloned from many parts of *Drosophila* at different development stages contain the identical 3' region (flybase). The second possibility is that every cell possesses a very low level of RBO-eGFP, which is hard to detect and distinguish from background by examining the fluorescence of RBO-eGFP. This seems the likely explanation and suggests a much more prominent, neural-specific role for RBO.

The *rbo* gene plays an essential role in both phototransduction and synaptic transmission in *Drosophila* (Huang et al., 2004; Huang et al., 2006). However, it is unknown which *rbo* isoform is involved in those two distinct biological processes. To resolve this question, P-element mediated germline transformation can be employed to introduce only the smaller or the bigger isoform into *rbo* TS mutants and examining the TS paralysis and blindness in those mutants.

The *rbo* gene product is predicted to be a multipass integral membrane protein. Consistent with this, RBO protein is strongly associated with plasma membrane, can be labeled by extracellular biotin and can be released from the membrane fraction only by detergent, but not by high pH or a high salt concentration (Huang et al., 2004). The *rbo* gene is conserved from yeast to

human being and all *rbo* homologs were predicted to encode integral membrane proteins (Faulkner et al., 1998). *Drosophila* RBO protein displays about 12% identity to the yeast YM62 protein and 34% identity to mouse KIAA0143 protein. Those two yeast and mouse proteins show the highest homology to *Drosophila* RBO protein (Blast) and are similarly associated with plasma membrane (Huh et al., 2003; Munemoto et al., 2004). *Drosophila* RBO is predicted to be a 2– or 3–pass transmembrane protein containing three catalytic sites of lypolytic enzymes (Faulkner et al., 1998; Huang et al., 2004). However, only in the 2-pass model can the catalytic triad assemble to form the catalytic center of lipolytic enzymes, indicating that RBO is likely a 2–pass transmembrane protein with both N- and C-termini located at cytoplasm. Protease protection assay can be used to determine the topology of RBO protein. Another integral membrane acylglycerol lipase identified in eukaryotic cells is the first sn1-DAG lipase (Bisogno et al., 2003). As integral membrane proteins, both RBO and the first sn1-DAG might be surrounded by a proper lipidic environment or some membrane cofactors, which are required for them to function.

Electrophysiological studies reveal that temperature-sensitive *rbo* mutants display a rapid (minutes), reversible block in both synaptic transmission and phototransduction, indicating that a common RBO-dependent mechanism in these highly divergent neural signaling pathways (Huang et al., 2004; Huang et al., 2006). Fly phototransduction is known to be completely mediated by PLC-dependent PIP_2-DAG signaling, which gates the cationic TRP and TRPL channels (Montell, 1999; Hardie, 2001; Hardie and Raghu, 2001; Hilgemann et

al., 2001; Hardie, 2003). At the synapse, certain excitatory postsynaptic current (EPSC) has been shown to be mediated by TRP-like channels, which are activated through G protein-PLC-PIP_2 signaling , such as TRPC1 mediating the GluR1 (metabotrophic glutmate receptor 1) activation-induced EPSC (Kim et al. 2003; Bengtson et al., 2004). In addition, Ca^{2+} influx through a TRP Channel (TRPC4) may be involved in neurotransmitter release (Munsch et al., 2003).

Apart from a possible conserved TRP regulatory function, PIP_2 and its hydrolysis product DAG also play direct functions in the synaptic vesicle (SV) cycle by regulating essential synaptic proteins, especially proteins involved in SV priming and calcium-dependent fusion, e.g., UNC-13, UNC-18, synaptotagmin and voltage-gated calcium channels (Lackner et al., 1999; Cremona and De Camilli, 2001; Martin, 2001; Brose and Rosenmund, 2002; Rosenmund et al., 2002; Di Paolo et al., 2004; Fratti et al., 2004; Jun et al., 2004; Wenk and De Camilli, 2004; Rohrbough and Broadie, 2005). PIP_2-DAG signaling is involved in both *Drosophila* phototransduction and mammalian/worm synaptic transmission, and, by analogy, likely in *Drosophila* synaptic transmission (Aravamudan and Broadie, 2003).

Disruption of PIP_2-DAG signaling may therefore be the common cause of the acute loss of both synaptic transmission and phototransduction in *rbo* TS mutants. Indeed, *rbo* TS mutants exhibit an activity-dependent depletion of DAG with concomitant accumulation of PIP/PIP_2, and an ERG phenotype reflecting down regulation of PLC activity in phototransduction pathway (Huang et al., 2004). Moreover, RBO protein is most closely related to a predicted DAG lipase

which hydrolyzes DAG into a free fatty acid and monoacylglycerol. Presumably, RBO's enzymatic activity is lost in *rbo* TS mutants at restrictive temperature, resulting in a defect in the regulation of turnover of lipidic components of PIP_2-DAG signaling pathway, and the lipid composition of plasma membrane. Further experiments need to examine the enzymatic activity of PLC and RBO in *rbo* mutants. Biosensors of PLC activity can be used to test this idea. TRPC6 is activated by PLC product DAG (Trebak 2003) and has been successfully used as a biosensor of PLC activity (Delmas, 2002; Kim, 2003; Hashimotodani, 2005). Thus, expression of TRPC6 might possibly be employed for real-time measurements of PLC activity and DAG levels in neurons in *rbo* mutants.

The block of synaptic transmission in *rbo* mutants appears due to a defect during SV priming or fusion (Huang et al., 2006). There are multiple possible explanations for how DAG depletion and PIP/PIP_2 accumulation might produce defective SV priming and fusion in *rbo* TS mutants. First, DAG depletion might cause the impairment of DAG-dependent recruitment and activation of UNC-13. The mammalian UNC13 (MUNC13) has three isoforms, MUNC13-1, 2, and 3; MUNC13-1 is neuron specific, contains one DAG-binding C1 domain and exists in two forms, soluble and insoluble (Brose et al. 1995; Betz et al., 1998 and Betz et al., 2001). In mice, the soluble MUNC13-1 is recruited to plasma membrane and is activated by DAG, and point mutation at the DAG binding C1 domain of MUNC13-1 abolishes the recruitment and activation by membrane DAG or DAG analogs (Betz et al., 1998). Evidences from both mamalian and *C. elegans* show that this interaction is required for SV priming during presynaptic stimulation at

high frequency, but not required for the SV priming under basic synaptic transmission condition (Betz et al., 1998; Lackner et al., 1999; Brose et al., 2002; Rhee et al., 2002; Rosenmund et al., 2002). Whereas the insoluble MUNC13-1 is tightly associated with presynaptic active zone matrix through proteineous linker (interaction with active zone proteins: Rab3 interacting molecule—RIM, cytomatrix of the active zone/proteins of the ELKS/Rab6-interacting protein 2/CAST family—CAST/ERC, and Bassoon) and is proposed to be responsible for DAG-independent SV priming (Betz, 2001; Rhee et al., 2002, Brose et al., 2004). Thus, the DAG depletion in *rbo* mutants may cause a defect in SV priming, specifically activity-dependent fast SV priming.

Second, DAG depletion should block the activation of protein kinase C (PKC), a C1-domain protein activated by DAG binding. PKC phosphorylates many synaptic proteins, including synaptotagmin (Hilfiker et al., 1999; Roggero et al., 2005), voltage-gated Ca^{2+} channel (Catterall, 2000), SNAP-25 (Shimazaki et al., 1996; Ciufo et al., 2005), and MUNC18-1 (Barclay et al., 2003; Ciufo et al., 2005). Particularly, the phosphorylation of SNAP-25 by PKC stimulates the localization of SNAP-25 to the plasma membrane (Iwasaki et al., 2000; Kataoka et al., 2000; Lee et al., 2003) and enhances the interactions of SNAP-25 with syntaxin and synaptotagmin (Shimazaki et al., 1996; Risinger and Bennett, 1999). PKC also potentiates the recruitment of vesicles to the plasma membrane (Nagy et al., 2002; Shoji-Kasai et al., 2002), and enhances the formation of SNARE complex (Lee et al., 2003). The phosphorylation of MUNC18-1 by PKC was suggested to disinhibit sytaxin1A

and regulate the kinetics of fusion pore opening (Fujita et al., 1998; Ciufo et al., 2005). Consistent with the effects of PKC phosphorylation of SNAP-25 and MUNC18-1, inhibition of PKC activity causes a depression of synaptic transmission even under stimulation of very low frequency (0.03Hz) (Rhee et al., 2002). In general, PKC phosphorylates and regulates many fusogenic proteins functioning at multiple stages of SV exocytosis, including facilitating readily releasable pool refilling and fusion downstream of Ca^{2+} (Ciufo et al., 2005). Besides PKC and MUNC13, there are several other uncharacterized C1-domain (DAG binding domain) containing proteins (e. g. DAG kinase ε, PLD, Ras guanyl nucleotide-releasing proteins, Chimaerins), which highly express in mamlian brain and may function in synaptic transmission (Brose et al., 2004). Depletion of DAG may cause down-regulation of these proteins and contribute to the block of exocytosis in *rbo* TS mutants. Antibody specific for the phosphorylated forms of PKC substrates might be used to examine their phosphorylation state in *rbo* TS mutants.

Third, PIP_2 and DAG misregulation may cause a block of Ca^{2+} influx at the presynaptic termini in *rbo* TS mutants at restrictive temperature. The Ca^{2+} influx through voltage-gated Ca^{2+} channel is the trigger of SV exocytosis. PIP_2 has dual, concentration-dependent effects on voltage-gated Ca^{2+} (P/Q type) channels, stimulating at low concentration, and inhibiting at high concentration *in vitro* and *in vivo* (Wu et al., 2002). In addition, Ca^{2+} influx through a TRP Channel (TRPC4) has been shown to be required for the serotonin receptor (type II, 5-HT_2R)-induced release of neurotransmitter from

termini in the dorsal lateral geniculate nucleus (Munsch et al., 2003). The activation of TRPC4 is caused by Gq activation of PLC (Clapham et al., 2005). Thus, the downregulation of PLC activity, accumulation of PIP/PIP_2 can impair the activation of voltage-gated Ca^{2+} channel and TRP channel involved in neurotransmitter release, therefore might block Ca^{2+} influx-induced synaptic transmission in *rbo* TS mutants. Transgenic Ca^{2+} indicators (e.g. cameleon constructs) can be employed to monitor the presynaptic Ca^{2+} in *rbo* TS mutants at restrictive temperature.

Fourth, DAG and its metabolite PUFA (polyunsaturated fatty acid) are "cone-shaped" lipids that directly facilitate the transition of plasma membrane from lamellar to non-lamellar phase by forming negative curvature (Goni and Alonso, 1999). The probability of fusion-pore opening depends on the tension and composition of the participating membranes. The DAG depletion and possible depletion of DAG metabolite PUFA presumably hinders the transition from double layer to non-double layer, and therefore would be predicted to reduce the probability of fusion-pore opening in *rbo* TS mutants.

Fifth, MUNC13-1 contains both C1 and C2 domains, which can bind to DAG and PIP_2 respectively. Its function may depend on the coordinate effects of PIP_2 and DAG binding, in either a parallel or a sequential mode. In the parallel mode, both lipids simultaneously bind to C1 and C2 domain containing protein and target it to plasma membrane. In the sequential mode, PIP_2 first binds to the C2 domain for AZ membrane targeting, then PIP_2 is hydrolyzed to produce DAG, which binds to C1 domain to activate the

recruited protein. Misregulation of PIP_2/DAG level, particularly caused by down-regulation of PLC activity may disrupt the coordination, and disrupt the function of C1 and C2 domain containing protein in SV exocytosis. This possibility is pure speculation, and I am aware of no available assay can be employed to test it.

Consistent with the role of RBO in the SV priming or fusion, the *rbo* TS mutant displays a strong synergistic interaction with the *syntaxin* 1A TS mutant (Huang et al., 2006). This interaction predicts that RBO and Syntaxin act in the same pathway, or a parallel pathway, required for neurotransmitter release. Syntaxin 1A assembles with SNAP25 and Synaptobrevin to form SNARE complex and drive SV fusion with presynaptic plasma membrane (Sollner et al., 1993; Weber et al., 1998; Sudhof, 2004). The *syntaxin* 1A TS mutation results in a defect in the formation of SNARE complex (Littleton et al., 1999). If RBO and Sytaxin 1A function in the same pathway, RBO protein may act in the same pathway involving SNARE complex formation. However, total SNARE complex abundance in *rbo; syntaxin* 1A double TS mutant is not detectably altered relative to the *sytaxin 1A* TS mutants at restrictive temperature, suggesting that RBO is not directly involved in SNARE complex formation. RBO may therefore act downstream of SNARE complex assembly or in a parallel pathway. In addition to the function in SNARE complex formation, Syntaxin 1A was recently suggested to form a part of the fusion pore through the polymerization of its transmembrane segment, and other protein or lipid may intercalate between the Syntaxin 1A segments to form the

pore across the pasma membrane (Han et al, 2004). Thus, it is possible that RBO might play a role in the formation of fusion pore by either directly interacting with Syntaxin 1A as a component or an accessory of the fusion pore, or indirectly interacting with syntaxin 1A by regulating or generating the production of a required lipid cofactor. Indeed, PIP, DAG and other lipids have been shown to accumulate at the “vertex”, which is the ring-shaped periphery of the boundary membrane of the opposed membranes of docked yeast vacuoles engaging homotypic SNARE-mediated fusion (Fratti et al., 2004), and DAG accumulation at vertex requires PLC (Jun et al., 2004). The experiments performed in Jun et al. (2004) can be borrowed to test these possibilites. Briefly, the experimental design would co-express wildtype or the TS mutant form of RBO with syntaxin 1A in PC12 cells and examine the flux of norepinephorine during single vesicle fusion, and also the effect of the manipulation of PLC activity on the norephinephorine flux through the fusion pore in this assay.

It should be pointed out that activity-dependent depletion of DAG and the accumulation of PIP/PIP_2 has to date only been analyzed at the whole brain level (Huang et al., 2004). We still need to examine whether these lipidic changes happen at presynaptic terminus, as predicted. In addition, electrospray ionization mass spectrometry analysis and other assays have indicated that PIP/PIP_2 possess many isomers with different fatty acid compositions (Fournier et al., 1995; Tsegaye et al., 2002; Wenk and Decamilli, 2003; Milne et al., 2005). Our measurement of PIP/PIP_2 and DAG

does not distinguish the change in the individual species of each one. It is important to resolve this issue because 1) different PIP/PIP_2 and DAG species have different biological activity (Meves, H, 1994; Chyb et al., 1999; Wenk and De Camilli, 2004), 2) the activities of PLC and DAG kinase are regulated by the acyl chain of these lipids (Rebecchi et al., 1993; Carricaburu and Fournier, 2001). Therefore, one likely possibility for RBO function is that it might regulate acyl chain composition of a PIP lipid substrate upstream of PLC activity in neurons.

Given PIP/PIP_2 accumulation and DAG depletion in the *rbo* mutant, the simplest hypothesis for the molecular role of RBO is that of a phosphoinositide lipase directly hydrolyzing PIP/PIP_2 into DAG. However, the PLC mediating this function in *Drosophila* phototransduction is already known. Therefore, an alternative hypothesis is that the RBO lipase produces a factor required for PLC function in both phototransduction and synaptic transmission. Given that RBO is most closely homologous to the first described cellular sn1-DAG lipase (Huang et al., 2004), and that DAG lipase product PUFA is a known stimulator of PLC (Meves, 1994), disruption of PUFA production is a plausible model. The role of PUFAs in synaptic transmission has been demonstrated by the effect of mutation of FAT-3 gene encoding a fatty acid desaturase essential for the production of PUFAs (Watts and Browse, 2002) on the neurosecretion in C. elegans (Lesa et al., 2003), and by the stimulation of massive SV release by presynaptic neurotoxins with PLA_2 activity which releases PUFA from phosphoinositides (Montecucco and Rossetto, 2000). SVs were found to contain

a very high level of PUFAs, particularly docosahexaenoic acid (20:6), which are protonated inside the acidic SV lumen, and rapidly flip-flop to the cytosolic leaflet, rendering SVs fusogenic (Deutsch and Kelly, 1981; Michaelson et al., 1983; Kamp et al., 1995; Montecucco and Rossetto, 2000).

PUFAs stimulate PLC gamma in the mammalian hippocampus, enhancing glutamate release from presynaptic termini (McGahon and Lynch, 1998). PUFAs also act as regulatory lipids in the SV cycle (Montecucco and Rossetto, 2000; Wenk and De Camilli, 2004). To test the hypothesis that RBO is a DAG lipase, purified RBO protein from cell lines or transgenic animals can be used to test its lipase activity with para-nitrophenol, which can be cleaved by all lipolytic enzymes (Gupta et al., 2003). RBO is an integral plasma membrane protein (Huang et al., 2004), it may require a proper lipidic environment or some cofactors to function. Thus, the purified RBO protein may be required to be integrated into a double layer membrane with a similar lipid composition as the plasma membrane of cells or neurons. Then, different lipids, particularly different species of phosphoinositides and DAGs can be used to test the specificity of RBO enzymatic activity, and determine its preferred or endogenous substrate, and product. When this is done, RBO enzymatic activity in *rbo* mutants can be explored by monitoring the levels of its specific substrate and product at both permissive and non-permissive temperature with mass spectrometry or high performance layer chromatography (HPLC).

Other than being a putative DAG lipase, RBO could be a lipolytic enzyme involved in the regulation of the acyl chain composition of phosphoinositides. It

has been shown that the acyl chain composition (e.g. the length of the acyl chain and the unsaturated bonds) of PIP_2 plays a critical role in the regulation of the PLC activity in mammals (Rebecchi et al., 1993; Carricaburu and Fournier, 2001). There are many species of phosphoinositides based on the profile of acyl chain composition of posphoinositides (Wenk et al., 2003). However, there is no correlation between the number of unsaturated ester bond or acyl chain length and their effects on PLC activity (Rebecchi et al., 1993; Carricaburu and Fournier, 2001). At restrictive temperature in *rbo* mutants, there may be a change in acyl chain composition of PIP_2, subsequently compromise the activity of PLC. To test this possibility, a PLC activity biosensor can be employed to monitor the PLC activity in *rbo* TS mutants, and mass spectrometry can be used to profile the fatty acyl chain composition of phosphoinostides in some neurons *rbo* TS mutants, particularly photoreceptor cells.

A fascinating aspect of *rbo*-TS mutant phototransduction block is that it is activity-dependent; mutant signal transduction rapidly recovers (minutes) in the dark. However, the loss of mutant synaptic transmission is not clearly activity dependent, because double $para^{ts1}$; rbo^{ts1} mutant display a similar recovery kinetics after 5 min exposure to 37^{o}C, indicating that synaptic transmission block occurs in *rbo* TS mutants under (presumably) no neuronal electrical activity. One possible explanation is that there is an alternative source for generating the RBO-dependent factor in photoreceptors, but this process is rate-limiting and unable to support the constant demand during fly phototransduction. Thus the requirement for RBO is activity-dependent. In larva NMJ synapses which do not

show a TS mutant phenotype, this source may be sufficient to support normal synaptic transmission. For example, if RBO is a sn2-DAG lipase and release the sn2 acyl chain from DAG, then the newly cloned sn1-DAG lipase which also releases sn2 fatty acid with less efficience can compensate for the loss of RBO sn2 activity in *rbo* TS mutants.

In summary, RBO is hereby identified as a putative DAG lipase and shown to be essential for both phototransduction and synaptic transmission in *Drosophila*. Further experiments need to 1) conclusively test the predicted lipase enzymatic activity, 2) determine the presumed endogenous lipid substrate and lipid product, 3) obtain direct evidence proving that RBO regulates PLC-PIP_2 signaling at the synapse and 4) provide mechanistic insight into the interaction between RBO and the T-SNARE Syntaxin 1A.

References

Acharya JK, Jalink K, Hardy RW, Hartenstein V, Zuker CS (1997) InsP3 receptor is essential for growth and differentiation but not for vision in Drosophila. Neuron 18:881-887.

Agam K, von Campenhausen M, Levy S, Ben-Ami HC, Cook B, Kirschfeld K, Minke B (2000) Metabolic stress reversibly activates the Drosophila light-sensitive channels TRP and TRPL in vivo. J Neurosci 20:5748-5755.

Ahmed S, Maruyama IN KR, Lee J, Brenner S, Lim L. (1992) The Caenorhabditis elegans unc-13 gene product is a phospholipid-dependent high-affinity phorbol ester receptor. Biochem J 287:995-999.

Allen MJ, Shan X, Murphey RK (2000) A role for Drosophila Drac1 in neurite outgrowth and synaptogenesis in the giant fiber system. Mol Cell Neurosci 16:754-765.

An SJ, Almers W (2004) Tracking SNARE complex formation in live endocrine cells. Science 306:1042-1046.

Aravamudan B, Fergestad T, Davis WS, Rodesch CK, Broadie K (1999) Drosophila UNC-13 is essential for synaptic transmission. Nat Neurosci 2:965-971.

Ashery U, Varoqueaux F, Voets T, Betz A, Thakur P, Koch H, Neher E, Brose N, Rettig J (2000) Munc13-1 acts as a priming factor for large dense-core vesicles in bovine chromaffin cells. EMBO J 19:3586-3596.

Augustin I, Rosenmund C, Sudhof TC, Brose N (1999) Munc13-1 is essential for fusion competence of glutamatergic synaptic vesicles. Nature 400:457-461.

Barbara J (2002) IP3-dependent calcium-induced calcium release mediates bidirectional calcium waves in neurones: functional implications for synaptic plasticity. Biochim Biophys Acta 1600:12-28.

Barclay JW, Craig TJ, Fisher RJ, Ciufo LF, Evans GJ, Morgan A, Burgoyne RD (2003) Phosphorylation of Munc18 by protein kinase C regulates the kinetics of exocytosis. J Biol Chem 278:10538-10545.

Barylko B, Binns D, Lin KM, Atkinson MA, Jameson DM, Yin HL, Albanesi JP (1998) Synergistic activation of dynamin GTPase by Grb2 and phosphoinositides. J Biol Chem 273:3791-3797.

Bayer MJ, Reese C, Buhler S, Peters C, Mayer A (2003) Vacuole membrane fusion: V0 functions after trans-SNARE pairing and is coupled to the Ca2+-releasing channel. J Cell Biol 162:211-222.

Belote JM, Lucchesi JC (1980) Male-specific lethal mutations of Drosophila melanogaster. Genetics 96:165-186.

Benesch S, Lommel S, Steffen A, Stradal TE, Scaplehorn N, Way M, Wehland J, Rottner K (2002) Phosphatidylinositol 4,5-biphosphate (PIP2)-induced vesicle movement depends on N-WASP and involves Nck, WIP, and Grb2. J Biol Chem 277:37771-37776.

Bengtson CP, Tozzi A, Bernardi G, Mercuri NB (2004) Transient receptor potential-like channels mediate metabotropic glutamate receptor EPSCs in rat dopamine neurones. J Physiol 555:323-330.

Benham CD, Davis JB, Randall AD (2002) Vanilloid and TRP channels: a family of lipid-gated cation channels. Neuropharmacology 42:873-888.

Bennett MK, Scheller RH (1993) The molecular machinery for secretion is conserved from yeast to neurons. Proc Natl Acad Sci U S A 90:2559-2563.

Berridge MJ (1993) Inositol trisphosphate and calcium signalling. Nature 361:315-325.

Berridge MJ, Bootman MD, Roderick HL (2003) Calcium signalling: dynamics, homeostasis and remodelling. Nat Rev Mol Cell Biol 4:517-529.

Betz A, Okamoto M, Benseler F, Brose N (1997) Direct interaction of the rat unc-13 homologue Munc13-1 with the N terminus of syntaxin. J Biol Chem 272:2520-2526.

Betz A, Ashery U, Rickmann M, Augustin I, Neher E, Sudhof TC, Rettig J, Brose N (1998) Munc13-1 is a presynaptic phorbol ester receptor that enhances neurotransmitter release. Neuron 21:123-136.

Betz A, Thakur P, Junge HJ, Ashery U, Rhee JS, Scheuss V, Rosenmund C, Rettig J, Brose N (2001) Functional interaction of the active zone proteins Munc13-1 and RIM1 in synaptic vesicle priming. Neuron 30:183-196.

Bisogno T, Howell F, Williams G, Minassi A, Cascio MG, Ligresti A, Matias I, Schiano-Moriello A, Paul P, Williams EJ, Gangadharan U, Hobbs C, Di Marzo V, Doherty P (2003) Cloning of the first sn1-DAG lipases points to the spatial and temporal regulation of endocannabinoid signaling in the brain. J Cell Biol 163:463-468.

Blackmer T, Larsen EC, Bartleson C, Kowalchyk JA, Yoon EJ, Preininger AM, Alford S, Hamm HE, Martin TF (2005) G protein betagamma directly regulates SNARE protein fusion machinery for secretory granule exocytosis. Nat Neurosci 8:421-425.

Bligh EG, Dyer WJ (1959) A rapid method of total lipid extraction and purification. Can J Med Sci 37:911-917.

Bloomquist BT, Shortridge RD, Schneuwly S, Perdew M, Montell C, Steller H, Rubin G, Pak WL (1988) Isolation of a putative phospholipase C gene of Drosophila, norpA, and its role in phototransduction. Cell 54:723-733.

Bowlby MR, Levitan IB (1995) Block of cloned voltage-gated potassium channels by the second messenger diacylglycerol independent of protein kinase C. J Neurophysiol 73:2221-2229.

Broadie K (2000) Functional assays of the peripheral and central nervous systems. In: Drosophila Protocols (Sullivan W AM, Hawley RS, ed), p 297–312. New York: Cold Spring Harbor laboratory Press.

Brose N, Rosenmund C (2002) Move over protein kinase C, you've got company: alternative cellular effectors of diacylglycerol and phorbol esters. J Cell Sci 115:4399-4411.

Brose N, Betz A, Wegmeyer H (2004) Divergent and convergent signaling by the diacylglycerol second messenger pathway in mammals. Curr Opin Neurobiol 14:328-340.

Brose N, Hofmann K, Hata Y, Sudhof TC (1995) Mammalian homologues of Caenorhabditis elegans unc-13 gene define novel family of C2-domain proteins. J Biol Chem 270:25273-25280.

Brown WJ, Chambers K, Doody A (2003) Phospholipase A2 (PLA2) enzymes in membrane trafficking: mediators of membrane shape and function. Traffic 4:214-221.

Carricaburu V and Fournier B (2001) Phosphoinositide fatty acids regulate phospholipase C and protein kinase C activities. Eur J Biochem 268:1238-1249.

Catterall WA (2000) Structure and regulation of voltage-gated Ca2+ channels. Annu Rev Cell Dev Biol 16:521-555.

Chandrashekaran S (1993) Mutations at the *stm A* locus of *Drosophila* melanogaster confer resistance to the sodium channel neuropoison veratridine. current science 65:80-82.

Chen X, Tomchick DR, Kovrigin E, Arac D, Machius M, Sudhof TC, Rizo J (2002) Three-dimensional structure of the complexin/SNARE complex. Neuron 33:397-409.

Chen YA, Scheller RH (2001) SNARE-mediated membrane fusion. Nat Rev Mol Cell Biol 2:98-106.

Chheda MG, Ashery U, Thakur P, Rettig J, Sheng ZH (2001) Phosphorylation of Snapin by PKA modulates its interaction with the SNARE complex. Nat Cell Biol 3:331-338.

Chyb S, Raghu P, Hardie RC (1999) Polyunsaturated fatty acids activate the Drosophila light-sensitive channels TRP and TRPL. Nature 397:255-259.

Ciufo LF, Barclay JW, Burgoyne RD, Morgan A (2005) Munc18-1 regulates early and late stages of exocytosis via syntaxin-independent protein interactions. Mol Biol Cell 16:470-482.

Clapham DE, Runnels LW, Strubing C (2001) The TRP ion channel family. Nat Rev Neurosci 2:387-396.

Cohen JS, Brown HA (2001) Phospholipases stimulate secretion in RBL mast cells. Biochemistry 40:6589-6597.

Constable JR, Graham ME, Morgan A, Burgoyne RD (2005) Amisyn regulates exocytosis and fusion pore stability by both syntaxin-dependent and syntaxin-independent mechanisms. J Biol Chem 280:31615-31623.

Cosens DJ, Manning A (1969) Abnormal electroretinogram from a Drosophila mutant. Nature 224:285-287.

Cremona O, De Camilli P (1997) Synaptic vesicle endocytosis. Curr Opin Neurobiol 7:323-330.

Cremona O, De Camilli P (2001) Phosphoinositides in membrane traffic at the synapse. J Cell Sci 114:1041-1052.

Cremona O, Di Paolo G, Wenk MR, Luthi A, Kim WT, Takei K, Daniell L, Nemoto Y, Shears SB, Flavell RA, McCormick DA, P. DC (1999) Essential role of phosphoinositide metabolism in synaptic vesicle recycling. Cell 99:179-188.

Dellinger B, Felling R, Ordway RW (2000) Genetic modifiers of the Drosophila NSF mutant, comatose, include a temperature-sensitive paralytic allele of the calcium channel alpha1-subunit gene, cacophony. Genetics 155:203-211.

Delmas P, Wanaverbecq N, Abogadie FC, Mistry M, Brown DA (2002) Signaling microdomains define the specificity of receptor-mediated InsP(3) pathways in neurons. Neuron 34:209-220.

Deutsch JW, Kelly RB (1981) Lipids of synaptic vesicles: relevance to the mechanism of membrane fusion. Biochemistry 20:378-385.

Di Paolo G, Moskowitz HS, Gipson K, Wenk MR, Voronov S, Obayashi M, Flavell R, Fitzsimonds RM, Ryan TA, De Camilli P (2004) Impaired PtdIns(4,5)P2 synthesis in nerve terminals produces defects in synaptic vesicle trafficking. Nature 431:415-422.

Dubnau J, Grady L, Kitamoto T, Tully T (2001) Disruption of neurotransmission in Drosophila mushroom body blocks retrieval but not acquisition of memory. Nature 411:476-480.

Dulubova I, Sugita S, Hill S, Hosaka M, Fernandez I, Sudhof TC, Rizo J (1999) A conformational switch in syntaxin during exocytosis: role of munc18. EMBO J 18:4372-4382.

Elkins T, Ganetzky B (1990) Conduction in the giant nerve fiber pathway in temperature-sensitive paralytic mutants of Drosophila. J Neurogenet 6:207-219.

Engel JE, Wu CF (1992) Interactions of membrane excitability mutations affecting potassium and sodium currents in the flight and giant fiber escape systems of Drosophila. J Comp Physiol [A] 171:93-104.

Estacion M, Sinkins WG, Schilling WP (2001) Regulation of Drosophila transient receptor potential-like (TrpL) channels by phospholipase C-dependent mechanisms. J Physiol 530:1-19.

Faulkner DL, Dockendorff TC, Jongens TA (1998) Clonal analysis of cmp44E, which encodes a conserved putative transmembrane protein, indicates a requirement for cell viability in Drosophila. Dev Genet 23:264-274.

Fergestad T, Broadie K (2001) Interaction of stoned and synaptotagmin in synaptic vesicle endocytosis. J Neurosci 21:1218-1227.

Ferro-Novick S, Jahn R (1994) Vesicle fusion from yeast to man. Nature 370:191-193.

Foletti DL, Blitzer JT, Scheller RH (2001) Physiological modulation of rabphilin phosphorylation. J Neurosci 21:5473-5483.

Fotin A, Cheng Y, Grigorieff N, Walz T, Harrison SC, Kirchhausen T (2004a) Structure of an auxilin-bound clathrin coat and its implications for the mechanism of uncoating. Nature 432:649-653.

Fotin A, Cheng Y, Sliz P, Grigorieff N, Harrison SC, Kirchhausen T, Walz T (2004b) Molecular model for a complete clathrin lattice from electron cryomicroscopy. Nature 432:573-579.

Fratti RA, Jun Y, Merz AJ, Margolis N, Wickner W (2004) Interdependent assembly of specific regulatory lipids and membrane fusion proteins into the vertex ring domain of docked vacuoles. J Cell Biol 167:1087-1098.

Fujita Y, Shirataki H, Sakisaka T, Asakura T, Ohya T, Kotani H, Yokoyama S, Nishioka H, Matsuura Y, Mizoguchi A, Scheller RH, Takai Y (1998) Tomosyn: a syntaxin-1-binding protein that forms a novel complex in the neurotransmitter release process. Neuron 20:905-915.

Fujita Y, Sasaki T, Fukui K, Kotani H, Kimura T, Hata Y, Sudhof TC, Scheller RH, Takai Y (1996) Phosphorylation of Munc-18/n-Sec1/rbSec1 by protein kinase C: its implication in regulating the interaction of Munc-18/n-Sec1/rbSec1 with syntaxin. J Biol Chem 271:7265-7268.

Fukami K, Matsuoka K, Nakanishi O, Yamakawa A, Kawai S, Takenawa T (1988) Antibody to phosphatidylinositol 4,5-bisphosphate inhibits oncogene-induced mitogenesis. Proc Natl Acad Sci U S A 85:9057-9061.

Fournier B, Wolff RL, Nogaro M, Radallah D, Darret D, Larrue J and Girardie A. (1995) Fatty acid composition of phospholipids and metabolism in rectal tissues of the African locust. Comp Biochem Physio 111B:361-370.

Fykse EM (1998) Depolarization of cerebellar granule cells increases phosphorylation of rabphilin-3A. J Neurochem 71:1661-1669.

Gad H, Ringstad N, Low P, Kjaerulff O, Gustafsson J, Wenk M, Di Paolo G, Nemoto Y, Crun J, Ellisman MH, De Camilli P, Shupliakov O, Brodin L (2000) Fission and uncoating of synaptic clathrin-coated vesicles are perturbed by disruption of interactions with the SH3 domain of endophilin. Neuron 27:301-312.

Gareus R, Di Nardo A, Rybin V, Witke W (2005) Mouse profilin 2 regulates endocytosis and competes with SH3-ligand binding to dynamin 1. J Biol Chem.

Geppert M, Archer BT, 3rd, Sudhof TC (1991) Synaptotagmin II. A novel differentially distributed form of synaptotagmin. J Biol Chem 266:13548-13552.

Gerachshenko T, Blackmer T, Yoon EJ, Bartleson C, Hamm HE, Alford S (2005) Gbetagamma acts at the C terminus of SNAP-25 to mediate presynaptic inhibition. Nat Neurosci 8:597-605.

Goni FM, Alonso A (1999) Structure and functional properties of diacylglycerols in membranes. Prog Lipid Res 38:1-48.

Greengard P, Benfenati F, Valtorta F (1994) Synapsin I, an actin-binding protein regulating synaptic vesicle traffic in the nerve terminal. Adv Second Messenger Phosphoprotein Res 29:31-45.

Grigliatti TA, Hall L, Rosenbluth R, Suzuki DT (1973) Temperature-sensitive mutations in Drosophila melanogaster. XIV. A selection of immobile adults. Mol Gen Genet 120:107-114.

Han X, Jackson MB (2005) Electrostatic interactions between the syntaxin membrane anchor and neurotransmitter passing through the fusion pore. Biophys J 88:L20-22.

Han X, Wang CT, Bai J, Chapman ER, Jackson MB (2004) Transmembrane segments of syntaxin line the fusion pore of Ca2+-triggered exocytosis. Science 304:289-292.

Hardie RC (2001) Phototransduction in Drosophila melanogaster. J Exp Biol 204:3403-3409.

Hardie RC (2003) Regulation of trp channels via lipid second messengers. Annu Rev Physiol 65:735-759.

Hardie RC, Minke B (1992) The trp gene is essential for a light-activated Ca2+ channel in Drosophila photoreceptors. Neuron 8:643-651.

Hardie RC, Raghu P (2001) Visual transduction in Drosophila. Nature 413:186-193.

Hardie RC, Raghu P, Moore S, Juusola M, Baines RA, Sweeney ST (2001) Calcium influx via TRP channels is required to maintain PIP2 levels in Drosophila photoreceptors. Neuron 30:149-159.

Hardie RC, Peretz A, Suss-Toby E, Rom-Glas A, Bishop SA, Selinger Z, Minke B (1993) Protein kinase C is required for light adaptation in Drosophila photoreceptors. Nature 363:634-637.

Harris TW, Hartwieg E, Horvitz HR, Jorgensen EM (2000) Mutations in synaptojanin disrupt synaptic vesicle recycling. J Cell Biol 150:589-600.

Hashimotodani Y, Ohno-Shosaku T, Tsubokawa H, Ogata H, Emoto K, Maejima T, Araishi K, Shin HS, Kano M (2005) Phospholipase Cbeta serves as a coincidence detector through its Ca2+ dependency for triggering retrograde endocannabinoid signal. Neuron 45:257-268.

Hay JC, Fisette PL, Jenkins GH, Fukami K, Takenawa T, Anderson RA, Martin TF (1995) ATP-dependent inositide phosphorylation required for Ca(2+)-activated secretion. Nature 374:173-177.

Hiesinger PR, Fayyazuddin A, Mehta SQ, Rosenmund T, Schulze KL, Zhai RG, Verstreken P, Cao Y, Zhou Y, Kunz J, Bellen HJ (2005) The v-ATPase V0 subunit a1 is required for a late step in synaptic vesicle exocytosis in Drosophila. Cell 121:607-620.

Hilfiker S, Pieribone VA, Nordstedt C, Greengard P, Czernik AJ (1999) Regulation of synaptotagmin I phosphorylation by multiple protein kinases. J Neurochem 73:921-932.

Hilgemann DW, Feng S, Nasuhoglu C (2001) The complex and intriguing lives of PIP2 with ion channels and transporters. Sci STKE 2001:RE19.

Hosaka M, Hammer RE, Sudhof TC (1999) A phospho-switch controls the dynamic association of synapsins with synaptic vesicles. Neuron 24:377-387.

Hotta Y, Benzer S (1969) Abnormal electroretinograms in visual mutants of Drosophila. Nature 222:354-356.

Huang FD, Woodruff E, Mohrmann R, Broadie K (2006) Rolling Blackout is required for synaptic vesicle exocytosis in Drosophila. J Neurosci in press.

Huang FD, Matthies HJ, Speese SD, Smith MA, Broadie K (2004) Rolling blackout, a newly identified PIP2-DAG pathway lipase required for Drosophila phototransduction. Nat Neurosci 7:1070-1078.

Huber A, Sander P, Bahner M, Paulsen R (1998) The TRP Ca2+ channel assembled in a signaling complex by the PDZ domain protein INAD is phosphorylated through the interaction with protein kinase C (ePKC). FEBS Lett 425:317-322.

Huh WK, Falvo JV, Gerke LC, Carroll AS, Howson RW, Weissman JS, O'Shea EK (2003) Global analysis of protein localization in budding yeast. Nature 425:686-691.

Hunt JM, Bommert K, Charlton MP, Kistner A, Habermann E, Augustine GJ, Betz H (1994) A post-docking role for synaptobrevin in synaptic vesicle fusion. Neuron 12:1269-1279.

Hussain NK, Jenna S, Glogauer M, Quinn CC, Wasiak S, Guipponi M, Antonarakis SE, Kay BK, Stossel TP, Lamarche-Vane N, McPherson PS (2001) Endocytic protein intersectin-l regulates actin assembly via Cdc42 and N-WASP. Nat Cell Biol 3:927-932.

Huttner WB, Schmidt AA (2002) Membrane curvature: a case of endofeelin'. Trends Cell Biol 12:155-158.

Ikeda K, Koenig JH (1988) Morphological identification of the motor neurons innervating the dorsal longitudinal flight muscle of Drosophila melanogaster. J Comp Neurol 273:436-444.

Ilardi JM, Mochida S, Sheng ZH (1999) Snapin: a SNARE-associated protein implicated in synaptic transmission. Nat Neurosci 2:119-124.

Inoue H, Yoshioka T, Hotta Y (1985) A genetic study of inositol trisphosphate involvement in phototransduction using Drosophila mutants. Biochem Biophys Res Commun 132:513-519.

Inoue H, Yoshioka T, Hotta Y (1989) Diacylglycerol kinase defect in a Drosophila retinal degeneration mutant rdgA. J Biol Chem 264:5996-6000.

Iwasaki S, Kataoka M, Sekiguchi M, Shimazaki Y, Sato K, Takahashi M (2000) Two distinct mechanisms underlie the stimulation of neurotransmitter release by phorbol esters in clonal rat pheochromocytoma PC12 cells. J Biochem (Tokyo) 128:407-414.

Jackson FR, Wilson SD, Hall LM (1986) The tip-E mutation of Drosophila decreases saxitoxin binding and interacts with other mutations affecting nerve membrane excitability. J Neurogenet 3:1-17.

Jahn R (2004) Principles of exocytosis and membrane fusion. Ann N Y Acad Sci 1014:170-178.

Jahn R, Sudhof TC (1999) Membrane fusion and exocytosis. Annu Rev Biochem 68:863-911.

Jahn R, Lang T, Sudhof TC (2003) Membrane fusion. Cell 112:519-533.

Jenkins GH, Fisette PL, Anderson RA (1994) Type I phosphatidylinositol 4-phosphate 5-kinase isoforms are specifically stimulated by phosphatidic acid. J Biol Chem 269:11547-11554.

Jordan R, Lemke EA, Klingauf J (2005) Visualization of synaptic vesicle movement in intact synaptic boutons using fluorescence fluctuation spectroscopy. Biophys J 89:2091-2102.

Jun Y, Fratti RA, Wickner W (2004) Diacylglycerol and its formation by phospholipase C regulate Rab- and SNARE-dependent yeast vacuole fusion. J Biol Chem 279:53186-53195.

Juusola M, Hardie RC (2001) Light adaptation in Drosophila photoreceptors: II. Rising temperature increases the bandwidth of reliable signaling. J Gen Physiol 117:27-42.

Kamp F, Zakim D, Zhang F, Noy N, Hamilton JA (1995) Fatty acid flip-flop in phospholipid bilayers is extremely fast. Biochemistry 34:11928-11937.

Kataoka M, Kuwahara R, Iwasaki S, Shoji-Kasai Y, Takahashi M (2000) Nerve growth factor-induced phosphorylation of SNAP-25 in PC12 cells: a possible involvement in the regulation of SNAP-25 localization. J Neurochem 74:2058-2066.

Kawasaki F, Ordway RW (1999) The Drosophila NSF protein, dNSF1, plays a similar role at neuromuscular and some central synapses. J Neurophysiol 82:123-130.

Kawasaki F, Mattiuz AM, Ordway RW (1998) Synaptic physiology and ultrastructure in comatose mutants define an in vivo role for NSF in neurotransmitter release. J Neurosci 18:10241-10249.

Kawasaki F, Felling R, Ordway RW (2000) A temperature-sensitive paralytic mutant defines a primary synaptic calcium channel in Drosophila. J Neurosci 20:4885-4889.

Kazanietz M, Bustelo XR BM, Kolch W, Mischak H, Wong G, Pettit GR, Bruns JD, Blumberg PM. (1994) Zinc finger domains and phorbol ester pharmacophore. Analysis of binding to mutated form of protein kinase C zeta and the vav and c-raf proto-oncogene products. J Biol Chem 269:11590-11594.

Kazanietz M, Lewin NE, Bruns JD, Blumberg PM. (1995a) Characterization of the cysteine-rich region of the Caenorhabditis elegans protein Unc-13 as a high affinity phorbol ester receptor. Analysis of ligand-binding interactions,

lipid cofactor requirements, and inhibitor sensitivity. J Biol Chem 270:10777-10783.

Kazanietz MG, Wang S, Milne G, Lewin NE, Liu HL, PM. B (1995b) Residues in the second cysteine-rich region of protein kinase C delta relevant to phorbol ester binding as revealed by site-directed mutagenesis. J Biol Chem 270:21852-21859.

Kessels MM, Qualmann B (2002) Syndapins integrate N-WASP in receptor-mediated endocytosis. Embo J 21:6083-6094.

Kessels MM, Engqvist-Goldstein AE, Drubin DG, Qualmann B (2001) Mammalian Abp1, a signal-responsive F-actin-binding protein, links the actin cytoskeleton to endocytosis via the GTPase dynamin. J Cell Biol 153:351-366.

Kidokoro Y, Kuromi H, Delgado R, Maureira C, Oliva C, Labarca P (2004) Synaptic vesicle pools and plasticity of synaptic transmission at the Drosophila synapse. Brain Res Brain Res Rev 47:18-32.

Kim SJ, Kim YS, Yuan JP, Petralia RS, Worley PF, Linden DJ (2003) Activation of the TRPC1 cation channel by metabotropic glutamate receptor mGluR1. Nature 426:285-291.

King DG, Wyman RJ (1980) Anatomy of the giant fibre pathway in Drosophila. I. Three thoracic components of the pathway. J Neurocytol 9:753-770.

Kitamoto T, Xie X, Wu CF, Salvaterra PM (2000) Isolation and characterization of mutants for the vesicular acetylcholine transporter gene in Drosophila melanogaster. J Neurobiol 42:161-171.

Koenig JH, Ikeda K (1996) Synaptic vesicles have two distinct recycling pathways. J Cell Biol 135:797-808.

Koenig JH, Saito K, Ikeda K (1983) Reversible control of synaptic transmission in a single gene mutant of Drosophila melanogaster. J Cell Biol 96:1517-1522.

Kumar M, Joseph M, Chandrashekaran S (2001) Effects of mutations at the stambh A locus of Drosophila melanogaster. J Genet 80:83-95.

Kuromi H, Kidokoro Y (1998) Two distinct pools of synaptic vesicles in single presynaptic boutons in a temperature-sensitive Drosophila mutant, shibire. Neuron 20:917-925.

Lackner MR, Nurrish SJ, Kaplan JM (1999) Facilitation of synaptic transmission by EGL-30 Gqalpha and EGL-8 PLCbeta: DAG binding to UNC-13 is required to stimulate acetylcholine release. Neuron 24:335-346.

Lee A, Frank DW, Marks MS, Lemmon MA (1999) Dominant-negative inhibition of receptor-mediated endocytosis by a dynamin-1 mutant with a defective pleckstrin homology domain. Curr Biol 9:261-264.

Lee E, De Camilli P (2002) Dynamin at actin tails. Proc Natl Acad Sci U S A 99:161-166.

Lee SJ, Xu H, Kang LW, Amzel LM, Montell C (2003) Light adaptation through phosphoinositide-regulated translocation of Drosophila visual arrestin. Neuron 39:121-132.

Lenburg ME, O'Shea EK (2001) Genetic evidence for a morphogenetic function of the Saccharomyces cerevisiae Pho85 cyclin-dependent kinase. Genetics 157:39-51.

Lesa GM, Palfreyman M, Hall DH, Clandinin MT, Rudolph C, Jorgensen EM, Schiavo G (2003) Long chain polyunsaturated fatty acids are required for efficient neurotransmission in C. elegans. J Cell Sci 116:4965-4975.

Lin RC, Scheller RH (1997) Structural organization of the synaptic exocytosis core complex. Neuron 19:1087-1094.

Lin RC, Scheller RH (2000) Mechanisms of synaptic vesicle exocytosis. Annu Rev Cell Dev Biol 16:19-49.

Littleton JT, Chapman ER, Kreber R, Garment MB, Carlson SD, Ganetzky B (1998) Temperature-sensitive paralytic mutations demonstrate that synaptic exocytosis requires SNARE complex assembly and disassembly. Neuron 21:401-413.

Liu M, Parker LL, Wadzinski BE, Shieh BH (2000) Reversible phosphorylation of the signal transduction complex in Drosophila photoreceptors. J Biol Chem 275:12194-12199.

Loughney K, Kreber R, Ganetzky B (1989) Molecular analysis of the para locus, a sodium channel gene in Drosophila. Cell 58:1143-1154.

Manifava M, Thuring JW, Lim ZY, Packman L, Holmes AB, Ktistakis NT (2001) Differential binding of traffic-related proteins to phosphatidic acid- or phosphatidylinositol (4,5)- bisphosphate-coupled affinity reagents. J Biol Chem 276:8987-8994.

Martin TF (2001) PI(4,5)P(2) regulation of surface membrane traffic. Curr Opin Cell Biol 13:493-499.

Martinez C, De Geus P, Lauwereys M, Matthyssens G, Cambillau C (1992) Fusarium solani cutinase is a lipolytic enzyme with a catalytic serine accessible to solvent. Nature 356:615-618.

Maruyama IN, Brenner S (1991) A phorbol ester/diacylglycerol-binding protein encoded by the unc-13 gene of Caenorhabditis elegans. Proc Natl Acad Sci U S A 88:5729-5733.

Mayer A, Scheglmann D, Dove S, Glatz A, Wickner W, Haas A (2000) Phosphatidylinositol 4,5-bisphosphate regulates two steps of homotypic vacuole fusion. Mol Biol Cell 11:807-817.

McKay RR, Zhu L, Shortridge RD (1994) Membrane association of phospholipase C encoded by the norpA gene of Drosophila melanogaster. Neuroscience 61:141-148.

McGahon B, Lynch MA (1998) Analysis of the interaction between arachidonic acid and metabotropic glutamate receptor activation reveals that phospholipase C acts as a coincidence detector in the expression of long-term potentiation in the rat dentate gyrus. Hippocampus 8:48-56.

McMahon HT, Missler M, Li C, Sudhof TC (1995) Complexins: cytosolic proteins that regulate SNAP receptor function. Cell 83:111-119.

McNiven MA, Kim L, Krueger EW, Orth JD, Cao H, Wong TW (2000) Regulated interactions between dynamin and the actin-binding protein cortactin modulate cell shape. J Cell Biol 151:187-198.

McPherson PS, Garcia EP, Slepnev VI, David C, Zhang X, Grabs D, Sossin WS, Bauerfeind R, Nemoto Y, De Camilli P (1996) A presynaptic inositol-5-phosphatase. Nature 379:353-357.

Merrifield CJ, Feldman ME, Wan L, Almers W (2002) Imaging actin and dynamin recruitment during invagination of single clathrin-coated pits. Nat Cell Biol 4:691-698.

Meves H (1994) Modulation of ion channels by arachidonic acid. Prog Neurobiol 43:175-186.

Michaelson DM, Barkai G, Barenholz Y (1983) Asymmetry of lipid organization in cholinergic synaptic vesicle membranes. Biochem J 211:155-162.

Miki H, Miura K, Matuoka K, Nakata T, Hirokawa N, Orita S, Kaibuchi K, Takai Y, Takenawa T (1994) Association of Ash/Grb-2 with dynamin through the Src homology 3 domain. J Biol Chem 269:5489-5492.

Miller KG, Emerson MD, Rand JB (1999) Goalpha and diacylglycerol kinase negatively regulate the Gqalpha pathway in C. elegans. Neuron 24:323-333.

Milne SB, Ivanova PT, DeCamp D, Hsueh RC, Brown HA (2005) A targeted mass spectrometric analysis of phosphatidylinositol phosphate species. J Lipid Res 46:1796-1802.

Minke B, Selinger Z (1991) Inositol lipid pathway in fly photoreceptors: excitation, calcium mobilization and retinal degeneration. Prog Retinal Res 11:99-124.

Minke B, Cook B (2002) TRP channel proteins and signal transduction. Physiol Rev 82:429-472.

Mochida S, Kobayashi H, Matsuda Y, Yuda Y, Muramoto K, Nonomura Y (1994) Myosin II is involved in transmitter release at synapses formed between rat sympathetic neurons in culture. Neuron 13:1131-1142.

Montecucco C, Rossetto O (2000) How do presynaptic PLA2 neurotoxins block nerve terminals? Trends Biochem Sci 25:266-270.

Montell C (1999) Visual transduction in Drosophila. Annu Rev Cell Dev Biol 15:231-268.

Montell C, Rubin GM (1989) Molecular characterization of the Drosophila trp locus: a putative integral membrane protein required for phototransduction. Neuron 2:1313-1323.

Morgan A, Burgoyne RD, Barclay JW, Craig TJ, Prescott GR, Ciufo LF, Evans GJ, Graham ME (2005) Regulation of exocytosis by protein kinase C. Biochem Soc Trans 33:1341-1344.

Muller O, Bayer MJ, Peters C, Andersen JS, Mann M, Mayer A (2002) The Vtc proteins in vacuole fusion: coupling NSF activity to V(0) trans-complex formation. Embo J 21:259-269.

Munemoto Y, Houtani T, Kase M, Sakuma S, Baba K, Yamashita T, Sugimoto T (2004) Mouse homolog of KIAA0143 protein: hearing deficit induces specific changes of expression in auditory brainstem neurons. Brain Res Mol Brain Res 128:131-140.

Munsch T, Freichel M, Flockerzi V, Pape HC (2003) Contribution of transient receptor potential channels to the control of GABA release from dendrites. Proc Natl Acad Sci U S A 100:16065-16070.

Nagy G, Matti U, Nehring RB, Binz T, Rettig J, Neher E, Sorensen JB (2002) Protein kinase C-dependent phosphorylation of synaptosome-associated protein of 25 kDa at Ser187 potentiates vesicle recruitment. J Neurosci 22:9278-9286.

Nurrish S, Segalat L, Kaplan JM (1999) Serotonin inhibition of synaptic transmission: Galpha(0) decreases the abundance of UNC-13 at release sites. Neuron 24:231-242.

Ordway RW, Pallanck L, Ganetzky B (1994) Neurally expressed Drosophila genes encoding homologs of the NSF and SNAP secretory proteins. Proc Natl Acad Sci U S A 91:5715-5719.

Orth JD, McNiven MA (2003) Dynamin at the actin-membrane interface. Curr Opin Cell Biol 15:31-39.

Pak WL, Grossfield J, White NV (1969) Nonphototactic mutants in a study of vision in Drosophila. Nature 222:351–354.

Pak WL, Grossfield J, Arnold KS (1970) Mutants of the visual pathway of Drosophila melanogaster. Nature 227:518-520.

Palczewski K, Saari JC (1997) Activation and inactivation steps in the visual transduction pathway. Curr Opin Neurobiol 7:500-504.

Pavlidis P, Tanouye MA (1995) Seizures and failures in the giant fiber pathway of Drosophila bang-sensitive paralytic mutants. J Neurosci 15:5810-5819.

Pearn MT, Randall LL, Shortridge RD, Burg MG, Pak WL (1996) Molecular, biochemical, and electrophysiological characterization of Drosophila norpA mutants. J Biol Chem 271:4937-4945.

Perin MS, Fried VA, Mignery GA, Jahn R, Sudhof TC (1990) Phospholipid binding by a synaptic vesicle protein homologous to the regulatory region of protein kinase C. Nature 345:260-263.

Peters C, Bayer MJ, Buhler S, Andersen JS, Mann M, Mayer A (2001) Trans-complex formation by proteolipid channels in the terminal phase of membrane fusion. Nature 409:581-588.

Peters C, Andrews PD, Stark MJ, Cesaro-Tadic S, Glatz A, Podtelejnikov A, Mann M, Mayer A (1999) Control of the terminal step of intracellular membrane fusion by protein phosphatase 1. Science 285:1084-1087.

Preiss J, Loomis CR, Bishop WR, Stein R, Niedel JE, Bell RM (1986) Quantitative measurement of sn-1,2-diacylglycerols present in platelets, hepatocytes, and ras- and sis-transformed normal rat kidney cells. J Biol Chem 261:8597-8600.

Pryer NK, Wuestehube LJ, Schekman R (1992) Vesicle-mediated protein sorting. Annu Rev Biochem 61:471-516.

Pyle JL, Kavalali ET, Piedras-Renteria ES, Tsien RW (2000) Rapid reuse of readily releasable pool vesicles at hippocampal synapses. Neuron 28:221-231.

Qualmann B, Kelly RB (2000) Syndapin isoforms participate in receptor-mediated endocytosis and actin organization. J Cell Biol 148:1047-1062.

Qualmann B, Kessels MM, Kelly RB (2000) Molecular links between endocytosis and the actin cytoskeleton. J Cell Biol 150:F111-116.

Raghu P, Usher K, Jonas S, Chyb S, Polyanovsky A, Hardie RC (2000) Constitutive activity of the light-sensitive channels TRP and TRPL in the Drosophila diacylglycerol kinase mutant, rdgA. Neuron 26:169-179.

Ranganathan R, Harris GL, Stevens CF, Zuker CS (1991) A Drosophila mutant defective in extracellular calcium-dependent photoreceptor deactivation and rapid desensitization. Nature 354:230-232.

Rao SS, Stewart BA, Rivlin PK, Vilinsky I, Watson BO, Lang C, Boulianne G, Salpeter MM, Deitcher DL (2001) Two distinct effects on neurotransmission in a temperature-sensitive SNAP-25 mutant. Embo J 20:6761-6771.

Rebecchi MJ, Eberhardt R, Delaney T, Ali S, Bittman R (1993) Hydrolysis of short acyl chain inositol lipids by phospholipase C-delta 1. J Biol Chem 268:1735-1741.

Reim K, Mansour M, Varoqueaux F, McMahon HT, Sudhof TC, Brose N, Rosenmund C (2001) Complexins regulate a late step in Ca2+-dependent neurotransmitter release. Cell 104:71-81.

Renganathan M, Godoy CM, Cukierman S (1995) Direct modulation of Na+ currents by protein kinase C activators in mouse neuroblastoma cells. J Membr Biol 144:59-69.

Rhee JS, Betz A, Pyott S, Reim K, Varoqueaux F, Augustin I, Hesse D, Sudhof TC, Takahashi M, Rosenmund C, Brose N (2002) Beta phorbol ester- and diacylglycerol-induced augmentation of transmitter release is mediated by Munc13s and not by PKCs. Cell 108:121-133.

Richards DA, Guatimosim C, Betz WJ (2000) Two endocytic recycling routes selectively fill two vesicle pools in frog motor nerve terminals. Neuron 27:551-559.

Richmond JE, Broadie KS (2002) The synaptic vesicle cycle: exocytosis and endocytosis in Drosophila and C. elegans. Curr Opin Neurobiol 12:499-507.

Richmond JE, Davis WS, Jorgensen EM (1999) UNC-13 is required for synaptic vesicle fusion in C. elegans. Nat Neurosci 2:959-964.

Richmond JE, Weimer RM, Jorgensen EM (2001) An open form of syntaxin bypasses the requirement for UNC-13 in vesicle priming. Nature 412:338-341.

Rickman C, Davletov B (2005) Arachidonic acid allows SNARE complex formation in the presence of Munc18. Chem Biol 12:545-553.

Rickman C, Jimenez JL, Graham ME, Archer DA, Soloviev M, Burgoyne RD, Davletov B (2005) Conserved Prefusion Protein Assembly in Regulated Exocytosis. Mol Biol Cell.

Risinger C, Bennett MK (1999) Differential phosphorylation of syntaxin and synaptosome-associated protein of 25 kDa (SNAP-25) isoforms. J Neurochem 72:614-624.

Ritchie JM (1979) A pharmacological approach to the structure of sodium channels in myelinated axons. Annu Rev Neurosci 2:341-362.

Rizo J, Sudhof TC (2002) Snares and Munc18 in synaptic vesicle fusion. Nat Rev Neurosci 3:641-653.

Rodriguez de Turco EB, Tang W, Topham MK, Sakane F, Marcheselli VL, Chen C, Taketomi A, Prescott SM, Bazan NG (2001) Diacylglycerol kinase epsilon regulates seizure susceptibility and long-term potentiation through arachidonoyl- inositol lipid signaling. Proc Natl Acad Sci U S A 98:4740-4745.

Roggero CM, Tomes CN, De Blas GA, Castillo J, Michaut MA, Fukuda M, Mayorga LS (2005) Protein kinase C-mediated phosphorylation of the two polybasic regions of synaptotagmin VI regulates their function in acrosomal exocytosis. Dev Biol 285:422-435.

Rohatgi R, Ma L, Miki H, Lopez M, Kirchhausen T, Takenawa T, Kirschner MW (1999) The interaction between N-WASP and the Arp2/3 complex links Cdc42-dependent signals to actin assembly. Cell 97:221-231.

Rohrbough J, Broadie K (2005) Lipid regulation of the synaptic vesicle cycle. Nat Rev Neurosci 6:139-150.

Rosenmund C, Rettig J, Brose N (2003) Molecular mechanisms of active zone function. Curr Opin Neurobiol 13:509-519.

Rosenmund C, Sigler A, Augustin I, Reim K, Brose N, Rhee JS (2002) Differential control of vesicle priming and short-term plasticity by Munc13 isoforms. Neuron 33:411-424.

Ryan TA (1999) Inhibitors of myosin light chain kinase block synaptic vesicle pool mobilization during action potential firing. J Neurosci 19:1317-1323.

Schmid SL (1997) Clathrin-coated vesicle formation and protein sorting: an integrated process. Annu Rev Biochem 66:511-548.

Schmidt A, Wolde M, Thiele C, Fest W, Kratzin H, Podtelejnikov AV, Witke W, Huttner WB, Soling HD (1999) Endophilin I mediates synaptic vesicle formation by transfer of arachidonate to lysophosphatidic acid. Nature 401:133-141.

Schreibmayer W (1999) Isoform diversity and modulation of sodium channels by protein kinases. Cell Physiol Biochem 9:187-200.

Sever S, Muhlberg AB, Schmid SL (1999) Impairment of dynamin's GAP domain stimulates receptor-mediated endocytosis. Nature 398:481-486.

Shimazaki Y, Nishiki T, Omori A, Sekiguchi M, Kamata Y, Kozaki S, Takahashi M (1996) Phosphorylation of 25-kDa synaptosome-associated protein. Possible involvement in protein kinase C-mediated regulation of neurotransmitter release. J Biol Chem 271:14548-14553.

Shoji-Kasai Y, Itakura M, Kataoka M, Yamamori S, Takahashi M (2002) Protein kinase C-mediated translocation of secretory vesicles to plasma membrane and enhancement of neurotransmitter release from PC12 cells. Eur J Neurosci 15:1390-1394.

Shyngle J, Sharma RP (1985) Studies on paralysis and development of second chromosome temperature sensitive paralytic mutants of Drosophila melanogaster. Indian J Exp Biol 23:235-240.

Siddiqi O, Benzer S (1976) Neurophysiological defects in temperature-sensitive paralytic mutants of Drosophila melanogaster. Proc Natl Acad Sci U S A 73:3253-3257.

Slepnev VI, De Camilli P (2000) Accessory factors in clathrin-dependent synaptic vesicle endocytosis. Nat Rev Neurosci 1:161-172.

Smith DP, Ranganathan R, Hardy RW, Marx J, Tsuchida T, Zuker CS (1991) Photoreceptor deactivation and retinal degeneration mediated by a photoreceptor-specific protein kinase C. Science 254:1478-1484.

Sollner T, Whiteheart SW, Brunner M, Erdjument-Bromage H, Geromanos S, Tempst P, Rothman JE (1993) SNAP receptors implicated in vesicle targeting and fusion. Nature 362:318-324.

Sorensen JB (2005) SNARE complexes prepare for membrane fusion. Trends Neurosci 28:453-455.

Standen NB, Quayle JM (1998) K+ channel modulation in arterial smooth muscle. Acta Physiol Scand 164:549-557.

Staneva G, Angelova MI, Koumanov K (2004) Phospholipase A2 promotes raft budding and fission from giant liposomes. Chem Phys Lipids 129:53-62.

Sudhof TC (2000) The synaptic vesicle cycle revisited. Neuron 28:317-320.

Sudhof TC (2004) The synaptic vesicle cycle. Annu Rev Neurosci 27:509-547.

Suh BC, Hille B (2002) Recovery from muscarinic modulation of M current channels requires phosphatidylinositol 4,5-bisphosphate synthesis. Neuron 35:507-520.

Sullivan J (2005) Finding the G spot on fusion machinery. Nat Neurosci 8:542-544.

Sutton RB, Fasshauer D, Jahn R, Brunger AT (1998) Crystal structure of a SNARE complex involved in synaptic exocytosis at 2.4 A resolution. Nature 395:347-353.

Suzuki DT, Grigliatti T, Williamson R (1971) Temperature-sensitive mutations in Drosophila melanogaster. VII. A mutation (para-ts) causing reversible adult paralysis. Proc Natl Acad Sci U S A 68:890-893.

Suzuki N, Wu CF (1984) Altered sensitivity to sodium channel-specific neurotoxins in cultured neurons from temperature-sensitive paralytic mutants of Drosophila. J Neurogenet 1:225-238.

Tanouye MA, Wyman RJ (1980) Motor outputs of giant nerve fiber in Drosophila. J Neurophysiol 44:405-421.

Terrian DM, White MK (1997) Phylogenetic analysis of membrane trafficking proteins: a family reunion and secondary structure predictions. Eur J Cell Biol 73:198-204.

Tian JH, Wu ZX, Unzicker M, Lu L, Cai Q, Li C, Schirra C, Matti U, Stevens D, Deng C, Rettig J, Sheng ZH (2005) The role of Snapin in neurosecretion: snapin knock-out mice exhibit impaired calcium-dependent exocytosis of large dense-core vesicles in chromaffin cells. J Neurosci 25:10546-10555.

Tokumaru H, Umayahara K, Pellegrini LL, Ishizuka T, Saisu H, Betz H, Augustine GJ, Abe T (2001) SNARE complex oligomerization by synaphin/complexin is essential for synaptic vesicle exocytosis. Cell 104:421-432.

Tolar LA, Pallanck L (1998) NSF function in neurotransmitter release involves rearrangement of the SNARE complex downstream of synaptic vesicle docking. J Neurosci 18:10250-10256.

Trebak M, Vazquez G, Bird GS, Putney JW, Jr. (2003) The TRPC3/6/7 subfamily of cation channels. Cell Calcium 33:451-461.

Trimarchi JR, Murphey RK (1997) The shaking-B2 mutation disrupts electrical synapses in a flight circuit in adult Drosophila. J Neurosci 17:4700-4710.

Tsegaye Y, Daasvatn KO, Holmsen H (2002) Acyl specificity of phospholipases A2 and C in thrombin-stimulated human platelets. Platelets 13:31-35.

Tsuboi T, Fukuda M (2005) The C2B Domain of Rabphilin Directly Interacts with SNAP-25 and Regulates the Docking Step of Dense Core Vesicle Exocytosis in PC12 Cells. J Biol Chem 280:39253-39259.

Tucker WC, Weber T, Chapman ER (2004) Reconstitution of Ca2+-regulated membrane fusion by synaptotagmin and SNAREs. Science 304:435-438.

Vallis Y, Wigge P, Marks B, Evans PR, McMahon HT (1999) Importance of the pleckstrin homology domain of dynamin in clathrin-mediated endocytosis. Curr Biol 9:257-260.

van der Bliek AM, Meyerowitz EM (1991) Dynamin-like protein encoded by the Drosophila shibire gene associated with vesicular traffic. Nature 351:411-414.

Varoqueaux F, Sigler A, Rhee JS, Brose N, Enk C, Reim K, Rosenmund C (2002) Total arrest of spontaneous and evoked synaptic transmission but normal synaptogenesis in the absence of Munc13-mediated vesicle priming. Proc Natl Actl Acad Sci U S A 99:9037-9042.

Verhage M, Maia AS, Plomp JJ, Brussaard AB, Heeroma JH, Vermeer H, Toonen RF, Hammer RE, van den Berg TK, Missler M, Geuze HJ, Sudhof TC (2000) Synaptic assembly of the brain in the absence of neurotransmitter secretion. Science 287:864-869.

Vinos J, Jalink K, Hardy RW, Britt SG, Zuker CS (1997) A G protein-coupled receptor phosphatase required for rhodopsin function. Science 277:687-690.

Vitale N, Caumont AS, Chasserot-Golaz S, Du G, Wu S, Sciorra VA, Morris AJ, Frohman MA, Bader MF (2001) Phospholipase D1: a key factor for the exocytotic machinery in neuroendocrine cells. Embo J 20:2424-2434.

Voets T, Toonen RF, Brian EC, de Wit H, Moser T, Rettig J, Sudhof TC, Neher E, Verhage M (2001) Munc18-1 promotes large dense-core vesicle docking. Neuron 31:581-591.

Waddell S, Quinn WG (2001) Neurobiology. Learning how a fruit fly forgets. Science 293:1271-1272.

Wagner ML, Tamm LK (2001) Reconstituted syntaxin1a/SNAP25 interacts with negatively charged lipids as measured by lateral diffusion in planar supported bilayers. Biophys J 81:266-275.

Wang P, Saraswati S, Guan Z, Watkins CJ, Wurtman RJ, Littleton JT (2004) A Drosophila temperature-sensitive seizure mutant in phosphoglycerate kinase disrupts ATP generation and alters synaptic function. J Neurosci 24:4518-4529.

Wang Y, Okamoto M, Schmitz F, Hofmann K, Sudhof TC (1997) Rim is a putative Rab3 effector in regulating synaptic-vesicle fusion. Nature 388:593-598.

Watts JL, Browse J (2002) Genetic dissection of polyunsaturated fatty acid synthesis in Caenorhabditis elegans. Proc Natl Acad Sci U S A 99:5854-5859.

Weber T, Zemelman BV, McNew JA, Westermann B, Gmachl M, Parlati F, Sollner TH, Rothman JE (1998) SNAREpins: minimal machinery for membrane fusion. Cell 92:759-772.

Wei S, Ong WY, Thwin MM, Fong CW, Farooqui AA, Gopalakrishnakone P, Hong W (2003) Group IIA secretory phospholipase A2 stimulates exocytosis and neurotransmitter release in pheochromocytoma-12 cells and cultured rat hippocampal neurons. Neuroscience 121:891-898.

Weimbs T, Mostov K, Low SH, Hofmann K (1998) A model for structural similarity between different SNARE complexes based on sequence relationships. Trends Cell Biol 8:260-262.

Weimbs T, Low SH, Chapin SJ, Mostov KE, Bucher P, Hofmann K (1997) A conserved domain is present in different families of vesicular fusion proteins: a new superfamily. Proc Natl Acad Sci U S A 94:3046-3051.

Weimer RM, Richmond JE, Davis WS, Hadwiger G, Nonet ML, Jorgensen EM (2003) Defects in synaptic vesicle docking in unc-18 mutants. Nat Neurosci 6:1023-1030.

Weis WI, Scheller RH (1998) Membrane fusion. SNARE the rod, coil the complex. Nature 395:328-329.

Wenk MR, De Camilli P (2004) Protein-lipid interactions and phosphoinositide metabolism in membrane traffic: insights from vesicle recycling in nerve terminals. Proc Natl Acad Sci U S A 101:8262-8269.

Wenk MR, Lucast L, Di Paolo G, Romanelli AJ, Suchy SF, Nussbaum RL, Cline GW, Shulman GI, McMurray W, De Camilli P (2003) Phosphoinositide profiling in complex lipid mixtures using electrospray ionization mass spectrometry. Nat Biotechnol 21:813-817.

Witke W, Podtelejnikov AV, Di Nardo A, Sutherland JD, Gurniak CB, Dotti C, Mann M (1998) In mouse brain profilin I and profilin II associate with regulators of the endocytic pathway and actin assembly. Embo J 17:967-976.

Wu CF, Ganetzky B (1980) Genetic alteration of nerve membrane excitability in temperature- sensitive paralytic mutants of Drosophila melanogaster. Nature 286:814-816.

Wu L, Niemeyer B, Colley N, Socolich M, Zuker CS (1995) Regulation of PLC-mediated signalling in vivo by CDP-diacylglycerol synthase. Nature 373:216-222.

Wu L, Bauer CS, Zhen XG, Xie C, Yang J (2002) Dual regulation of voltage-gated calcium channels by PtdIns(4,5)P(2). Nature 419:947-952.

Xu NJ, Yu YX, Zhu JM, Liu H, Shen L, Zeng R, Zhang X, Pei G (2004) Inhibition of SNAP-25 phosphorylation at Ser187 is involved in chronic morphine-induced down-regulation of SNARE complex formation. J Biol Chem 279:40601-40608.

Yang B, Steegmaier M, Gonzalez LC, Jr., Scheller RH (2000) nSec1 binds a closed conformation of syntaxin1A. J Cell Biol 148:247-252.

Yoshioka T, Inoue H, Hotta Y (1984) Absence of diglyceride kinase activity in the photoreceptor cells of Drosophila mutants. Biochem Biophys Res Commun 119:389-395.

Yoshioka T, Inoue H, Hotta Y (1985) Absence of phosphatidylinositol phosphodiesterase in the head of a Drosophila visual mutant, norpA (no receptor potential A). J Biochem (Tokyo) 97:1251-1254.

Zigmond SH (2000) How WASP regulates actin polymerization. J Cell Biol 150:F117-120.

Zinsmaier KE, Eberle KK, Buchner E, Walter N, Benzer S (1994) Paralysis and early death in cysteine string protein mutants of Drosophila. Science 263:977-980.